博士論文

Fabrication of Hollow Microcapsules from Microbubble Templates

(マイクロバブルをテンプレートとして用いた中空マイクロカプセルの製造)

モリノ　ジェイ　ヘスス

FABRICATION OF HOLLOW MICROCAPSULES FROM MICROBUBBLE TEMPLATES

(マイクロバブルをテンプレートとして用いた中空マイクロカプセルの製造)

Approved, Thesis committee (in alphabetical order):

_____

Daiguji, Hirofumi
Professor, Department of Mechanical Engineering
The University of Tokyo, Japan.

_____

Jimbo, Yasuhiko
Professor, Department of Human and Engineered Environmental Studies
The University of Tokyo, Japan.

_____

Maruyama, Shigeo
Professor, Department of Mechanical Engineering
The University of Tokyo, Japan.

_____

Takemura, Fumio
Deputy Director, Energy Technology Research Institute (ETRI) and
National Institute of Advanced Industrial Science and Technology (AIST), Japan.

_____

Torii, Toru
Professor, Department of Human and Engineered Environmental Studies
The University of Tokyo, Japan.

Abstract

Fabrication of Hollow Microcapsules from
Microbubble Templates
Professor Hirofumi Daiguji
By
Jay Jesus Molino
The University of Tokyo

Hollow microcapsules are expected to become an integral part in medical and industrial applications as such as drug delivery systems, ultrasound contrast agents, confinement fusion targets, light weight fillers, damping materials, and energy storage media. In essence the benefit of hollow capsules relies in the fact that these are small, have large inner volumes, and have better stability which is suitable for chemical loading. In this work we introduce new facile techniques to fabricate hollow biocompatible microcapsules. The disclosed techniques rely on the stabilization of micro bubbles in polymeric solutions for a time long enough to allow polymer adsorption onto the micro bubble surface. In the present study three different microcapsules were fabricated via bubble templating. Each capsule was fabricated to be potentially employed in different applications. Furthermore, the techniques are not restricted to the materials employed, which allow us to synthetize inorganic hollow capsules using the same principles. Yet, only those fabricated with biodegradable polymers are covered in the present study. Since microcapsules with tunable sizes are desired, we report on the size control of each of the capsules created using our bubble template method. Furthermore we also proved that the methods are scalable. Mass production can be achieved and the details for mass producing these capsules are disclosed in this study.

Concerning the study of microcapsules fabricated using PLA as the coating polymer, the conditions required to synthesize uniform microcapsules were clarified. The average size of these capsules was 1um and epifluorescence microscopy confirmed that there was a single hollow (air) core inside of them. Furthermore the conditions required for achieving a bigger stable micro bubble were clarified and capsules with an average size of 5um were fabricated. For tailoring the microcapsule size we focused on the effect of (1) PLA concentration, (2) PLA molecular weight, and (3) PVA in aqueous medium on the radius distribution of fabricated hollow PLA microcapsules. The experimental conditions for mass producing hollow PLA microcapsules are well documented.

Regarding the study of microcapsules fabricated using colloidal PAH as the coating polymer; we successfully controlled the microcapsule radius by changing the concentration of PAH in the Na_2CO_3 solution. The zeta potential of these PAH microcapsules is positive at pH = 8.5, which allowed the adsorption of poly-sodium styrene sulfonate (PSS) onto the PAH microcapsules, and a bilayer capsule was made. Furthermore, the bilayer PAH/PSS capsule solution was titrated until the pH was adjusted to 7.0 and they were stable at this pH, proving that they can be potentially used for pharmaceutical applications. The required conditions for successful synthesis of bilayer capsules were determined as well. On the basis of the analysis of the zeta potentials and Fourier transform infrared-attenuated total reflection (FTIR-ATR) spectra for both PAH and PAH/PSS hollow microcapsules, the adsorption mechanism of PSS onto hollow PAH microcapsules was elucidated as well.

Acknowledgement

I am utterly compelled to express my gratitude to all those who made this possible. First and foremost, I truly appreciate the valuable guidance and support received from Professor Hirofumi Daiguji who was my mentor during my tenure as a PhD student at the Microcapsule group. His scientific supervision shrewd questions, comments and precise reviewing style, were vital for the success of this work. Furthermore, I also owe my gratitude to Professor Fumio Takemura for believing and enduring with me. To both Professors I give my deepest gratefulness.

I want to thank Daichi Sakurai and Eitaro Matsuoka, my colleagues, for their great work and collaboration during these years as part of the microcapsule team.

To all the Professors who taught me during these years, all my labmates at Hihara Lab and to the staff of the University of Tokyo, they should also be commended for providing support during these years.

Last but not least, I extend my gratitude to the Japanese Government as they funded this research and financially sponsored my stay in Japan.

TABLE OF CONTENT

List of Figures

LIST OF TABLES

1

Fabrication of Hollow Polymer Microcapsules

1. Introduction

The encapsulation of materials consists in entrapping solid, liquid or gas cores inside a polymeric shell or matrix. The final product is named *microcapsule* and their sizes are in the micrometer range. If the size is in the nanometer range it is known as nanocapsule or nanoparticle. Thus, in general, a capsule is defined as any core surrounded by a shell whether this shell or core is organic or inorganic [1, 2, 3, 4]. This shell is a continuous non-porous or porous polymeric layer. A microcapsule ought not to be confused with a microsphere as microspheres display a single structure. This is, they are completely solid, with no internal reservoirs as a microcapsule.

Microencapsulation has found its way into industry and bioscience as microcapsules are an effective way to enhance the stability of the material being encapsulated, reduce toxic effects, and extend material release for different applications in various fields of manufacturing. Specifically, microencapsulation provides an effective method of protecting the encapsulated active components (isolate it) from a specific environmental condition, avoid denaturalization of the compounds (e.g. protect enzymes from strong sheering of traditional reactors, proteolysis by microbes or hydrophobic reactions) [5 6 7], and provide stability of drug substances (e.g. protection from biological fluids) [8, 9]. Furthermore, they can be utilized to enhance biocompatibility of conventional drugs, allow the controlled dosification of active molecules [10, 11, 12], eliminate incompatibles, and serve as inertial

confinement fusion targets [13], micro reactors [14, 15], scaffolds for cultivating tissue, [16] lightweight fillers/buoyancy, and spacers or dampers [17]. Microcapsules can also be employed as artificial cells, [18] as protective shells for enzymes and tissue [19 20], or as transferring vectors for gene therapy [21,22], dye dispersants [23], water purification systems [24], electrodes [25], gas storage media [26], as supports for catalysts, [27] for cosmetics [28] and, in general, as mass diffusion and transport enhancers [29]. Additionally, when hollow particles are sufficiently ordered, it is predicted that they can have very useful properties as optical devices (e.g. photonic band-gap), or as a dielectric defect in photonic crystals (micro cavities in crystals could lead to photonic states in the gap and thus, the properties of the material can be dictated by the nature of the defect) [30, 31]. Finally, they are affordable solutions for organic/inorganic functional coatings. From the aforementioned it can be inferred that microencapsulation is also a way to combine properties of very different materials, something very difficult to attain using other techniques. Several other applications have been discussed in the works of *Dubey et al* [32] and *Lachman et al* [33] but in general the value of a microcapsule is in its inherent properties such as their small size, large inner volume, spherical shape, and better stability suitable for chemical loading [34, 35, 36, 17]. Microcapsules size ranges from 0.5-5000 μm. If the microcapsules are intended to be employed for pharmaceutical applications the capsule must be biocompatible and biodegradable and within the 1 to 1000 μm range [37].

Microcapsules have great opportunities in the pharmaceutical industry. The human body sets very difficult requirements. For instance, the oral route has been the major route for drug delivery to provide treatment for any chronic treatment, however since nearly 40% of the new drug candidates are lipophilic, there is very poor oral bioavailability, high intra and intersubject variability, and lack of dose proportionality [38, 39]. For such compounds, the absorption rate from the GI lumen is controlled by dissolution. Modification of the physicochemical properties of the compound, such as salt formation and particle size reduction, may be one approach to improve the dissolution rate of the drug. This can be achieved using microcapsules. If parenteral delivery is chosen, the capsules should be less than 250μm in diameter (ideally less than 125μm) to allow injections with optimum needle diameter [1, 38] and, since the microcapsules size is highly tunable depending on the fabrication technique [40], it is possible to address the oral bioavailability issue. Another example is that microcapsules can address the "bubble stability problem" inside the body. Bubbles are well proven ultrasound contrast agents but to effectively employ them as ultrasound contrast agents they must be stable. To enhance the bubbles lifespan microcapsules can be employed to stabilize them. Capsules that are intended to be employed as ultrasound contrast agents should be in the range 1–4 μm to easily pass through the capillary blood circuit and ensure a long circulation time before they completely drain into the liver. [41, 42, 4]

The idea of a microcapsule is not new as it is already present in nature, e.g. vesicular structures and micelles. In the body the lipid bilayer is stable because water's affinity for hydrogen bonding never stops. It is the hydrogen bonding of water that holds a membrane together [43]. However, lipid bilayers have limitations since, if they are to be employed to stabilize microbubbles, they will easily disintegrate as the interaction between the lipids molecules is weak [44]; furthermore, lipid bilayers are not so useful for engineering applications. Fortunately, with the development of new techniques, biologically compatible microcapsules as well as capsules suited for several kinds of engineering application can be created.

2. Hollow microcapsules for UCAs

In general, hollow microcapsules are considered to be a structure filled with water or gas; this is so as many researchers denote hollow capsules as capsules that have a cavity or cavities filled with a fluid. However, this study only regards gas filled (empty) microcapsules as hollow. This is, a hollow microcapsule is a microbubble (CO_2, N_2, perfluorocarbons "PFC's") encapsulated in a thin polymer or protein shell[45-51].

The materials employed for encapsulating vary, as implied before, depending on the application. Capsules are made of liposomes, [52, 53] polymersomes, [54] colloidosomes, [55] hydrogel capsules [56] polyelectrolytes [57, 58 59], inorganic nanoparticles (e.g. gold, titanium, silica) [60, 61, 62, 63], melamine [64], lipid nanoparticles, assembled nanoparticles [65, 66], gums (e.g. sodium alginate) [67], cellulose (methylcellulose) proteins and even of carbohydrates (dextran, sucrose).

The fact is that hollow microcapsules are just stable microbubbles. This is the main focus of this thesis: Bubble Stabilization Using a Polymeric Shell. Even though a small container is of great usefulness, this study aims to design hollow capsules, which can be employed as ultrasound contrast agents. Ultrasound echoenhancers are stable and hemodynamically inert subcapillary sized microbubbles encapsulated in a thin shell, which have been introduced in recent years to improve blood flow visualization within organs to recognize tissue abnormalities. [68, 69]Microbubbles act as echoenhancers, this is, its backscattering echo is proportional to the change of acoustic impedance between the blood and the gas in the bubble. Since this impedance is very high the acoustic wave is completely reflected. Since wavelengths for diagnostic ultrasounds range from 1-0.1 mm (1.5-15 MHz), which are much larger than a bubble radius, it can be concluded that microbubbles behave as a Rayleight scatterer. The scattering cross-section φ for a linear scatterer whose characteristic length is smaller than the incident wave is given by equation (1.1),

$$\phi = \left(\frac{4}{9}\pi R^2 (kR)^4\right) \cdot \left(\left(\frac{\kappa_s - \kappa}{\kappa}\right)^2 + \frac{1}{3}\left(\frac{3(\rho_s - \rho)}{2\rho_s - \rho}\right)^2\right) \quad (1.1)$$

where R is the radius of the scatterer, λ is the wavelength, k=2π/λ is the wave number , k_s is the compressibility of the scatterer, K is the compressibility of the continuous phase. It can be seen from this equation that the increase in scattering cross section is regarded as the difference of densities and compressibility factors. Therefore using a gas as perfusion contrast agent assures maximum scattering cross section [70].

However, it is very interesting to realize that the sole reflection will not serve as ultrasound contrast agents because the microbubbles are very small and sparse when thinking on the bulk (blood). Here it is when the bubbles' second harmonic comes into play. Although its intensity is lower compared to the main resonant frequency, the second harmonic is still strong enough to be used for diagnostic purposes. Thus, it is possible to detect only the contrast agents and differentiate it from surrounding tissue since in general only contrast agents have harmonics. This Second Harmonic imaging, or best known as B-mode imaging, offers a high signal-to-noise ratio and allows imaging even at very slow flow conditions. [71]

Microbubbles by themselves have a very short lifespan in the system. The inner pressure in the bubble is the result of the equilibrium pressure (Henry's law), the *Laplace Pressure*, and the blood pressure and in turn the combination of these three, by far, exceeds the gas pressure in the blood. In fact, Laplace pressure is the main responsible for the movement of gas outside the bubble. This pressure drop across the interface is given by:

$$\Delta p = p_b - p_a = \frac{2\gamma}{r} \quad (1.2)$$

in which $\boldsymbol{r}$ is the radius of the bubble, γ is the interfacial surface tension and $\boldsymbol{\Delta P}$ the pressure difference experienced by a bubble. As the gas diffuses to the outside of the bubble, the radius decreases and thus the pressure difference increases as well. This implies a faster rate of dissolution. In addition, it is critical for microbubbles to be smaller than the capillaries to ensure passage through the pulmonary capillary bed, be stable enough to endure the whole circuit to allow proper examination and diagnosis (Plesset and Epstein calculated that a 10 μm air bubble will dissolve in 1.17 sec in degassed water and 6.63sec in air saturated water [72]), being also crucial for them to display a uniform size for optimizing backscattering.

One approach to the instability issue is to employ perfluorocarbons. It is of great interest to reduce the high partition coefficient of the gas (Air in the normal case) between the gaseous phase

and the liquid phase (known as Ostwald coefficient, *L)*. This reduction can be achieved by including PFC into the air bubbles. Thus, a combination of a low Ostwald coefficient ($<10^4$) and a relatively high saturated vapor pressure at body temperature ($> 3 \cdot 10^4$Pa) is required (only some PFC display this characteristics [73]). This is, since the larger amount of gas present in a microbubble will be PFC, the solution containing air is so diluted that the partial pressure of the most soluble gas (Air) is 1 atm. There can be diffusion of blood-soluble gasses in and out of the bubble and these changes of pressure can be withstand by the PFC. Figure 1.1 [73] shows a good representation of this phenomenon.

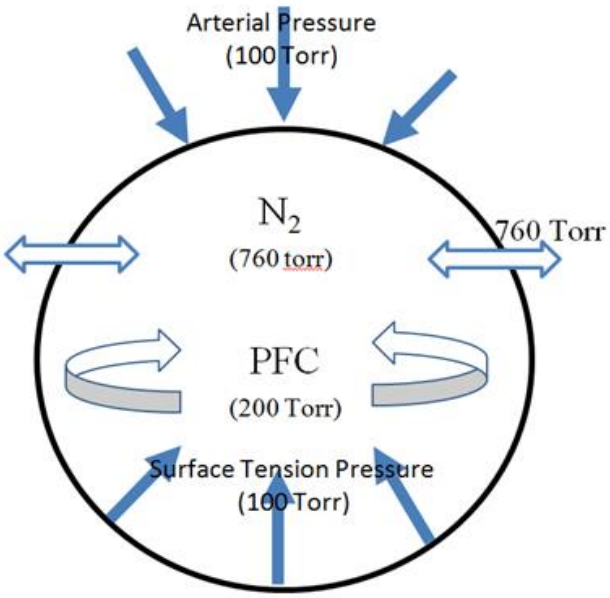

Figure 1.1: Osmotic Equilibrium. An osmotic equilibrium is set up where the water-soluble gases, whose partial pressure inside the bubble remains essentially constant at 1 atm, diffuse in and out of the bubble while the added partial pressure of the PFC vapor counterbalances the combined forces of blood pressure and Laplace pressure. [73]

The other option is to conveniently cover the bubbles (Air) so that it can be properly used as ultrasound contrast agents. The idea is not new; there exists several contrast agents which use lipids to protect the microbubble. Reference 69 summarized the commercially available contrast agents. This data is shown as Table 1.1.

Equation (1.3) [72, 74] is a modified version of the Epstein-Plesset equation for the lifetime of a microbubble which also considers the permeability of a layer surrounding the microcapsule.

$$-\frac{dr}{dt} = \frac{L}{r/D_w + R_{shell}} \cdot \left(\frac{1 + \left(2\sigma_{shell}/P_a \cdot r - f \right)}{1 + \left(4\sigma_{shell}/3P_a \cdot r \right)} \right) \tag{1.3}$$

Table 1.1: Microbubble contrast agents.

Name	Shell Material	Gas (solubility)	Size (μm)
Albumex	Albumin H	Air H	4.3
Optison™(FS069)	Albumin H	Octafluorpropane L	4.5
MP1950	Lipid L	Decafluorobutane L	2
PESDA	Albumin NA	Decafluorobutane L	4.7
Definity®(MRX-115)	Lipid/surfactant L	Octafluorpropane L	1.1–3.3
Imagent(AFO-150)	Lipid/surfactant L	Nitrogen/perfluorohexane L	6.0(median)
Sonovue®(BR-1)	Lipid L	Sulfur hexafluoride L	2 (median)
BR14	Lipid L	Perfluorobutane L	2.6
Levovist (SHU 508A)	Lipid/Galactose L	Air H	2–4
biSphere™ (PB127)	Polylactide/albumin H	Nitrogen H	3
Sonazoid (NC100100)	Lipid/surfactant NA	Perfluorobutane L	2.2
ST68-PFC	Lipid/surfactant L	Decafluorobutane L	1.8
Sonavist (SHU563a)	Cyanoacrylate H	Air H	NA

Shell stiffness is: high (H) and low (L) and gas solubility is noted as high (H), low (L) or not available (NA). [69]

Where L is the Ostwald's coefficient, D_w is the diffusivity of the gas in water, R_{shell} is the resistance of the shell to the encapsulated gas permeation, f is the ratio of the gas concentration in the bulk to saturation (i.e. f = 1 is for saturated), P_a is atmospheric pressure and σ_{shell} the surface tension at the gas-liquid interface. This equation (and all the analysis to be performed hereafter) assumes a spherical bubble. In addition, equation (1.3) does not take into account shell aging or even how the shell changes to the core size as gas permeates, yet it displays very useful and tangible information on the dissolution phenomena. Figure 1.2 shows the kinetics of bubble dissolution calculated from equation (1.3). From this graph it is understood that there is a need for a better "impermeable" shell and a better understanding on how PFC behaves.

Here it is the highlight based on all expressed hitherto: For a lifetime of days or even months the shell must be solid in order to eliminate surface tension and to decrease gas permeability through the shell matrix. An impermeable solid shell eliminates the Laplace pressure issue which is the driving force for "instant" bubble dissolution, but again, it ought to be thin and flexible enough to allow the bubble to resonate. Thus, this thesis focuses on synthesizing such shell around microbubbles.

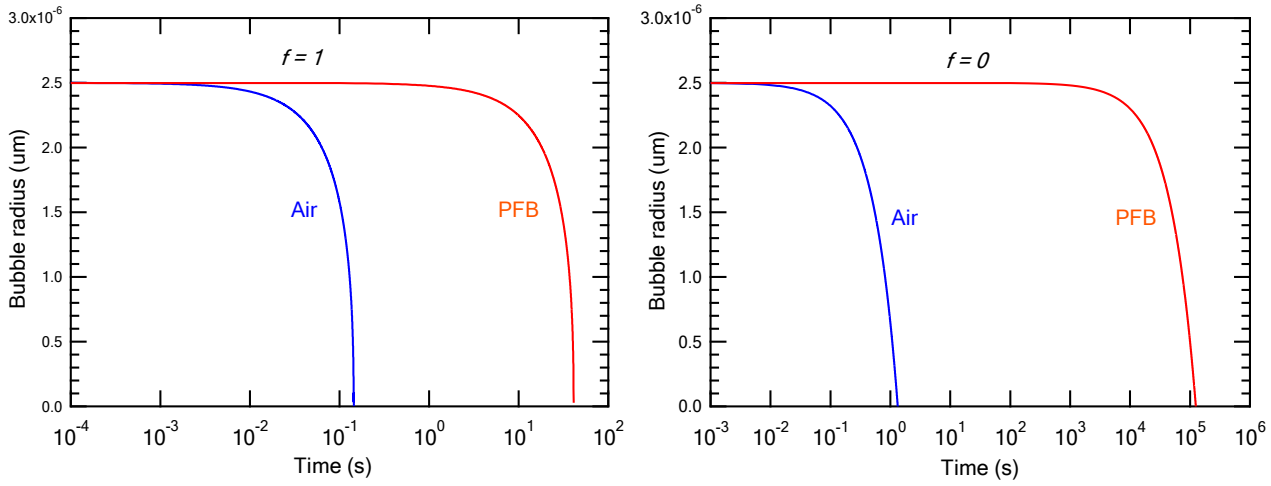

Figure 1.2: Dissolution kinetics. Calculated microbubble dissolution kinetics based on the modified-EP equation. (*a*) Radius-time curves of a free microbubble composed of air or perfluorobutane (PFB). Model parameters were σ_{shell}=72 mN m^{-1}, *Rshell*= 0, *Pa* = 101.3 kPa, and *f* = 1 (i.e., saturation). Diffusion parameters for air were L = 0.02 and Dw= 2 × 10−5 cm2 s^{-1}; those for PFB were L = 0.0002, Dw= 0.7 × 10−5 cm2 s^{-1}. (*b*) Radius-time curves of lipid-coated microbubbles in degassed water (*f* = 0). Model parameters were the same as above, except R_{shell}=104 s m^{-1} for air and 107 s m^{-1} for PFB and σshell= 0 mNm^{-1}.

3. Hollow microcapsules fabrication techniques

Even though there are several techniques to synthesize hollow microcapsules, in general, all of them can be classified into four main synthesis methods, namely: chemical methods, physico-chemical methods, electro-chemical and physico-mechanical methods. Among the chemical methods, the interfacial polymerization method is the most popular. In this technique the capsule shell is the result of a reaction among the polymer chain and the surface of a droplet or a solid particle that is being used as a core. In most cases, multifunctional monomers, i.e. isocyanates, are dispersed in the liquid cores, which are suspended in a dispersing/emulsyifing continuous phase. Another coreactant multifunctional polymer (e.g. amine) is dispersed in the continuous phase and this allows the reaction of both multifunctional polymers to take place at the droplet-dispersing phase (rapid polymerization at the interface), then the cores are removed to attain a hollow capsule. Polymerization can also occur at a bubble surface, and therefore hollow microcapsules are immediately created with a polymer shell [64, 75, 76].

Physico-chemical methods include the coacervation or phase separation method. Coacervation is a colloidal phenomenon, a process where a homogeneous polymer partially desolvates from a homogeneous polymeric solution into a polymer rich phase (coacervate) and a poor polymer phase. [3, 2] This method mainly consists of three steps carried out under continuous mixing: *1*. three

immiscible phases are formed, *2.* shell/coating material is deposited in the solution, and *3.* the coating solidifies. [77, 74]

A common technique, under the category of electro-chemical methods, for manufacturing polyelectrolyte microcapsules characterized for noncovalent interactions in the polymer chains to synthesize nano-thick layers around a liquid or solid core by the multiple adsorptions of polyanion and polycation groups, is the layer-by-layer (LbL) method. [78, 79, 80] The sequential addition of polyelectrolyte requires exact ratios of the polyelectrolyte; otherwise, the chance of forming free polyelectrolyte or particle aggregates increases. [81, 82]

As for physico-mechanical process, the solvent evaporation method is one of the best known. In this method first a water/oil/water (W/O/W) emulsion is created: core materials are dissolved in a solvent (oil) which is immiscible in the continuous phase (water) and mixed via agitation. The oil phase covers the liquid phase (water) and is emulsified in water to achieve a W/O/W mixture. The mixture is then heated and stirred to evaporate the solvent allowing the polymer to supersaturate at the water/oil interface. Finally freeze-drying is employed to remove the cores. [41]

Depending on the employed core, finally, after shell formation, the permeability and strength of the shell are intentionally degraded by aging or cross-linking so that the liquid or solid core can be removed by dissolution, evaporation, or thermolysis (e.g. calcination and freeze drying), thus yielding hollow capsules.

However it is still a challenge to find a proper procedure to effectively control all the characteristics of interest. This is, it is hard to control mechanical strength, permeability, porosity, capability, biocompatibility, and uniformity by a unique procedure. Through the current techniques it cannot be achieved as the fabrication of hollow microcapsules depends not only on the procedure but also the physico-chemical properties of the materials being employed.

This introduction focuses on some of the latest and novel methods to fabricate hollow microcapsules for engineering and biomedical applications. The next section focuses on four different techniques to fabricate hollow (gas filled) capsules, namely CAN-BD, LbL, electro hydrodynamic atomization, and tubular microfluidics.

3.1 Supercritical Fluids: CAN-BD

Recently many techniques that employ supercritical fluids have been developed and the interest relies in the fact that this technique has processing advantages as the organic solvent residue during microcapsule preparation is minimal and thus the purification process (cleaning) of the capsules is easier to achieve. Furthermore, the resultant product has a narrow size distribution; the fabrication

process takes seconds and since it operates at lower temperatures, thermally liable materials can be loaded on the capsule. [1]

A fluid is said to be supercritical when its pressure and temperature are higher than the critical pressure (Pc) and critical Temperature (Tc). In this region, the properties of the supercritical fluid can be finely tuned (e.g. viscosity, diffusivity, interfacial tension). This implies that the fluid properties can be controlled to fit different processing needs. For instance, if surface tension and viscosity can be controllable, the size of the sprayed droplets is controllable as well. In general CO_2 is widely used as supercritical fluid because it has low critical points (Pc = 73.8atm and Tc=31.1C), it is inexpensive, and it is also regarded as safe. Furthermore since CO_2 is nonpolar, it cannot dissolve lipophilic and hydrophilic compounds (most pharmaceutical compounds are lipophilic or hydrophilic) but it can solubilize low MW weight lipophilic substances, which is a great advantage as CO_2 can be a solvent and non solvent for pharmaceutical applications.

CAN-BD is classified among the SCF techniques. The acronym stands for Carbon Dioxide Assisted Nebulization with Bubble Dryer. It is a physico-chemical method. The process consists on the nebulization of a liquid solution which contains a solute formed of micro-nano particles that precipitate as the solubility of the solvent is reduced via solvent extraction. In other words, the supercritical solution, which contains a cosolvent and dissolved polymers (shell material), is maintained at high pressure and then sprayed through a nozzle or capillary to near atmospheric pressure. The rapid expansions yield to an aerosol, which is formed of micro droplets and micro bubbles. Thus, hollow capsules can be attained in this process. This flow is directed into a drying chamber filled with either nitrogen or heated air to keep a desired temperature during the drying process. The produced particles are then collected using a filter at the end of the chamber. The pore size of the filters is between 0.2 and 0.45μm. The typical flow rates on a lab scale are 0.3 to 0.6 ml/min. The process has been successfully scaled up by Sievers et al [83] and have more recently used flow rates as high as 30 ml/min, which is a commercial production scale for high value pharmaceutical products [84]. A schematic of the process is shown in Figure 1.3.

CAN-BD has been effectively employed for loading protein vaccines. Full retention of biological activity of Hepatitis B surface antigen (HBsAg) [83] in a protein vaccine was observed after preparing the vaccine using CAN-BD. Live attenuated measles virus have also been effectively loaded [83].

Furthermore a lyophilized measles vaccine has been loaded using CAN-BD for pulmonary delivery (dry vaccine) and it has been concluded that 107±23 of the viral activity has been preserved.

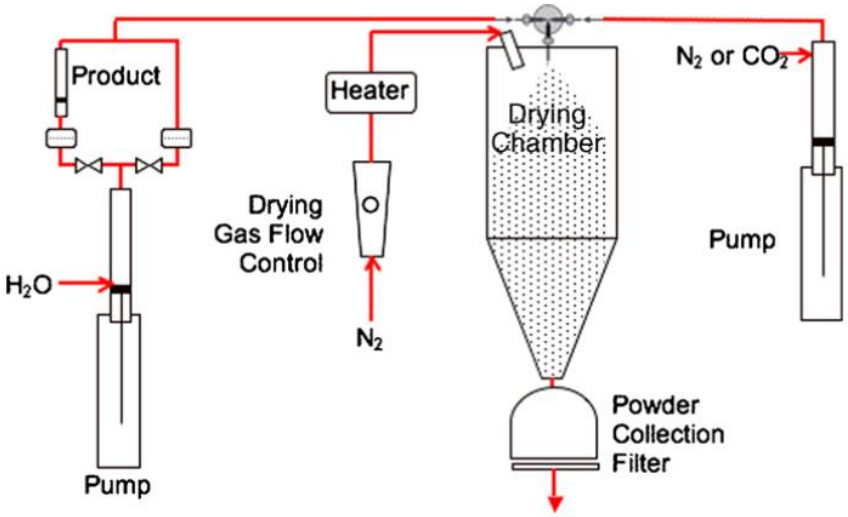

Figure 1.3: CAN-BD schematic. [83]

Cape et al. [85] reports being able to produce fine dry powders of anti-CD4 antibody, which is a primatized monoclonal antibody with potential clinical value in treating rheumatoid arthritis and other diseases. CAN-BD has also been employed to load ibuprofen.

CAN-BD offers a minimum decomposition of thermo liable drugs as the operation temperature is considerably lower than those in the usual solvent evaporation process, and furthermore, the final capsule size is below three micrometers, which is suitable for pulmonary delivery. [86] Figure 1.4 shows a SEM image of anti-CD4 antibody loaded microcaspules.

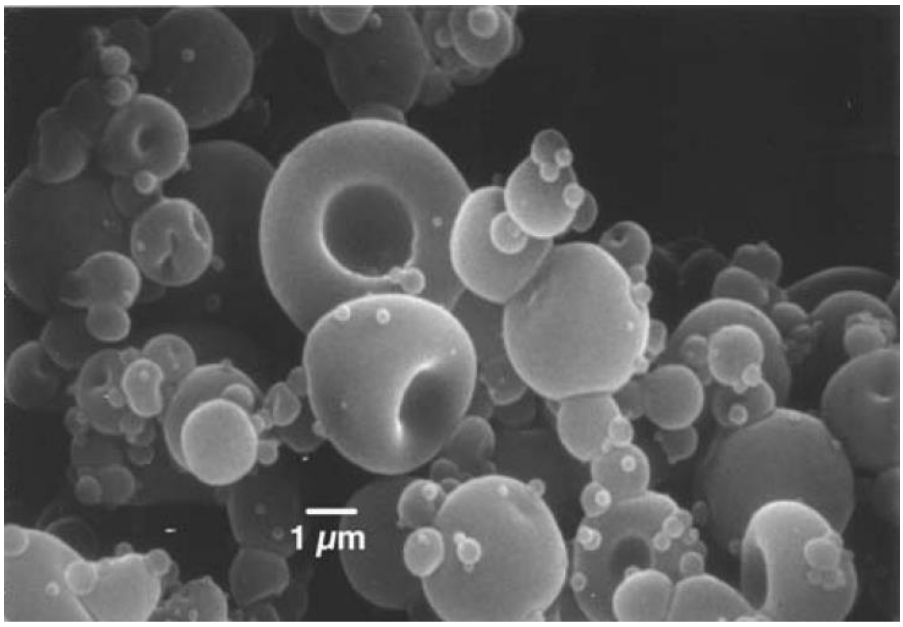

Figure 1.4:Anti-CD4 antibody. SEM image of particles of anti-CD4 antibody produced by CAN-BD [85]

3.2 Coaxial Electrospraying

Electrospraying or electrohydrodynamic atomization (EHDA) is a process employed to make droplets by applying a potential difference of thousands of volts between a plate and the tip of the capillary tube from which liquid is being supplied. The final droplet size, depending on the fabrication conditions, can be from millimeter to submicron size [87]. The technique dates back to the 1915 through the work of Zeleny, Vonneguton and Neubauer on aerosols [88, 89]. However, it was until very recently that Chang et al [87, 90] and Zhang et al [91] employed EHDA to effectively fabricate hollow capsules with tunable sizes and shell thickness. Chang et al employed perfluorohexane (PFH) as a liquid template and the biocompatible polymer polymethylsilsesquixane (PMSQ) as the shell material. The solutions were supplied via micro syringe. PFH was supplied via a needle of 150μm and PMSQ was supplied through a 300μm diameter needle. The needles were concentric so that at the end of the needles PFH was covered by the solution of PMSQA which yields to the core-shell structure. In this experiment PFH was supplied at a rate of 150μl/min and PMSQ was supplied at 650μL/min. Zhang et al produced hollow capsules using Polethersulfone (PES) dissolved in dimethyl sulfoxide DMSO as the shell material. For the core, they employed PVA and PEG in DMSO. The general schematic of EHDA is shown in the *panel 'a'* of Figure 1.5.

The process takes advantage of the differences in solubility and volatility of the liquids being employed. In general, the outer flow acceleration is dominated by the electrical field, whereas, the inner flow is driven by viscous stresses, thus flow rates must be adjusted to account for these differences so that both liquids can travel at the same velocity. The formation mechanism of hollow capsules from EHDA is different [92 87] since in order to remove the core either the core is miscible in water (the capsules are deposited in a water bath after fabrication) so that the hydrophilic core can be removed or the core has a low boiling point. In general the shell has nanopores that allow the transport of the gas or liquid from the interior to the exterior. It has been reported that not only hollow microcapsules can be formed but also highly porous materials can be obtained.

The fabricated hollow capsules are not limited to the pharmaceutical field. Hollow capsules made using EHDA can also be employed in engineering applications. The main issue to address when considering engineering applications is the yield of particles obtained. Multiple needles can be employed in EHDA as an efficient way to increase production or to develop capsules with different properties (double layer of different materials) [93, 94]

One of the advantages of EHDA is that it generates near monodisperse capsules. As it was stated in the introduction, the strictest requirements for encapsulation are given by the pharmaceutical applications and thus, due to the very gentle core evaporation method involved in EHDA, EHDA has great advantages over some more classical methods (e.g. WOW/OWO processes). [95, 86, 1]

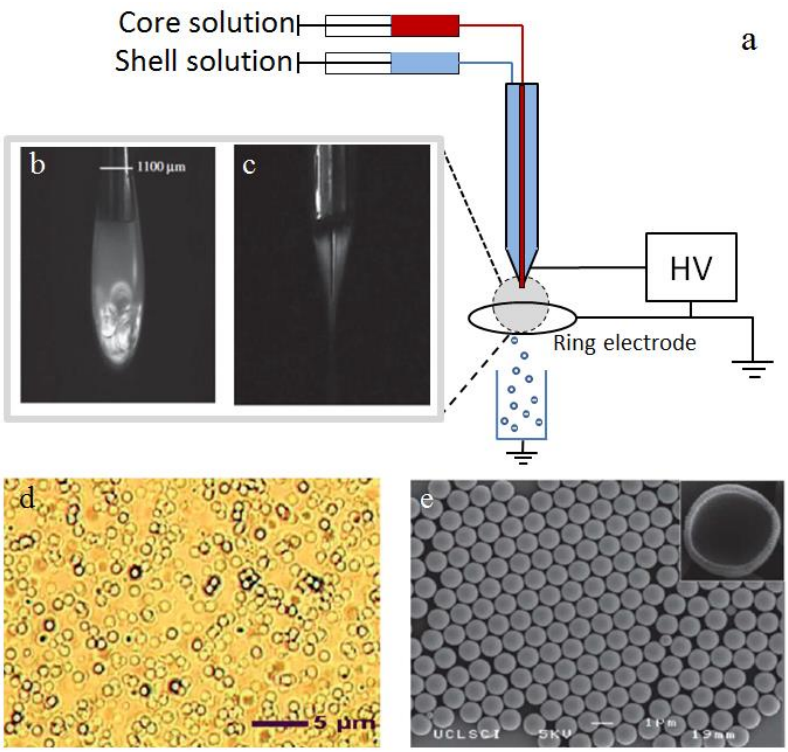

Figure 1.5: EHDA microcapsules. (a) The experimental set-up; (b) dripping and (c) stable jetting behavior of PMSQ/PFH, (c) Bright field image of hollow capsules immediately after preparation and (d) SEM image of hollow capsules with an inset image of the cross section showing the hollow cavity. [90, 87]

3.3 LBL: bubble and biological templates

Hollow polyelectrolyte microcapsules are normally fabricated by decomposing a core material after the formation of a capsule shell by the Layer by Layer (LbL) method. Microcapsules fabricated under this method are made by the "Layer by Layer" adsorption [96, 97, 98, 99] of charged polyelectrolytes onto charged colloidal particles, and then subsequent removal of the cores takes place to leave a hollow microcapsule. The sequential adsorption allows to tune these microcapsules in the nano meter range and it is dependant on ionic strenght [100, 101], temperature, and pH [102]. The main driving force for a multilayer shell formation is precisely electrostatic attraction between opposite charged species, resulting in overcharging of the films after deposition of each layer. Because of this, the system is stable against desorption, but since individual interactions are weak, the final layer structure depends on the fabrication conditions. The template material can vary, yet liquids are avoided in general as there are difficulties with the coating procedures or with the polidispersity of the cores, thus solid cores are suitable for LbL. When liquid cores are employed most of the time vesicles or emulsion droplets are employed [103, 104].Until very recently air and even cells are being used as templates [105]. As for the shell, silica, gold or zinc, can be used. [106, 107, 60, 61]

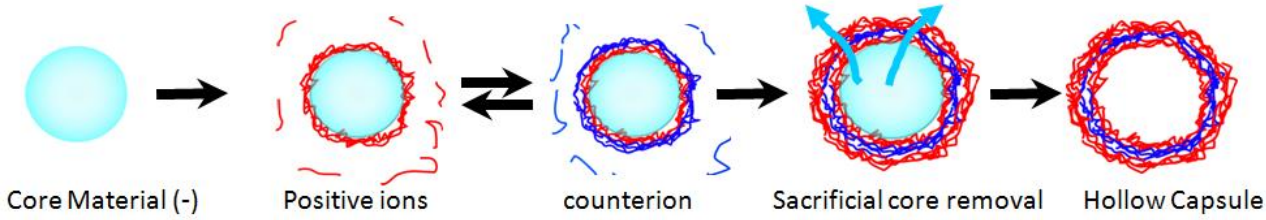

Figure 1.6: Layer-by-Layer method. Sequential adsorption of counter ions allows the formation of a shell.

Almost any coating can be applied to a polyelectrolyte microcapsule which makes it perhaps the most versatile of all the capsule fabrication techniques. A schematic of the sequential adsorption in the LbL process is shown in Figure 1.6. The removal of the core is done by using one of the processes listed previously (e.g. thermolysis, freeze drying).

The fabrication of hollow microcapsules using LbL can be simply attained. However it is of great convenience if there was no need for a core removal process (e.g. use air as template) or if it is possible to fabricate capsules of any shape.

3.3.1 Bubble template

Recently, Shchukin *et al.* [102] developed a technique to synthesize hollow microcapsules using microbubbles as templates. In these experiments microbubbles were generated via sonication in a tween/spam solution. Since the surface of the bubble was charged due to the adsorption of tween/spam, it allowed for sequential adsorption of PAH and PSS. A schematic of this fabrication technique is shown in Figure 1.7.

Furthermore, through the work of Daiguji et al. [58] it was demonstrated that hollow PAH microcapsules can be easily manufactured from microbubble templates without the need of surfactants. In a Na_2CO_3 solution, poly-allylamine hydrochloride (PAH) is broken down into colloidal particles of carbamate ions ($R\text{-}NHCOO^-$) and amino ions($R\text{-}NH3^+$) within a certain pH range. When CO_2 microbubbles nucleate in this solution, the colloidal particles of PAH stabilize the micro bubbles via adsorption. However, these capsules were only stable at pH= 8.5. Molino et al. [57] used the same methods aforementioned and attained size control of the capsule by changing the concentration of the Na_2CO_3 and, more important, they elucidated the conditions required to synthesize a hollow bilayer (and multilayer if required) microcapsule, as well as, the effective parameters to attain a condensed hollow PAH/PSS microcapsule solution at pH = 7.0. The final capsule is intended to be used for pharmaceutical purposes.

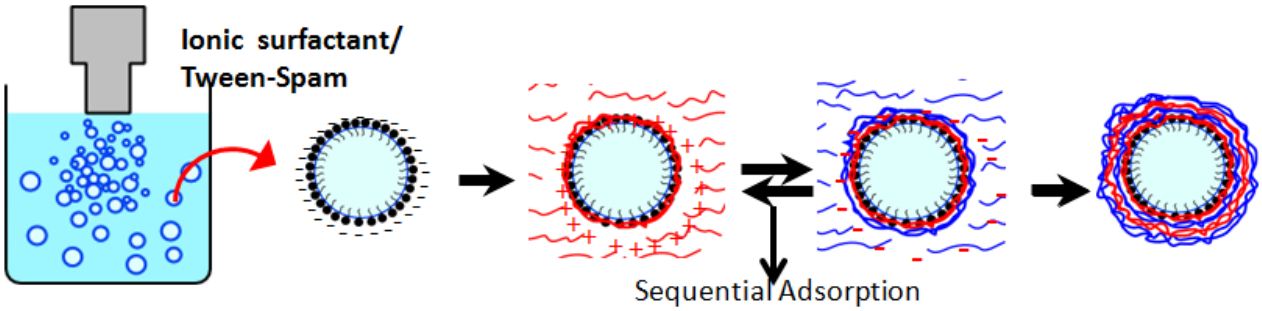

Figure 1.7: LbL using a microbubble as template via sonication. Synthesis of hollow microcapsules using micro bubbles as templates Micro bubbles are generated in a tween-spam solution that stabilize the micro bubbles and allows to sequentially adsorb counter ions to the bubble surface. The result is a hollow biodegradable microcapsule. [102]

3.3.2 Biotemplate

The advantages of employing biological structures as templates for fabricating microcapsules is that a wide variety of shapes and sizes can be attained without the need of designing or manufacturing solid sacrificial cores. Unless a solid core is employed, it is very difficult to attain a shape different from spheroids, as it is a spherical shape the lower state of energy for a drop or a bubble intended to be employed as a template core. Indeed the encapsulation of biomolecules and living organisms has several applications in the medical field, thus the understanding of such encapsulating procedures is of great relevance.

Neu et al [105] successfully used a red blood cell (RBC) as a template followed by the RBC removal to achieve a hollow capsule. Escherichia coli bacteria was employed as well. In their study, they employed PAH/PSS sequential adsorption to cover the surface of the cell. They deposited 10 layers onto the cell and bacteria respectively. By employing a solution of 140mM NaCl and 1.2% NaOCl, the cellular protein and lipid dissolved. In this work they commented that one of the disadvantages of using biological templates is their limited membrane stability.

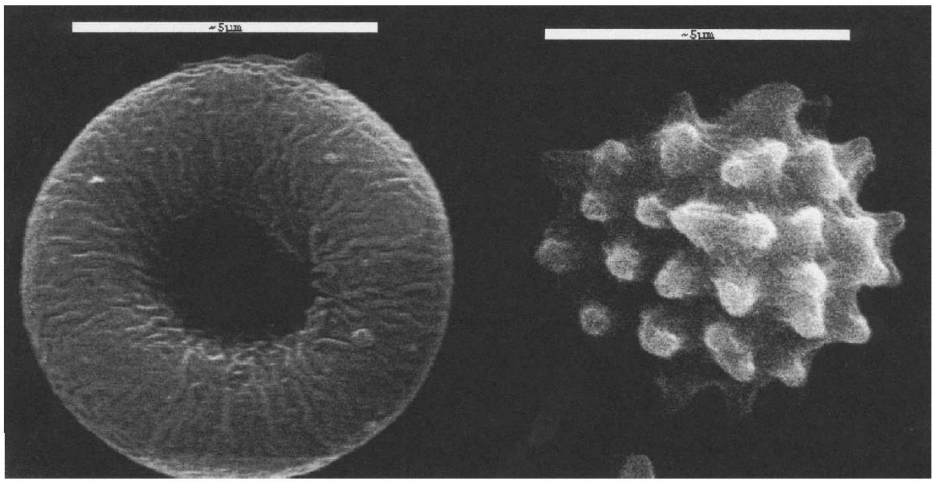

Figure 1.8: SEM image of hollow PAH/PSS microcapsule. From an. RBC template and b. e.Coli template [105].

Furthermore, if cell surface modification is desired, cell preservation is a must. However it has been proven that the cytotoxic effect depends on polycation concentration and exposure time, as the polycations (PAH in this case) could induce pores within the cell membrane as suggested by Vladimir and Srikanth [108]. Figure 1.8 shows the final discoid and echinocityc shape of RBC and E. Coli hollow polyelectrolyte capsules.

3.4 Tubular Microfluidics

Since the advent of microfluidic fabrication [109] several researchers have refined and attained several kind of particles for different purposes. Microfluidics offer the advantage of fabricating large microcapsules and the advantage of attaining monodisperse microcapsules (particles can be fabricated as well). The latter is a key feature for this fabrication technique. Although several other methods such as interfacial polymerization, coacervation or even spray drying can produce close to monodisperse microcapsules, the properties of the capsules produced are determined empirically as each fabrication parameter cannot be precisely controlled. If the size is not uniform, the mechanical and delivery properties are non-uniform as well. Since with microfluidic devices microcapsules are tailored individually, outstanding control can be achieved [110, 111, 112]. A microfluidic device is mainly characterized by laminar flow which leads to very typical easy to analyze microfluidic behavior and hence the resulting product is uniform. Furthermore, a microfluidic device is simple to fabricate. A basic schematic of a microfluidic device is shown in Figure 1.9.

In this image fluid A is the template solution. Fluid A could be an oil phase, fluid B could be water phase and Fluid C could be an oil phase which yields to a O/W/O (oil in water in oil) emulsion [113]. The inverse is also valid as it can be a W/O/W process. The important aspect of this fabrication is that the intermediate phase (e.g. Fluid B in the image) is poorly or completely inmiscible in either Fluid A or Fluid C. After the fabrication of the particles, the cores (if required) are removed.

Choi et al. [114] developed a one step synthetic approach to prepare hollow thermosensitive poly (N-isopropylacrylamide) (PNIPAM) microcapsules. This was the first time where hollow thermosensitive capsules have been produced. They reported using conventional photolithography and a mixture of PDMS and a curing agent to build the microfluidic device (normal method).

To attain hollow capsules, droplets of an aqueous solution containing a monomer are prepared and introduced into a continuous phase, which has an oil soluble photoninitiator. By irradiating the droplets with UV, radical polymerization at the aqueous solution/oil interface starts. The key aspect of the process is that upon UV irradiation, the capsules become hollow, contrary to other studies [115] where after fabrication sequential etching of the cores with strong solvents must be performed to remove them. The capsules were confirmed to be hollow via Ion Beam Milling.

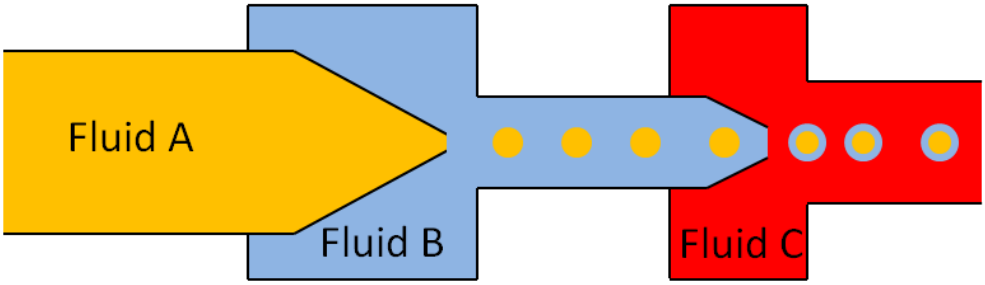

Figure 1.9: **General schematic of a microfluidic/ capillary device**.

In a different study, Zhang et al [116] designed long term glucose-responsive hydrogels (poly(N-isopropylacrylamide-co-3-aminophenylboronic acid-co-acrylic acid) (PNA) to fabricate hollow capsules using microfluidic devices. In general, hydrogels can respond to different environments inside the body through changes in temperature, pH and salinity. The way of fabricating these capsules is the same as the schematic shown in Figure 1.9. They also employed UV initiated polymerization to fabricate the hollow capsule. In their study they analyzed the effect of glucose concentration on the swelling behavior of the capsules. The PNA microcapsule exhibited a glucose swelling behavior, which was proportional to the amount of glucose in the Glucose Buffer solution (BFS).

The use of hydrogels is not limited to the shell; microgels are also used as sacrificial cores to fabricate hollow microcapsules. Gokmenn et al. showed this using microfluidics to create hydrogel cores, and combined with LbL it is possible to obtain a hollow capsules of several micrometers. In this study, the monodisperse microgels were coated by 6 alternating layers of Ptnp (platinum nanoparticle) and DAR (Diazoresin) [117]. Since Dex-Hema was employed to fabricate the sacrificial core, Sodium Hydroxide was employed to remove the cores as dex-Hema is degradable in NaOH. The resultant microcapsules had a size microcapsule in the order of hundreds of microns.

The aforementioned studies require the use of a sacrificial template, however in the work of Wan et al. [118] individual gas bubbles are wrapped with a polymer coating using a microfluidic device. The method consists on the fabrication of micro droplets with individual gas cores in a continuous oil phase. The oil phase contains precursors that allow for sol-gel reaction between the aqueous phase surrounding the gas bubbles and the continuous phase. The result is a hollow capsule (gas core) with a hard shell. One of the key parameters for keeping the bubbles stable inside the droplets is the viscosity of the aqueous phase. In this study, increasing the viscosity was achieved by adding glycerol. Since the precursors were silane and titanium butoxide, the final shells were made of either silica or titania. Figure 1.10 shows their microfluidic device and the resultant silica hollow capsules.

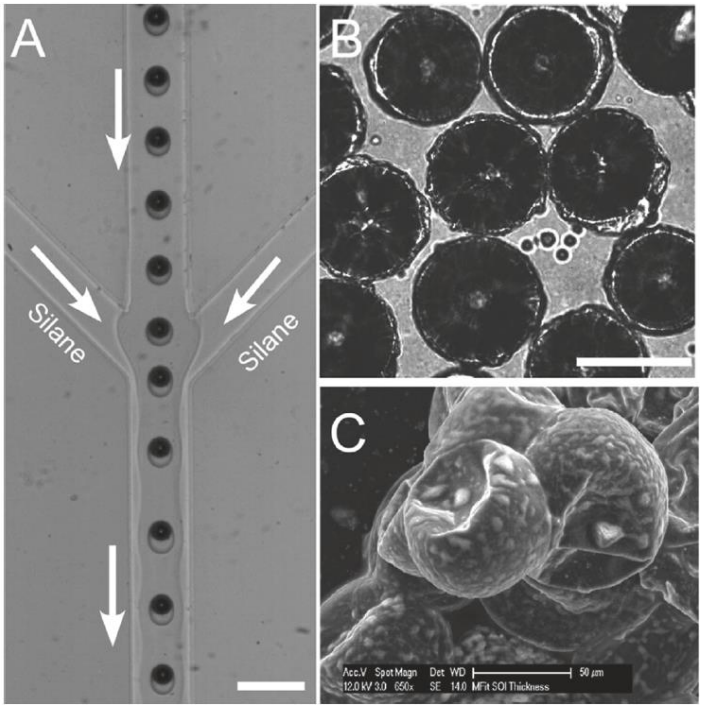

Figure 1.10: **Capsules from microfluidic devices.** The final capsule size was about 60μm, however other particles in the nano order were obtained as well. [118]

4. The objectives and contents of this thesis

In the research disclosed in this thesis, easy ways to make microcapsules from PLA or polyelectrolyte materials using bubbles as templates [119-121] are shown. When the reported techniques are compared to other techniques, the simplicity of this technique can be highlighted (e.g. no sacrificial cores are needed and bubbles can be enhanced with a hard shell). Furthermore, the theory developed by Ward et al.[122] was employed as the theoretical foundation to theoretically predict the conditions at which a bubble is stable inside a closed volume. This analysis considers the number of nucleated microbubbles and the initial amount of air dissolved in the solution. From these theoretical considerations, it was possible to produce microcapsules of different sizes. Mass production was attained as well.

Other studies use well refined methods to produce near monodisperse hollow microcapsules. Many of these techniques were covered in the first pages of this chapter. However, in general, the current fabrication methods consist of multistep fabrication procedures that include evaporation, polymerization and distillation. Some other techniques employ high porous particles that host gas mixtures (perfluorocarbon and Nitrogen) in order to achieve osmotic stabilization inside the blood stream. Via these mechanisms, and depending on the acoustic properties of the host particle/shells, ultrasound imaging can be achieved. In contrast to these techniques, this thesis presents a simple way

for fabricating biodegradable single-core hollow microcapsules that can be employed not only as perfusion contrast agents but also as DDS. Furthermore, since the mechanics of the process enable uniform bubble formation, stabilization and posterior encapsulation (self-assemble mechanism), other methods for controlled bubble formation were not employed in this work. Other methods can effectively achieve uniform sized bubbles and cover them with polymeric materials, however scale effects must be taken into account if further reduction in capsule size is to be achieved and, due to the diversity of substances used in the fabrication process these techniques must account for different effects; whereas the method shown in this study allows the utilization of other materials.

As aforementioned, this thesis discusses the stabilization of microbubbles inside open and close systems. One of the main priorities of this work is to achieve high uniformity in the resultant capsules. The capsules introduced in this thesis display high uniformity. Furthermore, whenever mass production is discussed, the conditions required to fabricate microcapsules with high uniformity is disclosed as well (attaining mass production, in general, compromises uniformity). PLA was used to fabricate the shell which surrounds the bubbles. Also employed polyelectrolyte material (PAH/PSS) was employed to enclose bubble templates and attain polyelectrolyte microcapsules.

Based on the materials used, this thesis features the works to develop two different kinds of microcapsules (PLA and Polyelectrolyte). This thesis discusses:

a. The development of new and facile ways to synthetize single void microcapsules using micro bubbles as templates. It was intended to employ them as ultrasound contrast agents, thus to fabricate mono disperse capsules is the target; nonetheless more engineering applications were also considered (Chapter 2, 6, and Appendix 1).
b. The characterization of both, the bubble template and the resulting hollow microcapsule from the physical point of view and the optimum fabrication conditions to attain highly uniform microcapsules were determined. (Chapter 2-6).
c. The stability of microbubbles inside closed system and its corresponding size control was experimentally confirmed. A mechanism for the formation of the hollow microcapsules was proposed as well.
d. Capsules size control (Chapter 3, and 6).
e. Capsules mass production (Chapter 4, 5 and Appendix 1)

An appendix is provided after the conclusions. Although chapters 1 through 6 are self-sustained, the appendix has information relevant to this investigation and will nurture even further the understanding of the chapters.

Throughout this document, to assess the size distribution and monodispersity of the synthesized capsules, an index termed Coefficient of Variation (CV) was employed, which is also known as

Polidispersity index (PI). This coefficient is defined as the ratio of the standard deviation size distribution to its arithmetic mean, this is,

$$CV = PI = 100\% \times \left(\sum_{i=1}^{N} \frac{(r_i - \overline{r_n})^2}{N-1}\right)^{1/2} / \overline{r_n} \quad (1.4)$$

Where r_i is the radius of the i^{th} capsule given in micrometers (μm) and $\overline{r_n}$ is the arithmetic mean in micrometers as well. Samples with a PI < 20% are considered to be uniform.

5. References

1. Benita, S. *Microencapsulation: Methods and Industrial Applications,* 2nd ed.; CRC Press: Boca Raton, FL, 2006.
2. Ghosh, S. L. *Functional Coatings by Polymer Encapsulation,* 1st ed.; WILEY-VCH Verlag GmbH & Co. KGaA, 2006.
3. Narayan, P.; Wheatley, M. Preparation and characterization of hollow microcapsules for use as ultrasound contrast agents. *Polymer Engineering and Science* **1999,** *39* (11), 2242-2255.
4. Lin, P.-L.; Eckersley, R. J.; Hall, E. A. H. Ultrabubble: A Laminated Ultrasound Contrast Agent with Narrow Size Range. *Advanced Materials* **2009,** *21,* 3949-3952.
5. Caussette, M.; Gaunand, A.; Planche, H.; Colombié, S.; Monsan, P.; Lindet, B. Lysozyme inactivation by inert gas bubbling: Kinetics in a bubble column reactor. *Enzyme and Microbial Technology* **1999,** *24,* 412-418.
6. Colombié, S.; Gaunand, A.; Lindet, B. Lysozyme inactivation and aggregation in stirred-reactor. *Journal of Molecular Catalysis B: Enzymatic* **2001,** *11,* 559-565.
7. Bommarius, A. S.; Karau, A. Deactivation of Formate Dehydrogenase (FDH) in Solution and at Gas-Liquid Interfaces. *Biotechnology Progress* **2005,** *21,* 1663-1672.
8. Barrat, G. Colloidal drug carriers: achievements and perspectives. *Cellular and Molecular Life Sciences* **2002,** *60,* 21-37.
9. Allen, T. M.; Cullis, P. R. Drug delivery systems: Entering the Mainstream. *Science* **2004,** *303,* 1818-1822.
10. Wise, D.; L, B.-P.; Klibanow AM, M. A.; Peppas, N.; Trantolo, D.; Wnek GE, Y. M. *Handbook of pharmaceutical Controlled Release Technology;* Marcel Dekker, 2000.
11. Yang, H.; Qiao, X.; Hong, W.; Dong, L. Core-Shell Microcapsules with Embedded Microactuators for Regulated Release. *Microelectromechanical Systems* **2013,** *22* (509-518).
12. Siepman, J.; A, G. Mathematical modeling of bioerodible, polymeric drug delivery systems. *Advanced Drug Delivery Review* **2001,** *48,* 229-247.
13. Sang, X. M.; Yang, X. J.; Cui, Z. D.; Zhu, S. L.; Sheng, J. J. Nano-SiO2 Doped Polystyrene Materials for Inertial Confinement Fusion Targets. *Macromolecular Science B* **2005,** *44,* 237-248.
14. Ikeuchi, M.; Tane, R.; Ikuta, K. Electrospray Deposition and Direct Patterning of Polylactic Acid Nanofibrous Microcapsules for Tissue Engineering. *Biomedical Microdevices* **2012,** *14,* 35-43.
15. Murphy, E. B.; Wudl, F. The World of Smart Healable Materials. *Progress in Polymer Science* **2010,** *35,* 223-251.
16. Sukhorukov, G. B.; Fery, A.; Mohwald, H. Intelligent micro-and nanocapsules. *Progress in Polymer Science* **2005,** *30,* 885-897.
17. Shchukin, D. G.; Sukhorukov, G. B. Nanoparticle Synthesis in Engnieered Organic Nanoscale Reactors. *Advanced Materials* **2004,** *16,* 671.
18. Ouyang, W.; Chen, H.; Jones, M. L.; Metz, T.; Haque, T.; Martoni, C.; Prakash, S. Artificial Cell Microcapsule for Oral Delivery of Live Bacterial Cells for Therapy: Design, Preparation, and In-Vitro Characterization. *Journal of Pharmaceutical Science* **2004,** *7,* 315-324.
19. Cao, L. *Carrier-bound Immobilized enzymes: Principles applications nd design,* 2nd ed.; wiley-VCH Verlag

GmBH, 2005.

20. Colvin, V. L. The Potential Environmental Impact of Engineered Nanomaterials. *Nature Biotechnology* **2003,** *21,* 1166-1170.
21. Selvam, S.; Thomas, S. P.; Hamm-Alvarez, S. F.; Schechter, J. E.; Stevenson, D.; Mircheff, A. K. Current Status of Gene Delivery and Gene Therapy in lacrimal gland using viral vectors. *Advanced Drug Delivery Reviews* **2006,** *58,* 1243-1257.
22. Baker, M. Homing in on Delivery. *Nature* **2010,** *464,* 1225-1228.
23. Luo Yan, C. S. Preparation and properties of disperse dye microcapsules. *Coloration Technology* **2002,** *119,* 37-40.
24. Sohn, K.; Na, Y.; Chang, H.; Roh, K.-M.; Jang, H.; Huang, J. Oil absorbing graphene capsules by capillary molding. *Chemical Communications* **2012,** *48,* 5968-5970.
25. Lee, K.; Jung, Y.; Oh, S. Synthesis of Tin-Encapsulated Spherical Hollow Carbon for Anode Material in Lithium Secondary Batteries. *Journal of American Chemical Society* **2003,** *125,* 5652-5653.
26. Tamae, H.; Sumi, T.; Yasuda, H. Preparation and Characteristics of Fine Hollow Carbon Particles. *Journal of Colloid and Interface Science* **1996,** *177,* 325-328.
27. Ikeda, S.; Ishino, S.; Harada, T.; Okamoto, N.; Sakata, T.; Mori, H.; Kuwabata, S.; Torimoto, T.; Matsumura, M. Ligand-Free Platinum Nanoparticles Encapsulated in a Hollow Porous Carbon Shell as a Highly Active Heterogeneous Hydrogenation Catalyst. *Angewandte Chemie* **2006,** *45,* 7063-7066.
28. Cheng, S. Y.; Yuen, M. C. W.; Kan, C. W.; Cheuk, K. K. L.; Chui, C. H.; Lam, K. H. Cosmetic textiles with biological benefits: Gelatin microcapsules containing Vitamin C. *International Journal of Molecular Medicine* **2009,** *24,* 411-419.
29. Zhu, Y.; Shi, J.; Chen, H.; Shen, W.; Dong, X. A Facile Method to Synthesize Novel Hollow Mesoporous Silica Spheres and Advanced Storage Property. *Microporous Mesoporous Materials* **2005,** *84,* 218-222.
30. Joannopoulos, J.; Johnson, S.; Winn, J.; Meade, R. *Photonic Crystals,* 2nd ed.; Princeton University Press, 2007.
31. Joannopoulos, J.; Villeneuve, P.; Fan, S. Photonic Crystals: putting a new twist on light. *Nature* **1997,** *386,* 143-149.
32. Lachman, L.; Lieberman, H. A.; Kanig, J. L. *The Theory and Practice of Industrial Pharmacy,* 3rd ed.; Lea and Febiger, 2010.
33. Dubey, R.; Shami, T.; Ku, R. B. Microencapsulation Tehcnology and Applications. *Defence Science Journal* **2009,** *59,* 82-95.
34. Lakshmi, S.; Figoli, A.; Buonomenna, M.; Colemme, G.; Drioli, E. Preparation and Characterization of Porous and Nonporous Polymeric Microspheres by the Phase Inversion Process. *Advances in Polymer Technology* **2012,** *00,* 1-11.
35. Choi, W. S.; Park, J.-H.; Koo, H. Y.; Kim, J.-Y.; Cho, B. K.; Kim, D.-Y. "Grafting-From" Polymerization inside a Polyelectrolyte Hollow-Capsule Microreactor. *Angewandte Chemie International Edition* **2005,** *44,* 1096-1101.
36. Wang, B.; Zhao, Q.; Wang, F.; Gao, C. Biologically Driven Assembly of Polyelectrolyte Microcapsule Patterns To Fabricate Microreactor Arrays†. *Angewandte Chemie International Edition* **2006,** *45,* 1560-1563.
37. N.V.N. Jyothi, M. P.; Prabha, S.; Ramaiah, P. S.; Srawan, G.; Sakarkar, S. N. Microencapsulation Techniques, Factors Influencing Encapsulation Efficiency: A Review. *The Internet Journal of Nanotechnology* **2009,** *3*.
38. Daham, A.; Hoffman, A. Rationalizing the selection of oral lipid based drug delivery systems by an invitro dynamic lipolysis model for improved oral bioavailabilitry of poorly water soluble drugs. *Journal of Controlled Release* **2008,** *129,* 1-10.
39. Waterbeend, H. v. d.; Dennis Smith, K. B.; Walker, D. Property-Based Design: Optimization of Drug Absorption and Pharmacokinetics. *Journal of Medicial Chemistry* **2001,** 1313-1332.
40. Kumar, S.; Nakka, S.; Rajabalaya, R.; Kumar, H.; Halder, T.; Palanisamy, M.; Khanam, J.; Nanda, A. Microencapsulation Techniques and its Practices. *International Journal of Pharmaceutical Science Technology* **2011,** *6,* 1-23.
41. Narayan, P.; Wheatley, M. Preparation and characterization of hollow micrpcapsles for use as ultrasound contrast agents. *Polymer Engineering and Science* **1999,** *39,* 2242-2255.
42. Lathia, J. D.; Leodore, L.; Wheatley, M. A. Polymeric contrast agent with targeting potential. *Ultrasonics* **2004,** *42,* 763-768.
43. Rave, P.; Johnson, G. *Biology,* 6th ed.; McGraw Hill, 2001.
44. Daiguji, H.; Takada, S.; Molino, J. J.; Takemura, F. Fabrication of Hollow Poly(lactic acid) Microcapsules from Microbubble Templates. *Journal of Physical Chemistry B* **2009,** *113,* 15002-150009.
45. Lakshmi, S.; Fioli, A.; Buonomenna, M. G.; Golemme, G.; Drioli, E. Preparation and Characterization of Porous

and Nonporous Polymeric Microspheres by the Phase Invertion Process. *Advances in Polumer Technology* **2012,** *00,* 1-11.

46. Schutt, E.; Klein, D.; Mattrey, R.; Riess, J. Injectable Microbubbles as Contrast Agents for Diagnostic Ultrasound Imaging: The Key Role of Perfluorochemicals. *Angewandte Chemistry International* **2003,** 3218-3235.
47. Kawahashi, N.; Matijevic, E. Preparation of Hollow Spherical PArticles of Yttrium Compounds. *Journal of Collooid and INterface Science* **1991,** *143* (103-110).
48. Preparation of hollow polylactide microcapsules through premix membrane emulsification-Effects of nonsolvent Properties. *Journal of Membrane Science* **2008,** *325,* 665-671.
49. Bejerknes, K.; Sontum, P. C.; Smistad, G.; Agerkvist, I. Preparation of polymeric Microbubbles: formulation studies and product characterization. *International Journal of Pharmaceutics* **1997,** *158,* 129-136.
50. Crotts, G.; Park, T. Preparation of porous and nonporous biodegradable polymeric hollow microspheres. *Journal of Controlled Release* **1995,** *35,* 91-105.
51. Bertling, J.; Blömer, J.; Kümmel, R. Hollow Microspheres. *Chemical Engineering Technology* **2004,** *27,* 829-837.
52. Fang, Y.-Y.; Lee, W.-R.; Shen, S.-C.; Huang., Y.-L. Effect of liposome encapsulation of tea catechins on their accumulatoin in basal cell carcinomas. *Journal Dermatological Science* **2006,** *42,* 101-109.
53. Chaize, B.; Fournier, D. Sorting out molecules reacting with acetylcholinesterase by enzyme encapsulation in liposome. *Biosensors and Bioelectronics* **2004,** *20,* 628-632.
54. Meng, F.; Zhong, Z.; Feijen, J. Stimuli-Responsive Polymersomes for Programmed Drug Delivery. *Biomacromolecules* **2009,** *10,* 197-209.
55. Kim, J.-W.; Fernandez-Nieves, A.; Nily Dan, A. U.; MArquez, M.; Weitz, D. Colloidal assembly route for responsive colloidosomes with tunable permeability. *Nano Letters* **2007,** *7,* 2876-2880.
56. Lawrence, D.; Cai, T.; Hu, Z.; Marquez, M.; Dinsmore, A. Temperature-Responsive Semipermeable Capsules Composed of Colloidal Microgel Spheres. *Langmuir* **2007,** *23,* 395-398.
57. Molino, J.; Matsuoka, E.; Daiguji, H. Size control of hollow poly-allylamine hydrochloride/poly-sodium styrene sulfonate microcapsules using the bubble template method. *Soft Matter* **2011,** *7,* 1897-1902.
58. Daiguji, H.; Matsuoka, E.; Muto, S. Fabrication of hollow poly-allylamine hydrochloride/poly-sodium styrene sulfonate microcapsules from microbubble templates. *Soft Matter* **2010,** *6,* 1892-1897.
59. Geest, B.; Déjugnat, C.; Sukhorukov, G.; Braeckmans, K.; DeSmedt, S.; Demeester, J. Self Rupturing Microcapsules. *Advanced Materials* **2005,** *17,* 2357-2361.
60. Wu, C.; Yu, C.; Chu, M. A gold nanoshell with a silica inner shell synthesized using liposome templates for dexorubicin loading and near-infrared photothermal therapy. *International journal of Nanomedicine* **2011,** *6,* 807-813.
61. Zhang, H.; Li, D.; Shao, G.; Yuan, Z. A simple method to prepare titania nanomaterials of core-shell structure, hollow nanospheres and mesoporous nanoparticles. *Science in China Series B: Chemistry/Springer* **2009,** *52,* 1498-1503.
62. Caruso, F. Hollow Capsule Processing through Colloidal Templating and Self-Assembling. *Chemistry: An European Journal* **2000,** *6,* 413-418.
63. Liu, J.; Wilcox, D. Factors influencing the formation of hollow ceramic microspheres by water extraction of colloidal droplets. *Journal of Material Research* **1995,** *10,* 84-94.
64. Daiguji, H.; Makuta, T.; Kinoshita, H.; Oyabu, T.; Takemura, F. Fabrication of Hollow melamine-formaldehyde microcapsules from microbubble templates. *Journal of Physical Chemistry B* **2007,** *111,* 8879-8884.
65. Bagaria, H.; Kadali, S.; Wong, M. Shell thickness control of nanoparticle-polymer assembled microcapsules. *Chemistry of Materials* **2011,** *23,* 301-308.
66. Pardeike, J.; Hommoss, A.; Muller, R. Lipid nanoparticles (SLN,NLC) in cosmetic and pharmaceutical dermal products. *INternational Journal of Pharmaceutics* **2009,** *366,* 170-184.
67. Zhao, Q.; Mao, Z.; Gao, C.; Shen, J. Assembly of multilayer microcapsules on CaCO3 particles from biocompatible polysaccharides. *Journal of Biomaterials Science, Polymer Edition* **2006,** *17,* 997-1014.
68. Schutt, E. G.; Klein, D. H.; Mattrey, R. M.; Riess, J. G. Injectable Microbubbles as Contrast Agents for Diagnostic Ultrasound Imaging: The Key Role of Perfluorochemicals. *Angewandte Chemie International Edition* **2003,** *42,* 3218-3235.
69. Sboros, V. Response of Contrast Agents to Ulrrasound. *Advanced Drug Delivery* **2008,** *60,* 1117-1136.
70. de Jong, N.; Ten Cate, F. J.; Lancee, C.; Roelandt, J. R. T. C.; Bom, N. Principles and recent developments in ultrasound contrast agents. *Ultrasonics* **1991,** *4,* 324-330.

71. Plesset, M. S.; Sadhal, S. S. On the stability of gas bubbles in liquid gas solutions. *Applied Science Research* **1982,** *38,* 133-141.

72. Borden, M.; Longo, M. Dissolution Behavious of Lipid Monolayer-Coated, Air filled Microbubbles: Effect of Lipid Hydrophobic Chain Lenght. *Langmuir* **2002,** *18,* 9225-9233.

73. Schutt, E. G.; Klein, D. H.; Mattrey, R. M.; Riess, J. G. Inyectable Microbubbles as Contrast Agents for Diagnostic Ultrasound Imaging: The Key Role of Perfluorochemicals. *Angewandte Chemie International Edition* **2003,** *42,* 3218-3235.

74. Shalaby, S. *Biomedical Polymers,* 1st ed.; Hanser Publishers, 1994.

75. Saihi, D.; Vroman, I.; Giraud, S.; Bourbigot, S. Microencapsulation of ammonium phosphate with a polyurethane shell. PartII. Interfacial polymerization tehcnique. *Reactyive and Functional Polymers* **2006,** *66,* 1118-1125.

76. Feng, Z.; Wang, Z.; Gao, C.; Shen, J. Hollow microcapsules with a complex polyelectrolyte shell structure fabricated by polymerization of 4-vinylpyridine in the presence of poly(sodium 4-styrenesulfonate) and silica particles. *Materials Letters* **2007,** *61,* 2560-2564.

77. Shun Li, S. K.; Feld, K.; Grim, w. Recent Advances in Microencapsulation Technology and equipment. *Drug Development and Industrial Pharmacy* **1988,** *14,* 353-376.

78. Zhao, Q.; Han, B.; Wang, Z.; Gao, C.; Peng, C.; Shen, J. Hollow chitosan-alginate multilayer microcapsules as drug delivery vehicle: doxorubicin loading and in vitro and in vivo studies. *Nanomedicine: Nanotechnology, Biology, and Medicine* **2007,** *3,* 63-74.

79. Decher, G. *Comprehensive Supramolecular chemistry,* 1st ed.; Pergamon Press, Oxford, 1996; Vol. 9.

80. Knoll, W. Self-Assembled microstructures at interfaces. *Current Opinions in Colloid & Interface Science* **1996,** *1,* 137-143.

81. Park, J.; Choi, Y.-W.; Kim, K.; Chung, H.; Sohn, D. Aggregation Processes of a Weak Polyelectrolyte, Poly(allylamine) Hydrochloride. *Bulletin of the Korean Chemical Society* **2008,** *29,* 104-110.

82. Peyratout, C.; Dahne, L. Tailor-Made Polyelectrolyte Microcapsules From Multilayers to Smart Containers. *Angewandte Chemie International Edition* **2004,** *43,* 3762-3783.

83. Sievers, R. E.; Quinn, B. P.; Cape, S. P.; Searles, J. A.; Braun, C. S.; Bhagwat, P.; L.G.Rebits; McAdams, D. H.; Burger, J. L.; Best, J. A.; Lindsay, L.; Hernandez, M. T.; Kisich, K. O.; Iacovangelo, T.; Kristensen, D.; Chen, D. Near-Critical fluid micronization of stabilized vaccines; antibiotics and anti-virals. *Journal of Supercritical Fluids* **2007,** *42,* 385-391.

84. Thiering, R.; Dehghani, F.; Foster, N. Current issues relating to anti-solvent micronisation techniques and their extension to industrial scales. *The Journal of Supercritical Fluids* **2001,** *21,* 159-177.

85. Cape, S.; Villa, J.; Huang, E.; Yang, T.-H.; Carpenter, J.; Sievers, R. Preparation of Active Proteins. vaccines and Pharmaceuticals as fine Powders using Supercritixcal or Near Critical fluids. *Pharmaceutical Research* **2008,** *25,* 1967-1990.

86. Parhi, R.; Suresh, P. Supercritical Fluid Technology: A Review. *Advanced Pharmaceuticval Science and Tehcnology 1,* 13-36.

87. Chang, M.-W.; Stride, E.; Edirisinghe, M. Controlling the thickness of hollow polymeric microspheres prepared by electrohydrodynamic atomization. *Journal of the Royal Society Interface* **2010,** *7,* 451-460.

88. Zeleny, J. On the conditions of instability of electrified drops with applications to the electrical discharge from liquid points. *Procedings of Cambridge Philosofica Society* **1915,** *18,* 71-83.

89. Vonnegut, B.; Neaubauer, R. Production of monodisperse liquid particles by electrical atomization. *Journal of Colloid Science* **1952,** *6,* 616-622.

90. Chang, M.-W.; Edirisinghea, M.; Stride, E. Ultrasound mediated release from stimuli-responsive core-shell capsules. *Journal of Material Chemistry B* **2013,** *1,* 3962-3971.

91. Zhang, Q.; Wang, L.; Wei, Z.; Wang, X.; Long, S.; Yang, J. A new simple method to prepare hollow PES microspheres. *Colloid Polymer Science* **2012,** *290,* 1257-1263.

92. Pisani, E.; Tsapis, N.; Paris, J.; Nicolas, V.; Cattel, L.; Fattal, E. Polymeric Nani/Microcapsules of Liquid Perfluorocarbons for Ultrasonic Imaging: Physical Characterization. *Langmuir* **2006,** *22,* 4397-4402.

93. Hwang, Y.; Jeong, U.; Cho, E. C. Production of uniform-sized polymer core-shell microcapsules by coaxial electrospraying. *Langmuir* **2008,** *18,* 2446-2451.

94. Kim, W.; Kim, S. Multishell Encapsulation Using a Triple Coaxial Electrospray System. *Analytical Chemistry* **2010,** *82,* 4644-4647.

95. Si, T.; Zhang, L.; Li, G.; Roberts2, C. J.; Jia, L.; Yin, X.; Xu, R. Coaxial electrospray for multinodal imaging and image-guided therapy. *Proceedings of SPIE* **2012,** *8216,* 1-10.

96. Bertrand, P.; Jonas, A.; Lashewsky, A.; Legras, R. Ultrathin polymer coatings by complexation of polyelectrolytes at interfaces-suitable materials, structure and properties. *Macromolecular Rapid Communiucations* **2000,** *21,* 319-348.

97. F. Caruso, R. C. a. H. M. Nanoengineering of Inorganic and Hybrid Hollow Spheres by colloidal Templating. *Science* **1998,** *282,* 1111-1114.

98. Caruso, F.; Lichtenfield, H.; Giersig, M.; Mohwald, H. Electrostatic Self-Assembly of Silica Nanoparticle-Polyelectrolyte Multilayers on Polyestyrene Latex Particles. *Journal of the American Chemical Society* **1998,** *120,* 8523-8524.

99. Yin, Y.; Lu, Y.; Gates, B.; Xia, Y. Synthesis and Characterization of Mesoscopic Hollow Spheres of Ceramic Materials with Functionalized Interior Surfaces. *Chemistry of Materials* **2001,** *13,* 1146-1148.

100. Korneev, D.; Lvov, Y.; G.Decher; Schmitt, J.; Yaradaikin, S. Neutron reflectivity of self assembled film superlattices with alternate layers of deuterated and hydrogenated polyesterenesulfonate and polyallylamine. *Physica B* **1995,** *1995,* 954-956.

101. Dubas, S. T.; Schlenoff, J. B. Factors Controlling the Growth of Polyelectrolyte Multilayers. *Macromolecules* **1999,** *32,* 8153-8160.

102. Shchukin, D. G.; Köhler, K.; Möhwald, H.; Sukhorukov, G. B. Gas-Filled Polyelectrolyte Capsules. *Angewandte Chemie International Edition* **2005,** *44,* 3310-3314.

103. Park, J.-H.; Oh, C.; Shin, S.-I.; Moon, S.-K.; Oh, S.-G. Preparation of hollow solica microspheres in W/O emulsions with polymers. *JOurnal of Colloid and Interface Science* **2003,** *266,* 107-114.

104. McKelvey, C. A.; Kaler, E. W.; Zasadzinski, J. A.; Coldren, B.; Jung, H.-T. Templating Hollow Polymeric Spheres from Cationic Equilibrium Vesicles: Synthesis and Characterization. *Langmuir* **2000,** *16,* 8285-8290.

105. Neu, B.; Voigt, A.; Hner, R. M.; eporatti, S.; Gao, C. Y.; Donath, E.; Kiesewetter, H.; Mowahld, H.; Meiselman, H. J.; Umler, H. B. Biological cells as templates for hollow microcapsules. *Journal of Microencapsulation* **2001,** *18,* 385-395.

106. Imhof, A. Preparation and Characterization of Titania-Coated Polysterene Spheres and Hollow Titania Shells. *Langmuir* **2001,** *17,* 3579-2585.

107. Xu, X.; Asher, S. A. Synthesis and Utilization of Monodisperse Hollow Polymeric Partciels in Photonic Crystals. *Journal of the American Chemical Society* **2004,** *126,* 7940-7945.

108. Tsukuk, V.; Singamaneni, S. *Scanning Probe Microscopy of Soft Matter: Fundamentals and Practices,* 1st ed.; Wiley-VCH Verlag GmbH & Co, 2012.

109. Thorsen, T.; Roberts, R.; Arnold, F.; Quake, S. Dynamic Patter Formation in a Vesicle-Generating Microfluidic Devie. *Physical Review Letters* **2001,** *86,* 4163-4166.

110. Shingo Okushima, T. N.; torii, T.; Higushi, T. Controlled Production of Monodisperse Double Emulsions by Two-Step Droplet Breakup in Microfluidic Devices. *Langmuir* **2004,** *20,* 9905-9908.

111. Nie, Z.; Xu, S.; Seo, M.; Lewis, p.; Kumacheva, E. Polymer Particles with Various Shapes and Morphologies Produced in Continuous Microfluidic Reactors. *Journal of American chemical Society* **2005,** *127,* 8058-8063.

112. Seo, M.; Nie, Z.; Xu, s.; Mok, M.; Lewis, P.; Graham, R.; Kumacheva, E. Continous Microfluidic Reactors for polymer Particles. *Langmuir* **2005,** *21,* 11614-11622.

113. Wei, J.; Ju, X.-J.; Xie, R.; Mou, C.-L.; Lin, X.; Chu, L.-Y. Novel cationic pH-responsive poly(N,N-dimethylaminoethyl methacrylate) microcapsules prepared by a microfluidic technique. *Journal of Colloid and Interface Science* **2011,** *357,* 101-108.

114. Choi, C.-H.; Jung, J.-H.; Kim, D.-W.; Chungc, Y.-M.; Lee, C.-S. Novel one-pot route to monodisperse thermosensitive hollow microcapsules in a microfluidic system. *Royal Society of Chemistry* **2008,** *8,* 1544-1551.

115. Kim, J.-W.; Utada, A.; Fernández-Nieves, A.; Hu, Z.; Weitz, D. Fabrication of Monodisperse Gel Shells and Functional Microgels in Microfluidic Devices. *Angewandte Chemie International Edition* **2007,** *1819-1822,* 46.

116. Zhang, M.-J.; Wei Wang; Xie, R.; Ju, X.-J.; Liu, L.; Gu, Y.-Y.; Chu, L.-Y. Microfluidic fabrication of monodisperse microcapsules for glucose-response at physiological temperature. *Soft Matter* **2013,** *9,* 4159-4159.

117. Gokmen, M. T.; Geest, B. G. D.; Hennink, W. E.; Prez, F. E. D. "Giant" Hollow Multilayer Capsules by Microfluidic Templating. *Applied Materials & interfaces* **2009,** *1,* 1196-1202.

118. Wan, J.; Stone, H. Coated Gas Bubbles for the Continuous Synthesis of Hollow Inorganic Particles. *Langmuir* **2012,** *28,* 37-41.

119. Makuta, T.; Takada, S.; Daiguji, H.; Talemura, F. Simple fabrication of hollow poly-lactic acid microspheres using uniform microbubbles as templates. *Materials Letters* **2009,** *63,* 703-705.

120. Molino, J. J.; Daiguji, H.; Takemura, F.Factors Affecting the Size and Uniformity of Hollow Poly(lactic acid) Microcapsules Fabricated from Microbubble Templates. *Journal of Physical Chemistry B* ***2011,***13828-13834.

121. Sakurai, D.; Molino, J.J.; Daiguji, H.; Takemura, F. Hollow Poly(lactic acid) Microcapsules Fabricated in Gas/O/W Method and Bubble Template Method. *Journal of Material Chemistry A* **2013,** 14562-14568.

122. Ward, C.A., Tikiusis, P., Venter, R.D. Stability of bubbles ina closed volume of liquid gas solution. *Journal of Applied Physics* **1982**, *53*, 6076-6084

2

The Stable Microbubble and its microencapsulation

Hollow microcapsules are expected to be integral components of drug delivery systems (DDS) in medical and pharmaceutical applications. Via the bubble template method microcapsules covered with biodegradable polymers should be easy to fabricate. In this study, the two conditions required to fabricate uniform hollow microcapsules using the bubble template method were clarified: the stability of uniformly sized microbubbles in a liquid droplet and the release of hollow microcapsules from the droplet. Furthermore, the experiments evaluated the radius distributions of the microbubble templates and the fabricated hollow poly-lactic acid (PLA) microcapsules.

1. Introduction

Hollow microcapsules of biodegradable polymers with diameter less than 10 μm are expected to be used as ultrasound contrast agents or carriers for drug delivery systems (DDS) in medical or pharmaceutical applications. [1, 2, 3, 4, 5] Hollow microcapsules are generally fabricated as follows: [6] First, solid particles or liquid droplets are dispersed in continuous gas or liquid phase. Then, shell materials are added to the dispersed cores or to the continuous phase. By controlling the temperature, pH, and/or pressure in the continuous phase, shells are formed around each of the dispersed core by supersaturating the concentration of the shell materials. Shells are also formed by adsorption or reaction of the shell materials onto the surface of the cores. Finally, the permeability and strength of the shell are intentionally degraded by aging or cross-linking so that the liquid or solid core can be removed by dissolution, evaporation, or thermolysis, thus yielding hollow capsules. Several other

fabrication methods have been proposed to produce hollow microcapsules for the shell materials of SiO_2, TiO_2, and amino resin. [7, 8, 9]

The direct encapsulation of microbubbles with shell materials is another method of fabricating hollow microcapsules. For medical and pharmaceutical applications, stabilized microbubbles covered with a lipid bilayer are expected to be used as ultrasound contrast agents or as carriers in DDS. [10, 11] Such shells, however, easily disintegrate because the interaction between lipid molecules is weak for bubbles covered with a lipid bilayer or because the shell for bubbles covered with a polymer film is too thin. Hollow microcapsules would be suitable for many applications if researchers could find ways to fabricate thicker shells.

For hollow microcapsules used in medical and pharmaceutical applications, biodegradable polymers that can be disintegrated using microbes or bacteria would make the best shell materials. Examples of such polymers include poly-lactic acid (PLA), poly-glycolic acid, and poly ε-caprolactone. Porous microcapsules of these biodegradable polymers made by using a spray drying method are being developed as an ultrasound perfusion contrast agent [12] and are currently in a clinical trial. [13] The structure of these microcapsules is not a single bubble covered with a biodegradable shell but a porous biodegradable particle that includes multiple internal voids of perfluorocarbon gas. Biodegradable polymers are synthesized from crude materials via a complex multistep fabrication that includes evaporation, distillation, and polymerization. [14] Therefore, it is difficult to encapsulate microbubbles with a biodegradable polymer using a direct poly-condensation reaction because microbubbles cannot stay in the liquid during the poly-condensation reaction time because of dissolution and bursting.

To fabricate hollow microcapsules covered with a relatively thick shell of a biodegradable polymer, Makuta et. al [15] introduced a simple method for fabricating hollow microcapsules covered with PLA by using microbubbles as templates. The method was called the "Bubble Template Method." In Makuta et al., the solution of PLA and the continuous phase were pressurized with Nitrogen at 300kPa. Thus, decreasing the pressure of the system to atmospheric pressure resulted in the super saturation of Nitrogen in the interior of the droplets and microbubbles were formed. For the present study no pressure was applied since the concentration of Nitrogen in the solutions was saturated at 1 atmosphere. Furthermore, in this chapter droplets of uniform size were formed. Below, each step of the modified fabrication process of the bubble Template Method is shown:

1) A 2 g/l methylene chloride solution of PLA and a 2% (w/w) poly-vinyl alcohol (PVA) aqueous solution was prepared. Then, droplets of the solution of PLA in dichloromethane (1mm in radius) were dispersed in the PVA aqueous solution through a micro syringe.

Because of the surface-active properties of PVA, the droplets did not coalesce in the aqueous solution.

2) As the droplet shrank due to the dissolution of dichloromethane into the PVA aqueous solution, which yields to the nucleation of microbubbles in the droplets because of solvent diffusion/extraction (in general terms, solvent evaporation), hollow PLA microcapsules that displayed microbubbles as inner templates were spontaneously released from the droplet's interior into the continuous aqueous phase.

This fabrication method can be categorized into the solvent evaporation methods. The nucleation of bubbles, physisorption of PLA onto microbubbles, the release of hollow PLA microcapsules into the PVA aqueous solution, and solvent evaporation take place as the droplet shrinks.

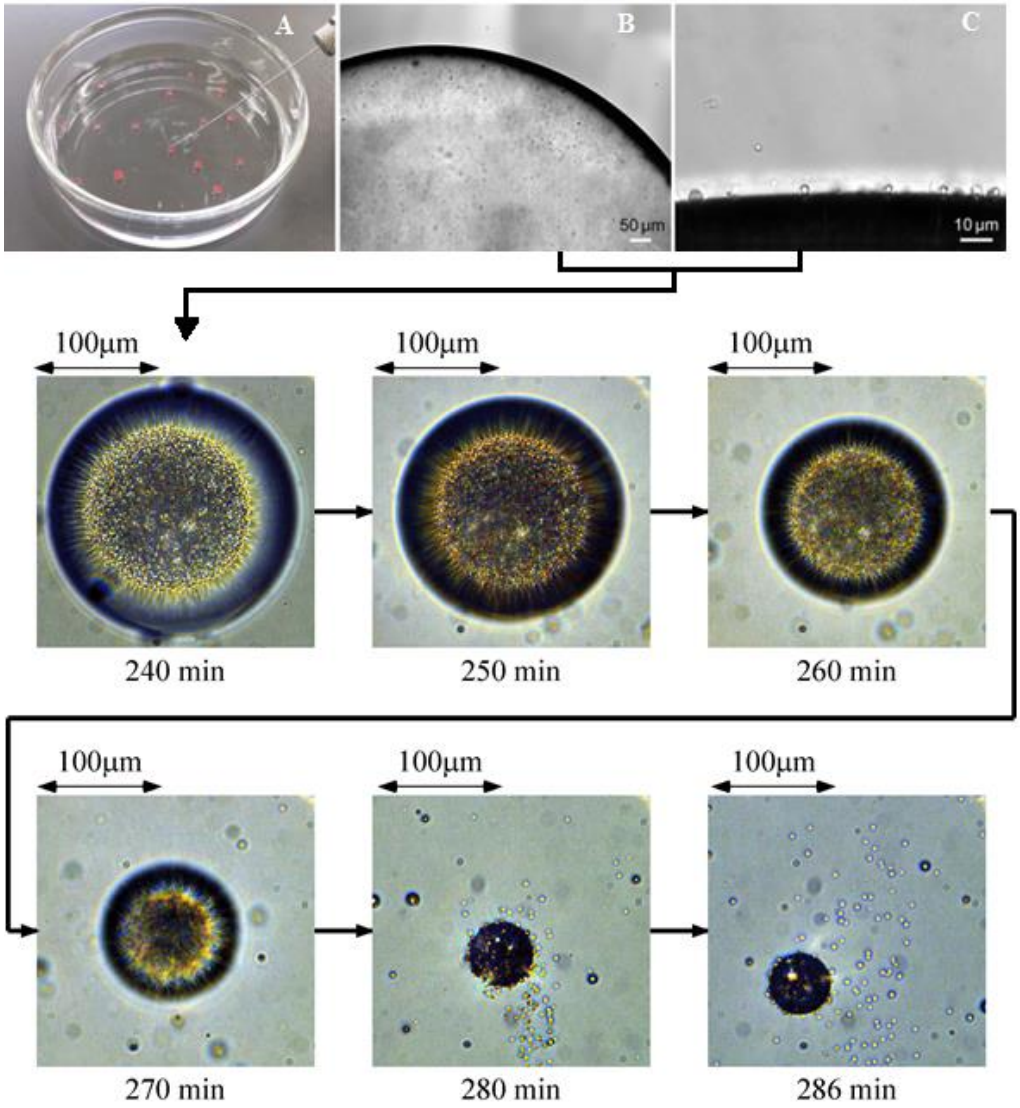

Figure 2.1: Fabrication of hollow PLA microcapsules in the bubble template method [15, 16]: (a) formation of droplets, (b) generation of microbubbles, (c) release of hollow microcapsules.

One of the advantages in the bubble template method is that all these processes take place spontaneously without the application of any external forces. Two important key processes in the bubble template method are the preparation of uniformly sized microbubbles as templates, as shown in Figure 2.1(b), and the encapsulation of microbubbles and the release from the droplet, as shown in Figure 2.1(c).

For the preparation of uniformly sized microbubbles, we focused on the phenomenon through which bubbles in a closed volume of liquid-gas solution have a uniform radius and can be thermodynamically stable.

It is critical to control precisely the bubbles' radius for the development of a uniformly sized hollow microcapsule. In the bulk liquid, some microbubbles coalesce into large bubbles and float into the air, and others disappear due to the dissolution of the gases into the liquid. In contrast, in a closed volume of liquid-gas solution, the bubble radius must be the same in the equilibrium state because the equilibrium radius, r, is determined by $2\gamma / p$, where p is the vapor pressure of the liquid, which is close to the saturation vapor pressure of the pure liquid, and γ is the surface tension. For the encapsulation process, the process proved to be successful for fabricating hollow PLA microcapsules without applying any external forces.

This chapter clarifies the following three conditions: (1) the conditions required for the stability of uniformly sized microbubbles inside a droplet of methylene chloride solution of PLA (2) the dependence of the equilibrium bubble size on the number of bubbles and the solubility of air in the solution and (3) the conditions required for the release of hollow PLA microcapsules from the droplet. The average radius of the microbubble and the final capsule were evaluated as well

2. Theory

2.1 Conditions required for the stability of uniformly sized microbubbles inside a droplet

The first step to fabricate uniformly sized hollow microcapsules is to maintain uniformly sized template bubbles in a liquid long enough to form a capsule shell. Ward *et al* [17] reported that bubbles in a closed volume of liquid-gas solution can be thermodynamically stable. The observed system was not completely closed because methylene chloride transferred to the surrounding PVA aqueous solution. However, the dissolution rate of methylene chloride into the PVA aqueous solution was much slower than the relaxation rate needed to achieve the liquid-vapor equilibrium. Furthermore, air bubbles were generated due to the dissolution of methylene chloride because the solubility of arbitrary gas in aqueous solution [18] was generally much smaller than that in methylene chloride. [19] However, the generation rate of microbubbles was also much slower than the relaxation rate needed to achieve the liquid-vapor equilibrium. Therefore, the observed system could be regarded as a

closed system.

Thermodynamic potentials are single functions of some variables from which all other equilibrium variables can be deduced. They are extensive state variables of dimensions of energy. In the studied system, microbubbles nucleated inside a droplet that is formed inside a continuous aqueous solution. This theoretical section employs the same thermodynamic potential employed by Ward et al[17] to establish a thermodynamic potential function for the virtual displacement in the bubble radius in the equilibrium state. Accordingly, a two component solution was considered: the liquid and its vapor component, and the gas component in its liquid and gas phase. The Gibbs free energy is defined by,

$$dG = \frac{dG}{dp}\Big|_{T,N_k} dp + \frac{dG}{dT}\Big|_{p,N_k} dT + \frac{dG}{dN_k}\Big|_{T,p} dN_k = Vdp - SdT + \sum_k^n \mu_k dN_k \tag{2.1}$$

Where T, p, N_k is the temperature, pressure and moles of the k^{th} component in the system respectively. Since our system is isobaric and isotropic, the above relation is as follows,

$$dG = \frac{dG}{dN_k}\Big|_{T,p} dN_k = \sum_k^n \mu_k dN_k \tag{2.2}$$

Thus, for a two-component system of air and liquid, the Gibbs free energy for the liquid phase is given by,

$$dG' = \mu_1' dN_1' + \mu_2' dN_2' \tag{2.3}$$

The Helmholtz free energy for the gas phase is given as

$$dF = \frac{dF}{dV}\Big|_{T,N_k} dV + \frac{dF}{dN_k}\Big|_{T,V} dN_k + \frac{dF}{dT}\Big|_{N_k,V} dT = -pdV - SdT + \sum_k^n \mu_k dN_k \tag{2.4}$$

$$dF'' = -p''dV'' + \mu_1'' dN_1'' + \mu_2'' dN_2'' \tag{2.5}$$

where the single and double primes refer to the liquid and gas phase respectively and the subscript 1 and 2 denote a volatile solvent (dichloromethane) and a no-condensable gas (air) respectively. Furthermore at the gas liquid interface of a bubble nucleated inside a liquid, a system of two parts separated by an interface has to be considered

$$\left.\frac{dF^{\sigma}}{dA}\right|_{T,V',V''} = \gamma \rightarrow dF^{\sigma} = \gamma dA \tag{2.6}$$

where γ is the surface tension and F^{σ} is the Helmholtz free energy of a system with an interface.

The liquid phase is maintained at a pressure p' (which is almost atmospheric) and the gaseous phase is at a pressure p''. The pressure in the bubble varies as the bubble radius is changing, thus the change of energy required for a change in volume of the bubble is

$$d(p'V'') = p'dV'' + V''dp' \tag{2.7}$$

given that the pressure is almost constant in the liquid phase, the above expression is reduced to

$$d(p'V'') = p'dV'' \tag{2.8}$$

Thus the thermodynamic potential of the system, B, can be written as

$$B = G'(T, P', N_1', N_2') + F''(T, V'', N_1'', N_2'') + F^{\sigma} + p'V'' \tag{2.9}$$

where $G', F''and\ F^{\sigma}$ are the Gibbs, Helmholtz and surface tension function for the liquid phase, the gas phase and the surface phase respectively. In our system, p', T, N_1, and N_2 are constants as it is a closed system. Thus the change of the total energy of the system, *dB*, is

$$\begin{aligned} dB &= q[dG' + dF'' + F^{\sigma} + p'dV''] \\ &= q[(p' - p'')dV''] + q[\gamma dA + \mu_1''dN_1'' + \mu_1'dN_1' + \mu_2''dN_2'' + \mu_2'dN_2' \\ &\qquad at\ p', T, N_1 and\ N_2 = constant \end{aligned} \tag{2.10}$$

At equilibrium, equality of chemical potentials and Laplace equation are satisfied. This is, it is assumed that the gas and liquid phase components form a weak solution in the liquid phase and an ideal mixture in the gaseous phase, then the chemical potentials can be written as

$$\mu_1'' = \nu_0 p_{\infty} + RT \ln \frac{p_1''}{p_{10}''} \tag{2.11}$$

$$\mu_2'' = \mu_{20}'' + RT \ln \left(\frac{p_2''}{p'}\right) \tag{2.12}$$

$$\mu_2' = \mu_{20}' + RT\ln\left(\frac{c_2'}{c_{2s}}\right) \tag{2.13}$$

$$\mu_1' = \nu_0 p' + RT\ln\left(\frac{c_2}{c_1' + c_2'}\right) = \nu_0 p' - RT\ln\left(1 + \frac{c_2'}{c_1'}\right)$$

$$\approx \nu_0 p' - RT\ln\left(\frac{c_2'}{c_1'}\right) \text{ for } c_2' \ll c_1' \tag{2.14}$$

$$p'' = p' + \frac{2\gamma}{r} \tag{2.15}$$

Where ν_0, p_{10}'' and $c_{2s}$are the specific volume of the pure liquid, the saturation pressure of the pure liquid and the saturation concentration of the gas in the liquid phase respectively. μ_{20}'' and μ_{20}' are the chemical potential of the gas in the gaseous and liquid phases when the gas is dissolved up to the saturation concentration ($p_2'' = p'$and $c_2' = c_{2s}$). Assuming that $c_1' \equiv N_1'/V' \equiv c_{01}\, c_{2s}$, the variables are only p_1'', p_2''andc_2'. It is also assumed that the derivatives of equation (2.11) through (2.15) are satisfied. Thus, $\mu_1'' = \mu_1'$ and $\mu_2'' = \mu_2'$. Taking the derivatives of equations (2.11) through (2.14) with respect to the bubble radius, the chemical potentials are given as:

$$\frac{d\mu_2''}{dr} = \frac{d\mu_2'}{dr} = \frac{RT}{dp_2''} \tag{2.16}$$

$$\frac{d\mu_1''}{dr} = \frac{RT}{p_1''}\frac{dp_1''}{dr} \tag{2.17}$$

$$\frac{d\mu_1'}{dr} = \frac{RT}{c_{01}}\frac{dc_2'}{dr} = \frac{RT}{K_H}\frac{dp_2''}{dr} \tag{2.18}$$

where Henry's law was assumed, namely,

$$p_2'' = K_{\mathrm{H}}\frac{c_2'}{c_{01}} \tag{2.19}$$

where K_H is a constant.

Hence, using the above equations and assuming equity of potentials, the derivatives of the chemical potentials into the thermodynamic potential in equation (2.10), dV'' and dA were replaced as a function of *dr*, which, after grouping yields to

$$\frac{dB}{dr} = q\left[4\pi r^2\left(p' - p'' + \frac{2\gamma}{r}\right) + (\mu_1'' - \mu_1')\frac{dN_1''}{dr} + (\mu_2'' - \mu_2')\frac{dN_2''}{dr}\right] \tag{2.20}$$

The second derivative of equation (2.20) was taken to determine the global minima (assuming that there is a minimum). This is, it is important to determine the lowest free energy point and for that, what is the radius.

$$\frac{d^2(B/q)}{dr^2} = 8\pi r\left(p' - p'' + \frac{2\gamma}{r}\right) + 4\pi r^2\left(-\frac{2\gamma}{r^2} - \frac{dp''}{dr}\right) + \left(\frac{d\mu_1''}{dr}\frac{dN_1''}{dr} - \frac{d\mu_1'}{dr}\frac{dN_1''}{dr}\right) + (\mu_1'' - \mu_1')\frac{d^2N_1''}{dr^2} + \left(\frac{d\mu_2''}{dr}\frac{dN_2''}{dr} - \frac{d\mu_2'}{dr}\frac{dN_2''}{dr}\right) + (\mu_2'' - \mu_2')\frac{d^2N_2''}{dr^2} \quad (2.21)$$

The above expression can be simplified. Using equation (2.15) through (2.18), the first two terms of the above expression are zero so as the fourth, fifth and the last term in the equation. The above equation is simplified to the following,

$$\frac{d^2(B/q)}{dr^2} = \left(\frac{d\mu_1''}{dr}\frac{dN_1''}{dr} - \frac{d\mu_1'}{dr}\frac{dN_1''}{dr}\right) + \left(\frac{d\mu_2''}{dr}\frac{dN_2''}{dr} - \frac{d\mu_2'}{dr}\frac{dN_2''}{dr}\right) \quad (2.22)$$

Substitution of the derivatives of the chemical potentials, the Henry's law constant constant and the derivative of the Laplace radius into equation (2.22) yield,

$$\frac{d^2(B/q)}{dr^2} = \left(\frac{RT}{p_1''}\frac{dp_1''}{dr}\frac{dN_1''}{dr} - \frac{RT}{K_H}\frac{dp_2''}{dr}\frac{dN_1''}{dr}\right) \quad (2.23)$$

Furthermore, since $N_1'' = V''\frac{p_1''}{RT}$ (from ideal gas law), the derivative of N_1'' is $\frac{dN_1''}{dr} = \left(\frac{dV}{dr}p_1'' + V''\frac{dp_1''}{dr}\right)\frac{1}{RT}$. Replacing into the above equation yields to

$$\begin{aligned}\frac{d^2(B/q)}{dr^2} &= \frac{RT}{p_1''}\frac{dp_1''}{dr}\frac{1}{RT}\left(\frac{dV}{dr}p_1'' + V''\frac{dp_1''}{dr}\right) + \frac{RT}{K_H}\frac{dp_2''}{dr}\frac{1}{RT}\left(\frac{dV}{dr}p_1'' + V''\frac{dp_1''}{dr}\right)\\ &= V''\frac{dp_1''}{dr}\left(\frac{1}{p_1''}\frac{dp_1''}{dr} + \frac{1}{K_H}\frac{dp_2''}{dr}\right) + \left(\frac{dp_1''}{dr} + \frac{p_1''}{K_H}\frac{dp_2''}{dr}\right)\frac{dV''}{dr}\\ &= \frac{4}{3}\pi r^3\left[\frac{dp_1''}{dr}\left(\frac{1}{p_1''}\frac{dp_1''}{dr} + \frac{1}{K_H}\frac{dp_2''}{dr}\right) + \frac{3}{r}\left(\frac{dp_1''}{dr} + \frac{p_1''}{K_H}\frac{dp_2''}{dr}\right)\right] \quad (2.24)\end{aligned}$$

Since it is a weak solution, $\frac{p_1''}{K_H} \ll 1$, and $p'' = p_1'' + p_2'' = \frac{2\gamma}{r} \rightarrow \frac{dp_1''}{dr} + \frac{dp_2''}{dr} = -\frac{2\gamma}{r^2}$, substitution into the above yields,

$$\frac{d^2(B/q)}{dr^2} = \frac{4}{3}\pi r^3\left[\frac{1}{p_1''}\left(1 - \frac{p_1''}{K_H}\right)\frac{dp_1''}{dr} - \frac{1}{K_H}\frac{2\gamma}{r^2}\right]\left(\frac{3p_1''}{r} + \frac{dp_1''}{dr}\right) \quad (2.25)$$

If the vapor pressure of a volatile liquid is independent of r, i.e., $dp_1''/dr = 0$, the system is unstable, i.e., $d^2B/dr^2 < 0$. This is the case in open systems where bubbles are in the bulk liquid instead of a liquid droplet. In contrast, in a closed systems, the total number of moles, N_1 and N_2, are constant, dp_1''/dr is non-zero and controlled by adjusting the dissolved gas concentration, c_2'.

For $\frac{d^2(B/q)}{dr^2} < 0$, the following is required,

$$\frac{dp_1''}{dr} + \frac{p_1''}{K_H}\frac{dp_2''}{dr} > 0 \tag{2.26}$$

The total number of moles of a volatile liquid and a non-condensable gas can be written as, [17]

$$N_1 = c_{01}V' + qN_1'' \tag{2.27}$$

$$N_2 = c_2'V' + qN_2'' \tag{2.28}$$

At fixed N_2 and N_1, the derivatives of equation (2.27) and (2.28) (considering ideal gas law and Henry's law) are as follow,

$$\frac{dp_1''}{dr} = -\left(\frac{RT}{V''}c_{01}\frac{dV'}{dr} + 3p_1''\right) \tag{2.29}$$

$$\frac{dp_2''}{dr} = -\frac{1}{\Psi}\left(\frac{RT}{V''}\frac{c_2}{q}\frac{dV'}{dr} + 3p_2''\right) \tag{2.30}$$

$$\text{Where, } \Psi = 1 + \frac{c_2'V'RT}{qp_2''V''} = 1 + \frac{N_2'}{qN_2''} \tag{2.31}$$

Substitution of equation (2.30) and (2.31) into $\frac{dp''}{dr} = -\frac{2\gamma}{r^2}$, $\frac{dV'}{dr}$ can be written as follow

$$\frac{dV'}{dr} = \frac{-3qp_1''V''}{c_{01}RTr}\left[\frac{\left(1-{}^{2\gamma}/_{3p_1''r}\right)\Psi + \left({}^{p_2''}/_{p_1''}\right)}{\Psi + \left({}^{c_2'}/_{c_{01}}\right)}\right] \tag{2.32}$$

From equation (2.26) and using equation (2.30), (2.31) and (2.32), the following was derived,

$$\frac{dp_1''}{dr} + \frac{p_1''}{K_H}\frac{dp_2''}{dr} = \frac{3p_1''}{r}\left\{\frac{\Psi + (p_1''/K_H)(c_2'/c_{01})}{\Psi + c_2'/c_{01}}\left[\left(1 - \frac{2\gamma}{3p_1''r}\right)\Psi + \frac{p_2''}{p_1''}\right] - \left(\Psi - \frac{c_2'}{c_{01}}\right)\right\} > 0 \tag{2.33}$$

The above inequality can be further simplified,

$$\Psi^2 - \frac{p_2''}{K_H}\left[\left(\frac{K_H}{p_1''} + \frac{p_1''}{K_H} - 2\right)\frac{3p_1''r}{2\gamma} - \frac{p_1''}{K_H}\right]\Psi > 0 \tag{2.34}$$

Solving the previous with respect to q it was arrived to the following inequality,

$$q > \frac{3c_{01}V'RT}{4\pi r^3 K_H}\left[\left(\frac{K_H}{p_1''}+\frac{p_1''}{K_H}-2\right)\frac{3p_1''p_2''r}{2\gamma K_H}-\left(\frac{K_H}{p_1''}+\frac{p_1''}{K_H}\right)\frac{p_2''}{K_H}\right]^{-1} \quad (2.35)$$

$$q > \frac{3c_{01}V'RT}{4\pi r^3 K_H}\left[\frac{3p_2''r}{2\gamma}-1\right]^{-1} \equiv q_0 \text{ for } \frac{p_1''}{K_H} \ll 1 \; at \; p', T, N_1 and \; N_2 = constant \quad (2.36)$$

The above relationship indicates that the system becomes stable when q is larger than a threshold number q_0. It also implies that when the number of nucleated bubbles (which is also given by the molar content of air, which in turn depends on the amount of dichloromethane) is below this threshold value, q_0, there is no equilibrium radius. Furthermore, when there are two possible equilibrium radiuses, the most stable radius is the larger one. When the above is satisfied, namely a specific minimum amount of bubbles are present in the solution, and the concentration of air in the liquid is saturated at the given temperature, the equilibrium radius is strictly given by Laplace's radius

$$r_{eq} = \frac{2\gamma}{p_{01}} \text{ and } p_2'' = p'$$

This theoretical prediction agreed with the average measured radius of the microbubbles nucleated inside the CH_2Cl_2 droplet. It is also understood that for microbubbles in equilibrium to exist, it is required a minimum concentration of air in the CH_2Cl_2 droplet and the surrounding PVA_{aq}. This condition is satisfied at saturation. After bubble nucleation and bubble stabilization, PLA absorbs to the bubble surface.

The above result is crucial as it opens room for the fabrication of bigger stable micro bubbles inside a closed system if the concentration of air in the solution could be adjusted. This is,

$$p'' = p' + \frac{2\gamma}{r} \rightarrow p_1'' + p_2'' = p' + \frac{2\gamma}{r} \quad (2.37)$$

Since $p_1'' = p_{01}'' \; and \; p_2'' = p'\frac{c_2'}{c_{2s}'}$, replacing into the above relation and solving for *r* yields to

$$p_{01}'' - p'\left(\frac{c_{2s}'-c_2'}{c_{2s}'}\right) = \frac{2\gamma}{r}$$

$$r = \frac{2\gamma}{p_{01}''-p'\left(1-\frac{c_2'}{c_{2s}'}\right)} \quad (2.38)$$

Equation (38) implies that if the concentration of air in the liquid is below the saturation

concentration of air in the liquid, $c'_{2s} > c'_2$, the radius of the bubble increases its size. For instance, if in the above equation the concentration of air in the solution is 10% below the solubility limit, $c'_{2s}/c'_2 = 0.9$, for a surface tension of $\gamma = 2.78\times10^{-2}$ N/m [20, 21] and a vapor pressure for pure dichloromethane of $p''_{01} = 5.81\times10^4$ Pa [22] and $p' = 101.3kPa$, the equilibrium radius is 1.15μm at 298 .15 K. If it is 20% below, then the equilibrium radius is 1.47μm at 298.15K. If so, given q_0, the bubble template method can be modified to attain bigger microcapsules (from bigger bubble templates), that are more suitable for engineering applications.

2.3 Relationship between the microbubble size, and air content

In the previous section, the stability of the bubble based on a thermodynamic potential was derived. The virtual displacement for a microbubble nucleated inside a liquid droplet was analyzed. In this analysis it was assumed that the process is isothermal and that microbubble nucleation is due to the diffusion of dichloromethane into the aqueous medium (aqueous solution of PVA or H_2O) but since the dissolution rate of methylene chloride into the PVA aqueous solution is much slower than the relaxation rate needed to achieve the liquid-vapor equilibrium, the system is considered in equilibrium. Keeping the notation introduced in the previous section [single and double primes refer to the liquid and gas phase respectively and the subscript 1 and 2 denote a volatile solvent (in this case a solution of PLA in dichloromethane) and a no-condensable gas (air) respectively], the focus of this section is to determine the direct relationship between the solubility of air in the solution and the microbubble size. It is assume that the Laplace equation is satisfied, Henry's law is satisfied and the equity of potential is satisfied:

$$\mu''_1 = v_0 p_\infty + RT \ln \frac{p''_1}{p''_{10}} \tag{2.39}$$

$$\mu''_2 = \mu''_{20} + RT \ln \left(\frac{p''_2}{p'}\right) \tag{2.40}$$

$$\mu'_2 = \mu'_{20} + RT \ln \left(\frac{c'_2}{c_{2s}}\right) \tag{2.41}$$

$$\mu'_1 = v_0 p' + RT \ln \left(\frac{c_2}{c'_1 + c'_2}\right) = v_0 p' - RT \ln \left(1 + \frac{c'_2}{c'_1}\right)$$
$$\approx v_0 p' - RT \ln \left(\frac{c'_2}{c'_1}\right) \text{ for } c'_2 \ll c'_1 \tag{2.42}$$

$$p'' = p' + \frac{2\gamma}{r} \tag{2.43}$$

In a liquid, bubbles usually have various sizes. Large bubbles may coalesce into even larger bubbles and float into the air, while the small ones may disappear due to the dissolution of gases in the liquid. Bubbles cannot keep their size stable in a bulk liquid. However, in a closed volume of liquid, it is known that the size of bubbles is stable. Considering the droplet system considered so far, assuming the ideal gas equation of state inside the bubbles, the total molar amounts of CH_2Cl_2 and nitrogen are given by[17]

$$N_1 = N_1' + qN_1'' = c_1'V' + q\frac{p_1''}{RT}\left(\frac{4}{3}\pi r_b^3\right) \tag{2.44}$$

$$N_2 = N_2' + qN_2'' = c_2'V' + q\frac{p_2''}{RT}\left(\frac{4}{3}\pi r_b^3\right) \tag{2.45}$$

where N_1 and N_2 without single/double primes denote the sum of each component and each phase, respectively. In equilibrium, the equality of chemical potentials in the liquid and gas phases should be satisfied for each component. Solving for the pressure of both components (air and dichloromethane) in the gas phase yields to the following relations:

$$p_1'' = \eta p_{01}'' \tag{2.46}$$

$$p_2'' = p'\frac{c_2'}{c_{2s}'} \tag{2.47}$$

where p''_{01} is the saturation vapor pressure of pure CH_2Cl_2, c'_{2s} is the saturation concentration of nitrogen in the liquid phase, and η is defined by the following equation:

$$\eta = e^{\left[\frac{v_0\left(p'-p_{01}''\right)}{RT}-\frac{c_2'}{c_1'}\right]} \tag{2.48}$$

where v_0 is the specific volume of pure CH_2Cl_2 in the liquid phase. The Laplace relation should also be satisfied at the equilibrium condition:

$$p'' = p' + \frac{2\gamma}{r_b} \tag{2.49}$$

where γ is the surface tension of CH_2Cl_2. By substituting eqs 3 and 4 into eq 6, c'_2 is given by

$$c_2' = c_{2s}'\left(1 - \eta\frac{p_{01}''}{p'} + \frac{2\gamma}{r_b p'}\right) \tag{2.50}$$

Since for a weak solution, c'_1 is approximately equal to the molar concentration of pure CH_2Cl_2, c'_{01}:

$$c'_1 = c'_{01}. \tag{2.51}$$

By substituting equation (2.42) and (2.46) into equation (2.39), and equations (2.41) and (2.47) into equation (2.40), and eliminating V', the relation between the total molar amount of nitrogen, N_2, and the equilibrium radius of bubbles, r_b, for different numbers of bubbles, q, at constant p', T, and N_1 is given by the following equation:

$$N_2 = \left[\frac{c'_{2s}}{c'_{01}}\left(N_1 - q\eta\frac{p''_{01}}{RT}\frac{4}{3}\pi r_b^3\right) + q\frac{p'}{RT}\frac{4}{3}\pi r_b^3\right]\left[1 - \eta\frac{p''_{01}}{p'} + \frac{2\gamma}{r_b p'}\right] \tag{2.52}$$

where η is given as a function of r_b by substituting equations (2.48) and (2.49) into equation (2.47). The above relationship correlates to the Henry's law constant since

$$\frac{c'_{2s}}{c'_{01}} = \frac{p'}{K_H}$$

p' is the atmospheric pressure, and K_H is the Henry's Law constant

By using the stability condition attained in equation (2.35) and using equations (2.44), (2.45), (2.48) and (2.51), the stability condition of equation (2.35) can also be expressed as follow

$$-\left(\frac{3N_1RT}{q4\pi r_b^3 K_H} + 1 - \frac{p''_1}{K_H}\right) - \left(\frac{p''_1 p''_2}{K_H^2} - \frac{3r_b p''_2}{2\gamma}\left(1 - \frac{p''_1}{K_H}\right)^2\right) > 0$$

$$\rightarrow \left[\frac{c'_{2s}}{c'_{01}}\left(N_1 - q\eta\frac{p''_{01}}{RT}\frac{4}{3}\pi r_b^3\right) + q\frac{p'}{RT}\frac{4}{3}\pi r_b^3\right]\frac{d}{dr_b}\left(1 - \eta\frac{p''_{01}}{p'} + \frac{2\gamma}{r_b p'}\right) + \frac{d}{dr_b}\left[\frac{c'_{2s}}{c'_{01}}\left(N_1 - q\eta\frac{p''_{01}}{RT}\frac{4}{3}\pi r_b^3\right) + q\frac{p'}{RT}\frac{4}{3}\pi r_b^3\right]\left(1 - \eta\frac{p''_{01}}{p'} + \frac{2\gamma}{r_b p'}\right) > 0$$

$$\frac{dN_2}{dr_b} > 0 \tag{2.53}$$

The relevance of this result relies on the fact that the bubbles are stable only at $dN_2/dr_b > 0$. The above analysis also provides the theoretical foundation for manufacturing bigger microcapsules. In Sakurai et al. [16] this was called the Gas/O/W method and it is shown in Appendix 1.

2.3 Conditions required for the release of hollow PLA microcapsules from a droplet

In the bubble template method,[1] microbubbles were stable in the droplet of the methylene chloride solution of PLA, as shown in Figure 2.1(b). However, microbubbles coalesced or disappeared in the droplet without PLA. This result suggests that PLA adsorbs to the surface of microbubbles because of its surface-active property. Sequentially, microbubbles covered with PLA were released from the droplet to the surrounding PVA aqueous solution, as shown in Figure 2.1(c). The droplet shrank due to the dissolution of methylene chloride into the PVA aqueous solution, and the PLA concentration increased. However, the release of microcapsules stopped before dissolving methylene chloride completely into the surrounding PVA aqueous solution. This section focuses on the concentration of PLA in the methylene chloride solution, c_3, as a parameter to identify the start and stop times for the release of hollow PLA microcapsules from the droplet. By assuming that the total volume of bubbles in comparison to the total volume of a droplet, V_d, is negligible, and a part of PLA adsorbs onto the bubbles and capsules, the mass conservation equation of PLA can be expressed as follows:

$$c_3 V_\mathrm{d} = c_{30} V_{\mathrm{d}0} - \Gamma_\mathrm{bc}^\mathrm{eq}(c_3) \sum S_\mathrm{bc}, \tag{2.54}$$

where c_{30} and $V_{\mathrm{d}0}$ are the initial values of c_3 and V_d, $\Gamma_\mathrm{bc}^\mathrm{eq}(c_3)$ is the equilibrium area density of PLA on the surface of bubbles and capsules at c_3, and $\sum S_\mathrm{bc}$ is the total surface area of bubbles and capsules. Here, the relationship between c_3 and V_d was modeled by assuming that the release of hollow PLA microcapsules started at $c_{3\mathrm{min}}$ and stopped at $c_{3\mathrm{max}}$, where $c_{3\mathrm{min}}$ is a threshold value of c_3 at which PLA adsorbs on the surface of bubbles so much that bubbles can keep stable, and $c_{3\mathrm{max}}$ is the solubility of PLA in methylene chloride. For simplicity, bubbles are unstable, that is, $\sum S_\mathrm{bc} = 0$ at $c_3 < c_{3\mathrm{min}}$, whereas bubbles are stable and PLA is fully adsorbed on the surface of bubbles and capsules, that is, $\Gamma_\mathrm{bc}^\mathrm{eq}(c_3)$ is a constant value of $\Gamma_\mathrm{bc}^\mathrm{max}$ at $c_3 \geq c_{3\mathrm{min}}$. Specifically,

$$c_3 V_\mathrm{d} = c_{30} V_{\mathrm{d}0} \text{ at } c_3 < c_{3\mathrm{min}}, \tag{2.55}$$

$$c_3 V_\mathrm{d} = c_{30} V_{\mathrm{d}0} - \Gamma_\mathrm{bc}^\mathrm{max} \sum S_\mathrm{bc} \text{ at } c_3 \geq c_{3\mathrm{min}}, \tag{2.56}$$

At $c_3 \geq c_{3\mathrm{min}}$, if all bubbles and capsules have an equilibrium radius, r_eq, $\sum S_\mathrm{bc}$ is given by the following equation:

$$\sum S_{\mathrm{bc}} = \frac{3}{r_{\mathrm{eq}}} \sum V_{\mathrm{bc}} , \tag{2.57}$$

where $\sum V_{\mathrm{bc}}$ is the total volume of bubbles and capsules. Here, the following two assumptions were employed:

1) As the droplet shrinks, air dissolving in the solution forms bubbles because the solubility of air in the solution is much higher than that in the PVA aqueous solution.
2) When the generated bubbles arrive at the interface between the droplet and the surrounding PVA aqueous solution, a part of the bubbles stay, and others collapse at the interface.

Because the diffusion rate of PLA is much slower than the nucleation rate of bubbles, the average area density of PLA at the surface of bubbles, $\overline{\Gamma}_{\mathrm{bc}}$, is smaller than $\Gamma_{\mathrm{bc}}^{\max}$ just when the bubbles arrive at the interface. If the diffusion of PLA is negligible, $\overline{\Gamma}_{\mathrm{bc}}$ is given by $\Gamma_{\mathrm{bc}} = c_3 \bar{d} A_{\mathrm{bc}} / S_{\mathrm{bc}}$, where $\bar{d}$ is the average traveling distance of bubbles, which is proportional to the radius of a droplet, r_{d}, ($\bar{d} = \delta r_{\mathrm{d}}$), and A_{bc} is the collision cross section. Here, the survival ratio of bubbles at the interface, R_{s}, is assumed to be proportional to $\overline{\Gamma}_{\mathrm{bc}} / \Gamma_{\mathrm{bc}}^{\max}$ ($R_{\mathrm{s}} = \varepsilon \overline{\Gamma}_{\mathrm{bc}} / \Gamma_{\mathrm{bc}}^{\max}$). From these two assumptions, the derivative of $\sum V_{\mathrm{bc}}$ with respect to time can be expressed as follows:

$$\frac{d}{dt}\left(\sum V_{\mathrm{bc}}\right) = -\alpha \frac{dV_{\mathrm{d}}}{dt} \times R_{\mathrm{s}} , \tag{2.58}$$

where α is the ratio between the saturation concentration of air in the methylene chloride solution and air density in the gas phase, that is, $\alpha = c_{2\mathrm{s}} RT / p_2''$. From equations (57) and (58), equation (59) becomes

$$c_3 V_{\mathrm{d}} = c_{30} V_{\mathrm{d0}} + \frac{\alpha\beta}{r_{\mathrm{eq}}} \int \frac{dr_{\mathrm{d}}}{dt} c_3 V_{\mathrm{d}} dt , \tag{2.59}$$

where $\beta = \delta \varepsilon A_{\mathrm{bc}} / S_{\mathrm{bc}}$. If dr_{d} / dt is constant, equation (59) can be simplified as follows:

$$\frac{d}{dt}(c_3 V_d) = \kappa (c_3 V_d), \tag{2.60}$$

where $\kappa = \frac{\alpha\beta}{r_{eq}} \frac{dr_d}{dt}$. The condition for constant dr_d/dt is explained in Appendix 1. By solving equation (60), the total mass of PLA in the bulk solution, $c_3 V_d$, is given by

$$c_3 V_d = c_{30} V_{d0} \exp(\kappa t). \tag{2.61}$$

By employing the above assumptions, equation (56) was transformed to equation (61). In summary, if $c_{30} < c_{3min}$, the release of hollow PLA capsules starts at c_{3min} and stops at c_{3max}. From equation (55) and (61), the release of capsules starts at the droplet size of $V_d = (c_{30}/c_{3min}) V_{d0}$ and stops at $V_d = (c_{30}/c_{3max}) V_{d0} \exp(\kappa t)$.

3. Experiment

3.1 Chemicals

The shell material was PLA with a molecular weight of 2000 (PolyScience, Niles, IL). Methylene chloride (Wako Pure Chemical Industries, Ltd., Osaka, Japan) was used for the PLA solution. The continuous phase was 2% (w/w) PVA aqueous solution made from anionic polyvinyl alcohol (Gohsenal T-350, Nippon Gohsei, Osaka, Japan). All chemicals used in this study were reagent grade.

3.2 Methods

Hollow PLA microcapsules were fabricated by generating microbubbles inside droplets of PLA solution. Because the initial concentration of dissolving air in a methylene chloride solution of PLA was close to the saturation concentration and the solubility of air in a PVA aqueous solution was much smaller than that in a methylene chloride solution of PLA, microbubbles were generated due to the dissolution of methylene chloride into the surrounding PVA aqueous solution. The radius distribution of bubbles was obtained by processing several bright field images of bubbles using an inverted microscope system (ECLIPSE Ti-E, Nikon Corporation, Tokyo, Japan). The generated hollow PLA microcapsules were purified, dried, and then observed. Because PLA was stained with Nile Red, hollow PLA microcapsules were visualized as fluorescence images. The inner and outer

radius distributions of hollow PLA capsules were obtained by processing several bright field images of capsules.

To verify the conditions for the release of hollow PLA microcapsules from a droplet, a 500-μm-radius droplet of the methylene chloride solution of PLA with five different initial concentrations of PLA— c_{30} = 20, 2, 0.2, 0.02, and 0.002 g/l—was formed inside a 2% (w/w) PVA aqueous solution by using a microsyringe, and the shrinkage of a droplet and the release of hollow PLA capsules were recorded as a movie by using the microscope. The time evolution of the droplet radius of methylene chloride solutions of PLA, r_d, and the start and stop times for the release of hollow PLA microcapsules were obtained by analyzing the movie. All the experiments were executed at 298 K.

3.3 Results and discussion

Figure 2.2 shows the frequency histogram of bubble radius, r_b. The mean radius and the standard deviation were 1.03 and 0.14 μm, respectively. The polydispersivity index (PI = standard deviation/mean) values for the bubbles was 13.6%. By substituting $\gamma = 2.78\times10^{-2}$ N/m [20] and $p''_{01} = 5.81\times10^{4}$ Pa [22] at 298 .15 K into equation (37), r_{eq} was calculated as 0.95 μm. The measured bubble radius agreed with the theoretical prediction.

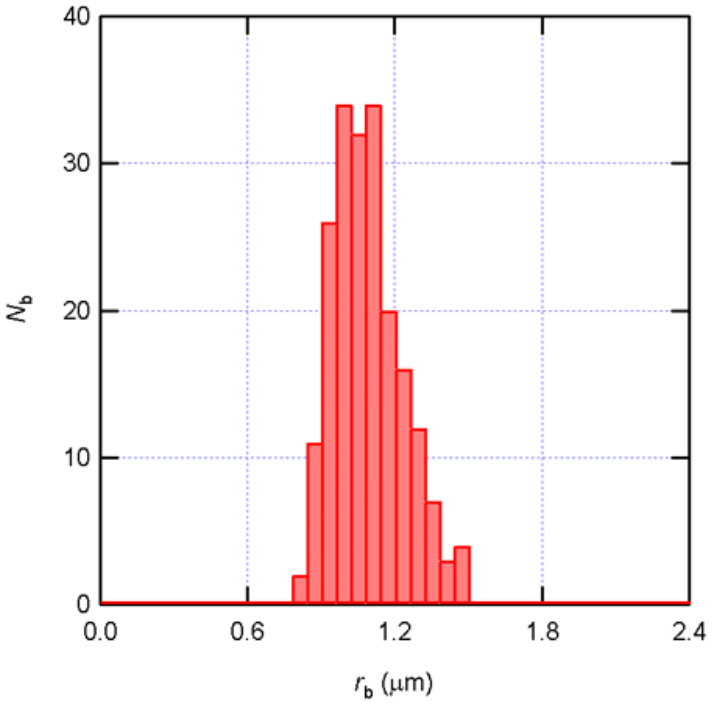

Figure 2.2: Number of bubbles, N_b, vs. radius, r_b, histogram.

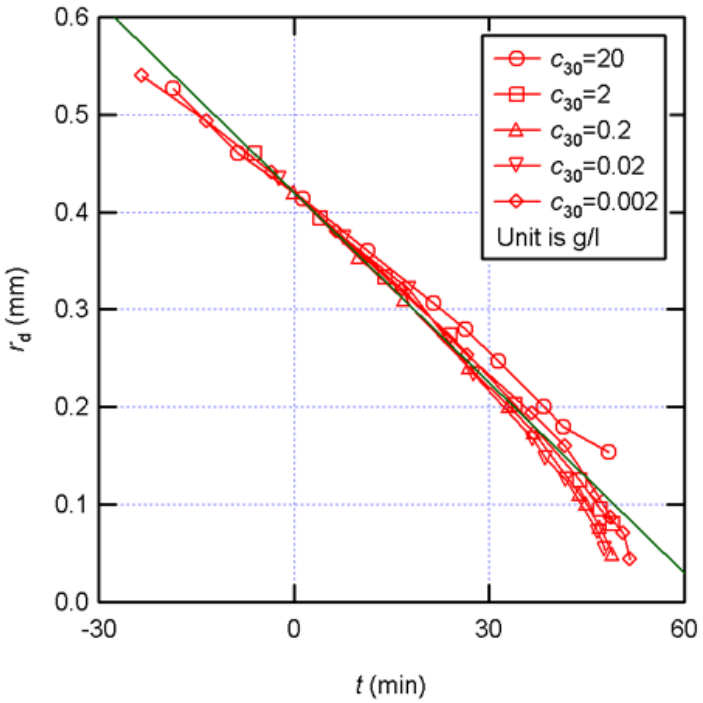

Figure 2.3: Droplet dissolution. Time evolution of the droplet radius of methylene chloride solutions of PLA, r_d, for five different initial concentrations of PLA, c_{30}. Time (x-axis) was set as $t = 0$ at $r_d = 0.42$ mm. The line fitted to all the data except for $c_{30} = 20$ g/l within the range of $0 \le t \le 45$ min was $r_d\,(\mathrm{mm}) = 0.42 - 0.0065 \times t\,(\mathrm{min})$.

Figure 2.3 shows the time evolution of the droplet radius of methylene chloride solutions of PLA, r_d, for five different c_{30}. In the x axis, time was set as $t = 0$ at $r_d = 0.42$ mm. Except for the region at t>45 min, r_d decreased almost linearly with respect to t. The line fitted to all the data except for $c_{30} = 20$ g/l within the range of $0 \le t \le 45$ min was $r_d\,(\mathrm{mm}) = 0.42 - 0.0065 \times t\,(\mathrm{min})$. If the dissolution rate of methylene chloride into the surrounding PVA aqueous solution is restricted by the surface area of a droplet and is not restricted by the diffusion in the PVA aqueous solution, dr_d/dt keeps constant (refer to Appendix 1).

This experimental result confirmed the validity of the transformation of equation 2.59 into equation 2.61. Furthermore, at t>20 min, $\left|dr_d/dt\right|$ of $c_{30} = 20$ g/l was smaller than that of other c_{30}. This experimental result suggested that c_3 increased beyond the solubility around $t = 20$ min for $c_{30} = 20$ g/l, and the diffusion of methylene chloride inside the droplet could restrict the overall dissolution rate. For $c_{30} = 20$ and 2 g/l, the release of hollow PLA microcapsules started just after the formation of a droplet and stopped at $t = 20$ and 44 min, respectively. For these two c_{30}, the fluidity of a droplet was not lost when the release of hollow PLA microcapsules stopped. However, for $c_{30} = 0.2$, 0.02, and 0.002 g/l, hollow PLA microcapsules did not release just after the formation of a

droplet. The release of hollow PLA microcapsules started at t = 17, 39, and 49 min, respectively, and stopped when a droplet became a solid particle.

Figure 2.4 shows the time evolution of c_3 for five different c_{30} that was calculated from equation (2.55) and (2.61). In the x axis, time was also set as $t = 0$ at $r_d = 0.42$ mm. The threshold value of $c_{3\min}$ was determined from equation (2.54) by using c_{30}, V_{d0} and the volume of a droplet when the capsule release started. The calculated $c_{3\min}$ were 0.50, 0.52, and 0.48 g/l for $c_{30} = 0.2$, 0.02, and 0.002 g/l, respectively. Therefore, the threshold value of $c_{3\min}$ could be determined about 0.5 g/l. At $c_3 < c_{3\min}$, c_3 was calculated from equation (37), whereas, at $c_3 \geq c_{3\min}$, c_3 was calculated from equation (2.43) by assuming $\kappa = -0.01\,\mathrm{min}^{-1}$. Assuming that r_{eq}=0.95 μm, $dr_d/dt = -6.5\mu m/\mathrm{min}$ (from Figure 2.4) and $\alpha = c_{2s}RT/p_2'' \approx 0.5$, the parameter $\kappa\left(=\frac{\alpha\beta}{r_{eq}}\frac{dr_d}{dt}\right)$ is given by $\kappa = -3.4\beta\,\mathrm{min}^{-1}$. The parameter $\beta\left(=\delta\varepsilon A_{bc}/S_{bc}\right)$, consists of three parameters of ε, δ, and A_{bc}/S_{bc}. The last parameter A_{bc}/S_{bc} can be approximated as $A_{bc}/S_{bc} = \pi r_{eq}^2 / 4\pi r_{eq}^2 = 0.25$.

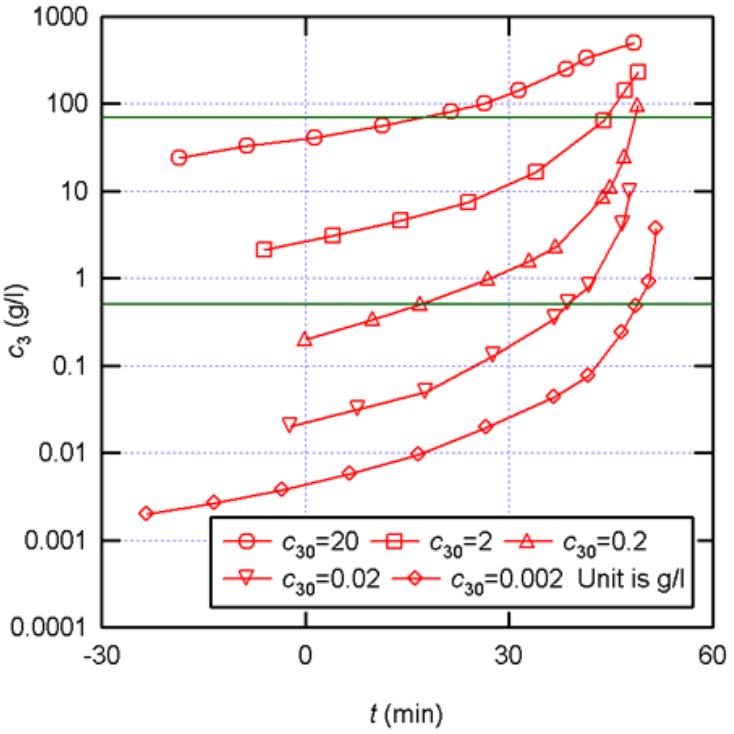

Figure 2.4: Time evolution of the concentration of methylene chloride solutions of PLA, c_3, for five different initial concentrations of PLA, c_{30}. Time (x-axis) was set as $t = 0$ at $r_d = 0.42$ mm. The lines show $c_3 = 0.5$ and 70 g/l. Hollow PLA microcapsules released from a droplet within the range of $0.5 \leq c_3 \leq 70$ g/l.

It is difficult to make models to identify these parameters, ε and δ, but if it is assumed that δ= 1 and ε=0.01, i.e., $\bar{d} = r_d$ and 1% of PLA fully absorbed bubbles survived, $\kappa = -0.01 min^{-1}$ but each parameter should be 1. Thus, the parameter κ was assumed –0.01min^{-1}. The solubility of c_{3max} was determined from equation (43) by using c_{30}, V_{d0} and the volume of a droplet when the capsule release stopped. The calculated c_{3max} were 82 and 64 for c_{30} = 20 and 2 g/l, respectively. Because the measured solubility of PLA in methylene chloride was 70 g/l at room temperature, the calculated c_{3max} was close to the solubility. By using the theoretical model shown in the previous section, the experimental results could be reasonably explained if the release of hollow PLA microcapsules started at c_3 = 0.5 g/l and stopped at 70 g/l independent of the initial concentration of PLA and initial radius of a droplet.

Figure 2.5 (left) shows the epifluorescence image of hollow PLA microcapsules. PLA was stained with Nile Red and the excitation wavelength was 552 nm. Figure 2.5 show low-fluorescence intensity rings with a dark area inside the spheres, clearly indicating that fabricated microspheres were hollow microcapsules with a single internal void.

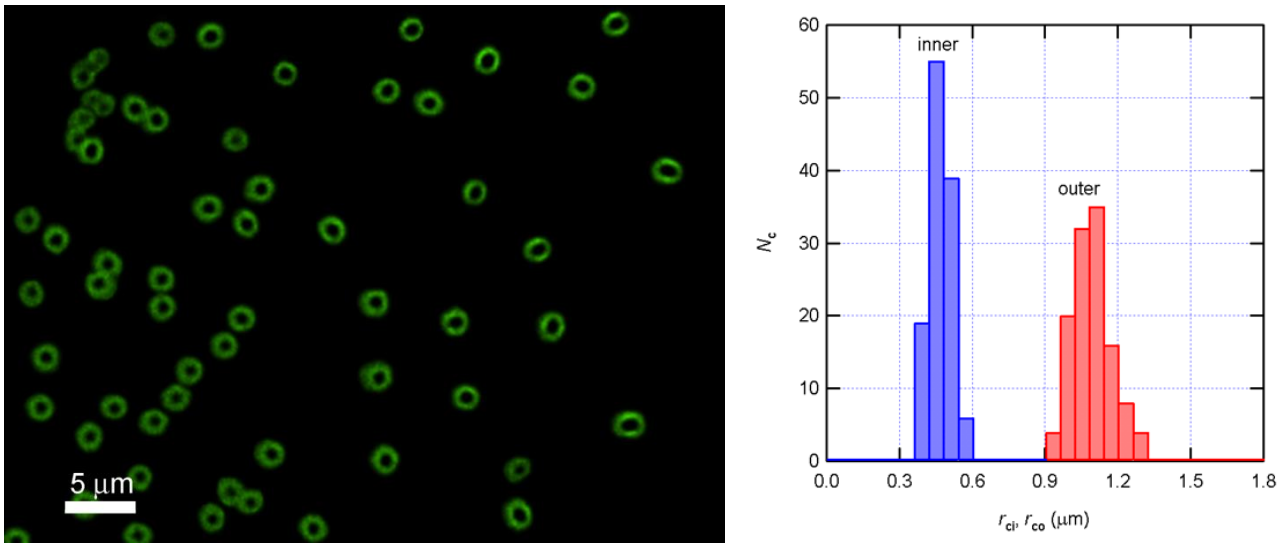

Figure 2.5: Hollow microcapsules and distribution. (Left) Epifluorescence image of hollow PLA microcapsules. (Right) Number of hollow PLA capsules, N_c, vs. either inner radius, r_{ci} or outer radius, r_{co}, histogram.

Figure 2.5 (right) shows the number of hollow PLA capsules, N_c, vs. either inner radius, r_{ci}, or outer radius, r_{co}, histogram. The average inner radius was 0.41µm and the standard deviation was 0.04 µm (PI = 10%). The average outer radius was 1.03 µm and the standard deviation was 0.08µm (PI = 7.7%). The shell thickness calculated from the difference between the average inner and outer radiuses was 0.62µm. Because the mean value of template bubble radius was about 1.03µm, the inner

radius of capsules was smaller than that of template bubbles. This experimental result suggested that hollow PLA capsules shrank before the shell was solidified. The successful control of the shrinkage enables the bubble template method to be more controllable.

4. Conclusions

Two important processes in the bubble template method are the preparation of uniformly sized microbubbles as templates, and the encapsulation of microbubbles and the release from the droplet. About these two processes, the following conclusions could be drawn both from the theoretical and experimental studies:

1) In the theoretical analysis, when determining the condition for the stability of uniformly sized microbubbles inside a droplet, it is concluded that the number of bubbles, q, must be larger than the threshold number of q_0. When the stability condition was satisfied and the concentration of air in the liquid phase achieved the saturation concentration, the equilibrium radius of the bubbles was approximated to be $r_{eq} = 2\gamma / p''_{01}$ (e), where p''_{01} is the saturation vapor pressure of the pure liquid and γ is the surface tension. The mean value of the measured bubble radius was 1.03 μm and agreed with the theoretical prediction of 0.95 μm.
2) The relationship between the concentration of PLA, c_3, and the volume of a droplet, V_d, was modeled by assuming that the release of hollow PLA microcapsules started at c_{3min} and stopped at c_{3max}, where c_{3min} was the threshold value of c_3 at which PLA adsorbed on the surface of bubbles so much that the bubbles remained stable, and c_{3max} was the solubility of PLA in methylene chloride. By using this model, the experimental results could be reasonably explained if the release of hollow PLA microcapsules started at $c_{3min} = 0.5$ g/l and stopped at $c_{3max} = 70$ g/l, independent of the initial concentration of PLA and initial radius of a droplet.
3) The average outer radius of hollow PLA microcapsules was 1.03 μm and the standard deviation was 0.08μm. The average shell thickness was 0.62μm. The average inner radius was smaller than that of template bubbles, suggesting that hollow PLA capsules shrank before the shell was solidified.

5. References

1. Stein, M.; Heldmann, D.; Fritzsch, T.; Siegert, J.; Roessling, G. U. S. 6,264,959, 2009.
2. Straub, J. A.; Chikering, D. E.; Church, C. C.; Shah, B.; Hanlon, T.; Bernstein, H. Porous PLGA microparticles: Ai-700, an intravenously administered ultrasound contrast agent for use in echocardiography. *Journal of Controlled Release* **2005,** *108,* 21-32.

3. Wheatley, M. A.; Forsberg, F.; Oum, K.; Ro, R.; El-Sherif, D. Comparison of in vitro and in vivo acoustic response of a novel 50:50 PLGA contrast agent. *Ultrasonics* **2006,** *44,* 360-367.
4. Rouzes, C.; Leonard, M.; Durand, A.; Dellacherie, E. Influence of polymeric surfactants on the properties of drug-loaded PLA nanospheres. *Colloids and Surfaces B: Biointerfaces* **2003,** *32,* 125-135.
5. Pisani, E.; Tsapis, N.; Paris, J.; Nicolas, V.; Cattel, L.; Fattal, E. Polymeric Nano/Microcapsules of Liquid Perfluorocarbons for Ultrasonic Imaging: Physical Characterization. *Langmuir* **2006,** *22,* 4397-4402.
6. Bertling, J.; Blömer, J.; Kümmel, R. Hollow Microcapsules. *Chemical Engineering Technology* **2004,** *27,* 829-837.
7. Caruso, F. Hollow capsule processing through colloidal tenplating and self assembly. *Chemical European Journal* **2000,** *6,* 413-419.
8. Kawahashi, N.; Matijevi, E. J. Preparation of hollow spherical particles of yttrium compounds. *Journal of Colloid Interface Science* **1991,** *143,* 103-110.
9. Strohm, H.; Sgraja, M.; Bertling, J.; Lobmann, P. Preparation of TiO2-polymer hybrid microcapsules. *Journal of Material Science* **2003,** *38,* 1605-1609.
10. Kaul, S. Myocardial Contrast Echocardiography: 15 Years of Research and Development. *Circulation* **1997,** *96,* 3745-3760.
11. Schutt, E. G.; Klein, D. H.; Mattrey, R. M.; Riess, J. G. Inyectable Microbubbles as Contrast Agents for Diagnostic Ultrasound Imaging: The Key Role of Perfluorochemicals. *Angewandte Chemie International Edition* **2003,** *42,* 3218-3235.
12. Walovitch, R.; Bernstein, H.; Chickering, D.; Straub, J. US Patent. 0,271,591, 2005.
13. Senior, R. Magify™ (perflubutane polymer microspheres) injectable suspension for the assessment of coronary artery disease. *Expert Review in Cardiovascular Therapy* **2007,** *5,* 413-421.
14. Gruber, P. R.; Hall, E. S.; Kolstad, J. J.; Iwen, M. L.; Benson, R. D.; Borchardt, R. L. US. Patent. 5,142,023, 1992.
15. Makuta, T.; Takada, S.; Daiguji, H.; Takemura, F. Simple fabrication of hollow poly-lactic acid microspheres using uniform microbubbles as templates., *Journal of Materials Letters* **2009**, 63, 703-705
16. Sakurai, D.; Molino, J.J.; Daiguji, H.; Takemura, F. Hollow polylactic acid microcapsules fabricated by gas/oil/water and bubble template methods. *Journal of Material Chemistry A* **2013,** No. 10.1039/c3ta12587d.
17. Ward, C. A.; Tikuisis, P. Bubble stability in closed systems. *journal of Applied Physics* **1982,** *53,* 6076-6084.
18. Wilhelm, E.; Battino, R.; Wilcock, R. Low-pressure solubility of gases in liquid water. *Journal Chemistry Review* **1977,** *77,* 219-262.
19. Shirono, K.; Morimatsu, T.; Takemura, F. Gas Solubilities (CO2, O2, Ar, N2, H2, and He) in Liquid Chlorinated Methanes. *Journal of Chemical Engineering Data* **2008,** *53,* 1867-1871.
20. Yaw, C. L. *Thermophysical Properties of Chemicals and Hydrocarbons,* 1st ed.; William Andrew Publishing: New York, 2008.
21. Molino, J.J.; Daiguji, H.; Takemura, F. Factors Affecting the Size and Uniformity of Hollow Poly(lactic acid) Microcapsules Fabricated from Microbubble Templates. *Journal of Physical Chemistry B* **2011,** *115,* 13828-13834.
22. Perry, R. H.; Green, D. W. *Perry's Chemical Engineers' Handbook,* 7th ed.; McGraw-Hill, 1997.

3

Size Tuning of Hollow PLA Microcapsules Fabricated Using Micro Bubbles as Templates

The present chapter focuses on the effects of the initial PLA concentration, addition of PVA to the aqueous medium, and PLA molecular weight on the radius distribution of the hollow PLA microcapsules. The results show that a low initial concentration of PLA, the addition of PVA, and low molecular weight PLA are required to form uniform hollow microcapsules. It is suggested that these factors reduce the energy barrier at the liquid–liquid interface; this allows the PLA-covered microbubbles to pass smoothly through the interface. Furthermore, the release of the microbubbles from the dichloromethane droplets was observed through a microscope and the relationship between the uniformity of the hollow PLA microcapsules and the bubble-release mechanism was clarified.

1. Introduction

Ultrasound is the most versatile, non-invasive, low-cost, and low-risk real-time imaging technique to visualize the condition of internal tissues. However, despite its widespread application, the capabilities of this method are hindered by a lack of effective ultrasound contrast agents. [1, 2]. Contrast agents are used to alter the image contrast to improve the diagnostic yield, thereby enabling physicians to easily and clearly distinguish between normal and abnormal conditions. [3]

Microbubbles can potentially be used as echo enhancers. [4, 5, 6, 7] However, if microbubbles are to be used as standalone ultrasound contrast agents, several issues must be addressed. They have a short

lifespan in the system, which is further shortened in the presence of an ultrasound field. [8-12]In addition, microbubbles must be in the size range of 1–4 μm to easily pass through the capillary blood circuit and ensure a long circulation time before they completely drain into the liver. [13]Yet, it is difficult to control the size of microbubbles. Furthermore, it is vital for microbubbles to be uniformly sized in order to attain a narrow backscatter signal.

The aforementioned limitations were overcome by functionalizing the microbubbles with a PLA shell via the bubble template method. Furthermore they were single void. These two characteristics are highly desirable as stated in the Introduction Chapter of this thesis. Thus, if the potential applications are considered, they could be suitable for DDS and ultrasound contrast agents.

This chapter focuses on tuning the size of the capsules introduced in Chapter 2. This is, while achieving high uniformity, it was desired to (1) vary the microcapsule sizes and (2) determine the optimum conditions at which the highest uniformity is attained (even though the produced capsule is within the medical size constraint and from that alone the manufactured capsules in chapter 2 are already considered uniform). For these purposes, the effects of the initial PLA concentration, addition of PVA to the aqueous medium, and PLA molecular weight on the radius distribution of the fabricated hollow PLA microcapsules were studied. Furthermore, a discussion of the bubble release mechanism of the hollow PLA microcapsule is presented.

2. Experimental Methods

2.1 Chemicals

The polymeric shell material comprised PLA with molecular weights of 2, 45, and 100 kDa (PolyScience, Niles, IL, USA), dichloromethane of 99.99% purity (Wako, Osaka, Japan), and aqueous phase 2% (w/w) PVA (Gohsenal T-350, Nippon Gohsei, Osaka, Japan). All the chemicals used in this study were reagent grade. Water from a Milli-Q Advantage A10 water purification system was used.

2.2 Method

The synthesis method employed in this study is the same as that described in Chapter 2. In a glass dish with 2% (w/w) PVA aqueous solution, several 1mm radius size droplets of a solution of PLA (MW = 2 kDa) in CH_2Cl_2 were placed via microsyringe. Immediately, after droplet formation, CH_2Cl_2 diffuses into the surrounding aqueous phase and thus this yields to microbubble nucleation inside the droplet. These bubbles are covered with PLA and then spontaneously released from the droplets interior. After the capsules were fabricated, they were collected, purified and dried. During the purification of the microcapsule solution, Millipore water at 313 K was employed to remove

absorbed PVA from the capsule shell. The hollow PLA microcapsules were dried in a desiccator at 0.7 kPa for 36 h. Silica gel was used as a desiccant. The final product of hollow PLA microcapsules had a white powder appearance. It is worth to mention that the shells of the obtained hollow PLA microcapsules were sufficiently solid to retain their forms in the dry condition.

Attempts were made to control the capsule size distribution by changing one of the following three parameters: (1) the initial PLA concentration of the dichloromethane solution, (2) the concentration of PVA in the aqueous medium, and (3) the PLA molecular weight. To assess the effect of each parameter on the final capsule size, several bright-field and fluorescent images of the dried hollow PLA microcapsules were obtained using an inverted microscope (ECLIPSE Ti-E, Nikon Corporation, Tokyo, Japan). To determine the effect of the initial PLA concentration, 1, 2, 3, 4, 5, 6, 7, 10, and 20 g L^{-1} dichloromethane solutions of 2 kDa PLA were prepared. To clarify the effect of the addition of PVA, pure water and a 2% (w/w) PVA aqueous solution as the surrounding aqueous medium were employed. The initial PLA concentration was 2 g L^{-1} and a 2 kDa PLA was employed in this experiment. Additionally, dichloromethane solutions of 2, 45, and 100 kDa PLA were prepared to assess the effect of the molecular weight of PLA. In this experiment, the initial concentration of PLA was set at 2 g L^{-1} and hollow PLA microcapsules were fabricated both in a 2% (w/w) PVA aqueous solution and in pure water. All experiments were performed at room temperature and atmospheric pressure.

3. Results

3.1 Effect of initial PLA concentration

Previously in Chapter 2, [14] the effect of the initial PLA concentration was investigated to determine the conditions required for the release of the PLA-covered microbubbles from the droplets. The results showed that the release of the bubbles began when the PLA concentration of the dichloromethane solution surpassed 0.5 g L^{-1} regardless of the initial concentration. However, the sizes of the fabricated hollow PLA microcapsules were not evaluated. In this chapter, the initial concentration of 2 kDa PLA in dichloromethane was varied to analyze its effect on the final microcapsule size. Figure 3.1 shows the mean inner and outer radii of the hollow PLA microcapsules fabricated in the 2% (w/w) PVA aqueous solution.

Although the data were scattered, it was found that the outer and inner radii decreased with an increase in the initial PLA concentration. The thickness of the microcapsule shell also decreased with an increase in the initial PLA concentration.

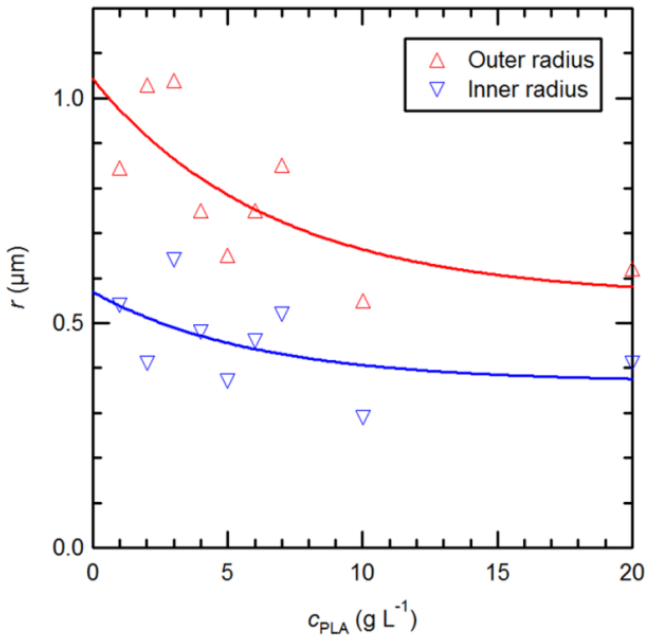

Figure 3.1: Mean inner and outer radii of hollow PLA microcapsules in PVA. Capsules were fabricated in a 2% (w/w) PVA aqueous solution as a function of the initial PLA concentration.

Table 3.1: Measured capsule radius as a function of the initial PLA concentration. The molecular weight of PLA was 2 kDa and the aqueous medium was a 2% (w/w) PVA aqueous solution.

PLA conc. (g L^{-1})	Radius	Mean radius (µm)	Standard dev. (µm)	PI (%)
1	Outer	0.84	0.24	28.57
	Inner	0.54	0.20	37.03
2	Outer	1.03	0.07	7.710
	Inner	0.41	0.04	10.25
3	Outer	1.04	0.06	5.760
	Inner	0.64	0.08	12.50
4	Outer	0.75	0.16	21.61
	Inner	0.48	0.15	32.12
5	Outer	0.65	0.14	21.53
	Inner	0.37	0.12	32.43
6	Outer	0.75	0.23	30.60
	Inner	0.46	0.15	32.60
7	Outer	0.85	0.21	24.70
	Inner	0.52	0.16	30.76
10	Outer	0.55	0.21	38.18
	Inner	0.29	0.13	44.82
20	Outer	0.62	0.24	38.70
	Inner	0.41	0.20	48.78

The mean values, standard deviations, and polydispersity indices (PI = standard deviation/mean) of the outer and inner radii are summarized in Table 3.1. The PI values of the outer and inner radii were around 10% when the initial PLA concentration was either 2 or 3 g L^{-1}, which suggests that hollow PLA microcapsules fabricated under these conditions were highly uniform.[15]

These results suggest that the initial PLA concentration should be much less than 5 g L^{-1} to delay the release of the bubbles until the dissolving PLA molecules adsorb on the nucleated bubble surface. When the initial PLA concentration was too high, the dissolving PLA adsorbed on the interface between the droplet and the surrounding aqueous medium thus preventing the bubbles from passing smoothly through the interface. On the other hand, when the initial PLA concentration was too low, the PI value increased, which suggests that the bubbles were not effectively covered with PLA.

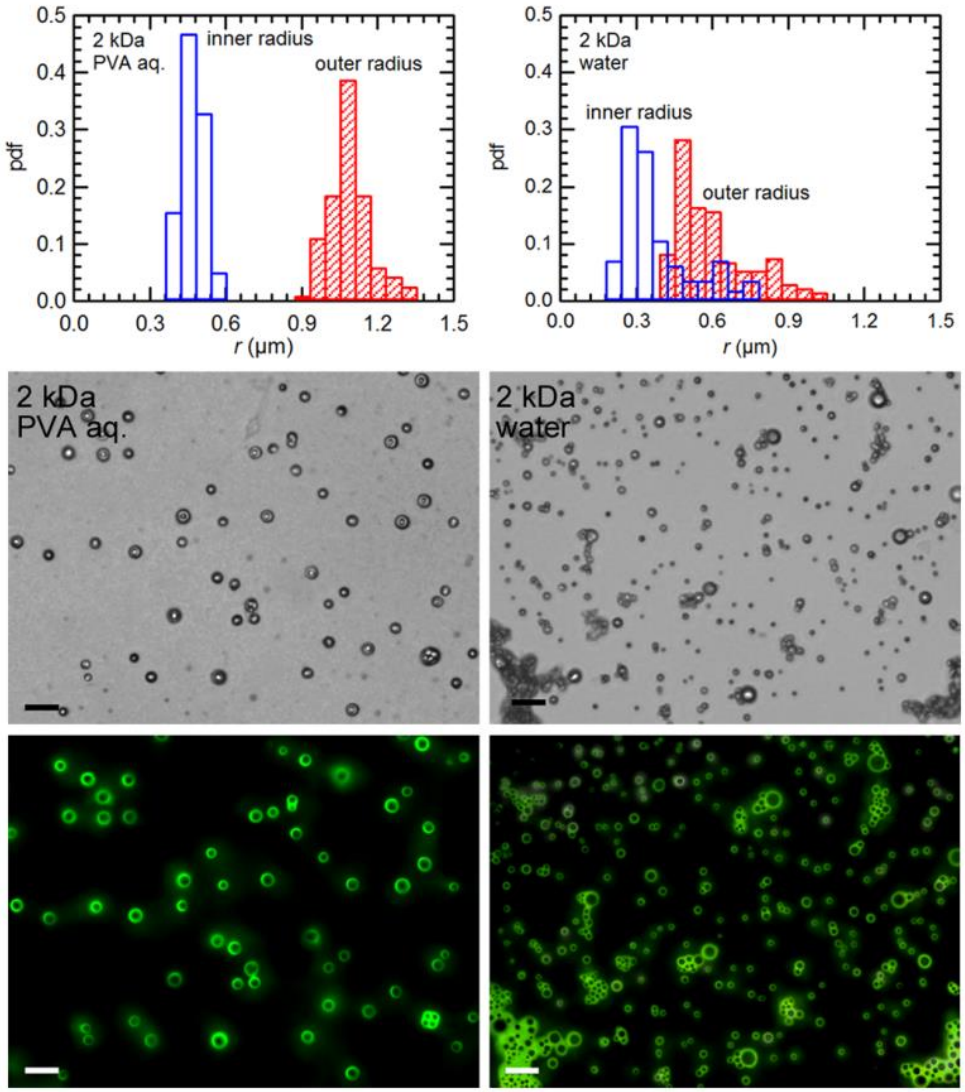

Figure 3.2: Microcapsule size distribution (top) and typical bright field (middle) and fluorescent (bottom) images of the hollow PLA microcapsules fabricated in a 2% (w/w) PVA aqueous solution (left) and water (right). The initial PLA concentration was 2 g L^{-1} and the PLA molecular weight was 2 kDa. The scale bar is 5 μm long.

3.2 Effect of PVA

Figure 3.2 shows the probability density function and typical bright-field and fluorescent images of hollow PLA microcapsules fabricated in either a 2% (w/w) PVA aqueous solution or water. The initial PLA concentration was 2 g L^{-1} and the PLA molecular weight was 2 kDa.

The inner and outer radii of the hollow PLA microcapsules fabricated in water were smaller than those fabricated in the 2% (w/w) PVA aqueous solution. In addition, the standard deviation of the radii of the microcapsules was larger when they were fabricated in water rather than in the 2% (w/w) PVA aqueous solution.

In Chapter 2, a 2% (w/w) PVA aqueous solution as a continuum medium was employed to prevent the droplets of dichloromethane from coalescing due to the surface active properties of PVA on the droplet surface. Figure 3.2 shows that hollow PLA microcapsules can be formed in both 2% (w/w) PVA aqueous solution and water; thus, the addition of PVA is not required to form the microcapsules, although it does affect the capsule size distribution.

3.3 Effect of PLA molecular weight

Figure 3.3 shows the probability distribution for the hollow PLA microcapsules manufactured using three different molecular weights of PLA (i.e., 2, 45, and 100 kDa) fabricated in either 2% (w/w) PVA aqueous solution or water. The initial PLA concentration was 2 g L^{-1}. The measured inner and outer radii of these hollow PLA microcapsules are summarized in Table 3.2.

Table 3.2: Measured inner and outer radii of the hollow PLA microcapsules. The initial PLA concentration of the dichloromethane solution was 2 g L^{-1}.

MW of PLA & type of aqueous medium	Radius	Mean (μm)	Standard dev. (μm)	PI (%)
2 kDa in 2% (w/w) PVA aq.	Outer	1.03	0.08	7.7
	Inner	0.41	0.04	10.3
45 kDa in 2% (w/w) PVA aq.	Outer	0.58	0.15	26.7
	Inner	0.36	0.13	37.8
100 kDa in 2% (w/w) PVA aq.	Outer	0.58	0.14	25.0
	Inner	0.36	0.07	20.1
2 kDa in water	Outer	0.55	0.15	27.5
	Inner	0.32	0.14	43.3
45 kDa in water	Outer	0.57	0.13	23.2
	Inner	0.37	0.13	34.7
100 kDa in water	Outer	0.65	0.17	26.0
	Inner	0.39	0.13	33.4

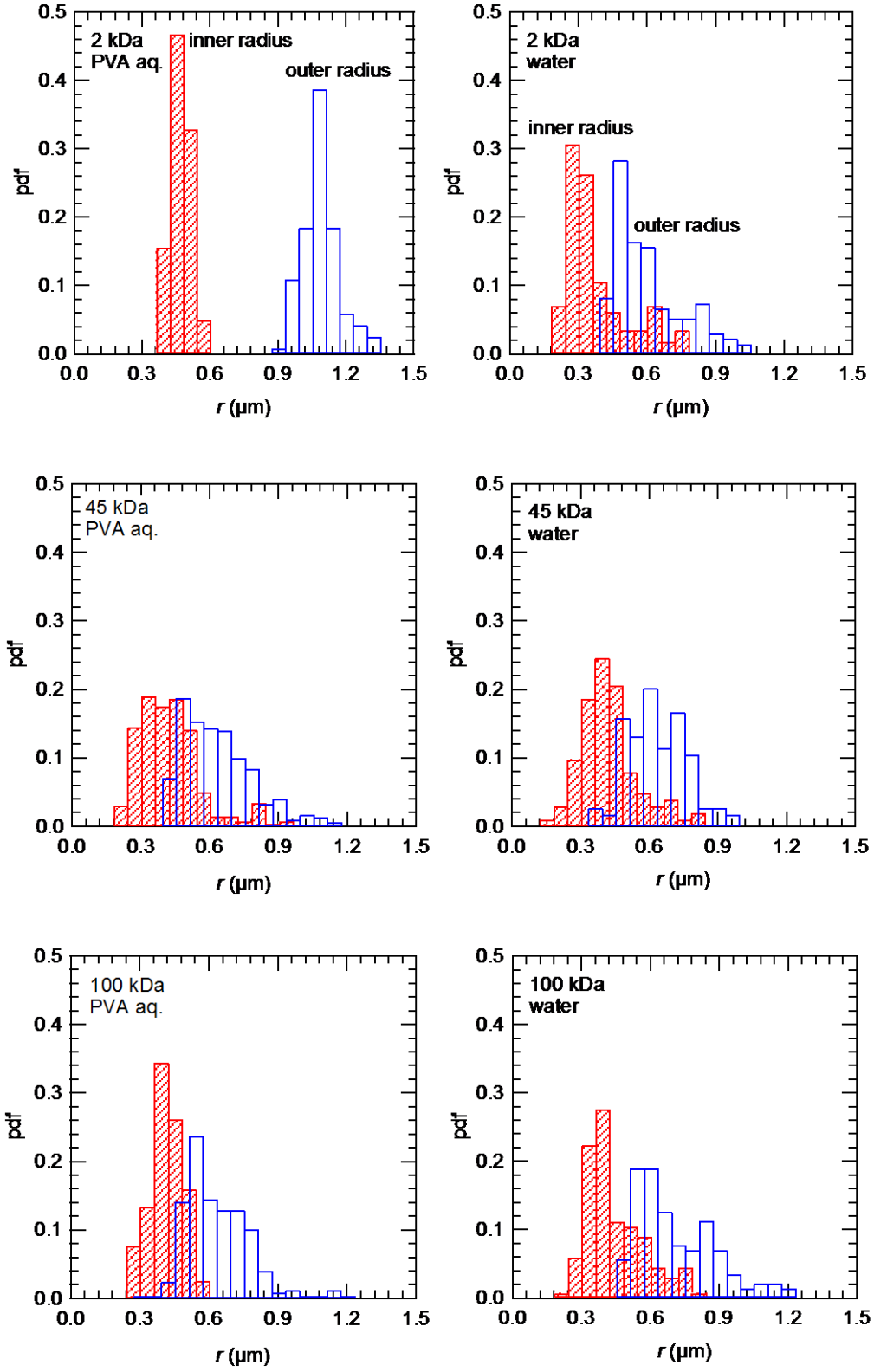

Figure 3.3: The effect of surfactant and molecular weight on capsule size. The microcapsule size distribution (PDF) of hollow PLA microcapsules of different molecular weights: 2 kDa (top), 45 kDa (middle), and 100 kDa (bottom), fabricated in either a 2% (w/w) PVA aqueous solution (left) or water (right). The initial PLA concentration was 2kDa.

Figure 3.4 shows the corresponding typical bright-field images. In 2% (w/w) PVA aqueous solution, the outer radius and shell thickness of the hollow PLA microcapsules decreased and the uniformity deteriorated as the molecular weight increased. PLA microparticles, in addition to hollow PLA microcapsules were produced at molecular weights of 45 and 100 kDa. However, the fabricated microcapsules showed high PI values regardless of the molecular weight.

It was observed that the number of PLA microparticles and aggregates of hollow PLA microcapsules increased with increased molecular weight.

These results indicate that the addition of PVA and low molecular weight PLA yielded large and highly uniform hollow PLA microcapsules. Among the six conditions shown in Figures 3.3 and 3.4, the uniformity of the hollow PLA microcapsules was only very high when the PLA molecular weight was 2 kDa and the aqueous medium was 2% (w/w) PVA aqueous solution.

Additionally, using these conditions very few micro particles and aggregates of hollow microcapsules were observed. This indicates that the mechanism of capsule shell formation depends on the PLA molecular weight as well as the addition of PVA.

4. Discussion

4.1 Observation of microbubble release from the dichloromethane droplet

In the bubble-template method, the size and uniformity of the fabricated PLA microcapsules should correlate with the bubble release mechanism. First, the release of the microbubbles from the dichloromethane droplets was observed through a microscope; two typical snapshots are shown in Figure 3.5. As shown in Figure 3.5a, each microbubble independently appeared on the droplet surface, detached from the surface, and moved into the aqueous medium. This mechanism was observed under most experimental conditions.

However, the PLA-covered microbubbles are smoothly released from the interior with a low initial concentration of PLA, the addition of PVA, and a low molecular weight of PLA. Except for under these experimental conditions, as dichloromethane diffuses from the droplet into the surrounding aqueous medium the droplet shrinks and a high-PLA-concentration region grows at the liquid–liquid interface. Thus, when the microbubbles reach the interface, they stay there. Since the bubbles keep nucleating as a result of solvent diffusion, more and more bubbles aggregate. Under these conditions, the release of microbubbles shown in Figure 3.5b was observed. The shadow in the aqueous medium reflects the differences in density, that is, dichloromethane flow from the droplet is accompanied with microbubble emission. From these two images, the bubble-release mechanism can be classified as either single-bubble release due to solvent evaporation (Figure 3.5a) or multiple-

bubble release as a result of bubble eruption (Figure 3.5b). The first mechanism is required for the fabrication of uniformly sized hollow PLA microcapsules.

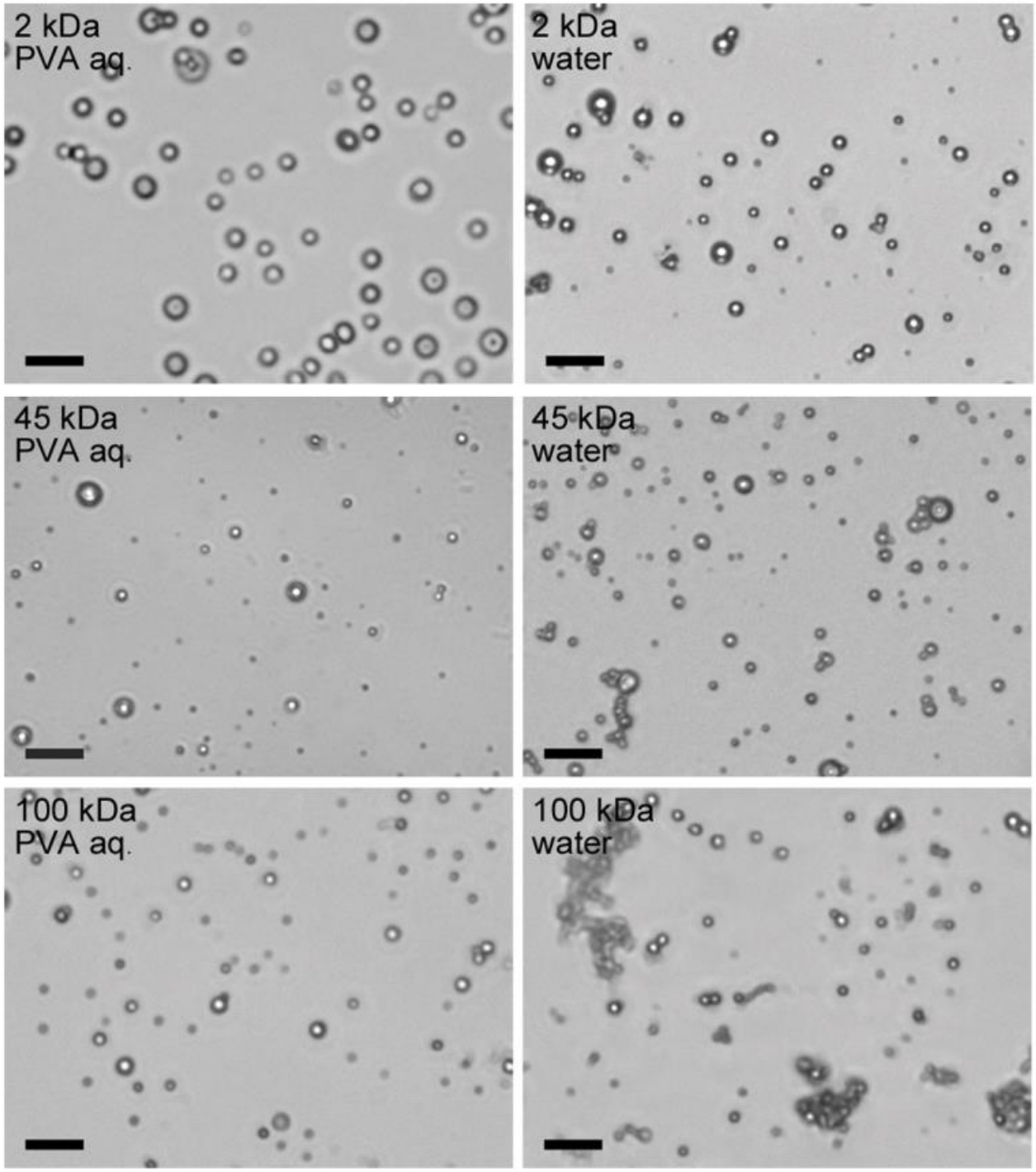

Figure 3.4: Typical bright field images of hollow PLA microcapsules. Different molecular weights, i.e., 2 kDa (top), 45 kDa (middle), and 100 kDa (bottom) were employed to fabricate in a 2% (w/w) PVA aqueous solution (left) and water (right). The initial PLA concentration was 2 g L^{-1}. The scale bar is 5 μm long.

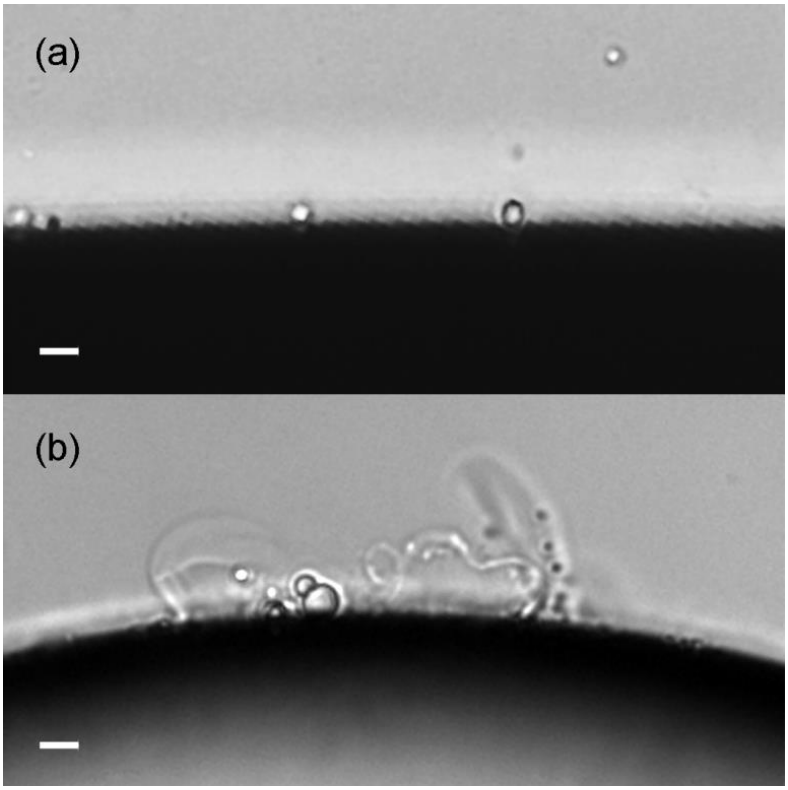

Figure 3.5: Two release mechanisms of microbubbles. (a) single-bubble release as a result of solvent evaporation and (b) multiple-bubble release as a result of bubble eruption. The initial PLA concentrations of the dichloromethane solutions are (a) 2 and (b) 20 g L^{-1}. The PLA molecular weight was 2 kDa and the surrounding aqueous medium was 2% (w/w) PVA aqueous solution in both cases. The scale bar is 10 μm long.

4.2 Microbubble release mechanism

To quantitatively discuss the bubble-release mechanism, the interfacial tension, droplet reduction rate, and viscosity were measured. The interfacial tensions were measured by the pendant drop method using the Drop Master Series DM-501 (Kyowa Interface Science, Japan) (see Supporting Information S1) and are summarized in Table 3.3. The measured interfacial tensions between dichloromethane–water and dichloromethane–2% (w/w) PVA aqueous solution were 2.81×10^{-2} and 1.94×10^{-2} N m^{-1}, respectively, at 298 K. This result suggests that PVA adsorbed on the interface between the droplet and the surrounding aqueous medium resulting in decreased the interfacial tension.[19]

If a 2 g L^{-1} PLA (2 kDa) dichloromethane solution was employed instead of pure dichloromethane, the measured interfacial tensions slightly decreased, as shown in Table 3.3. Although the effect of PLA on the interfacial tension was small, the PLA reduced the diffusivity of dichloromethane into the surrounding aqueous medium, which was confirmed by the difference of the size reduction rate of the droplets (Appendix 2). Therefore, the addition of PLA creates a more stable liquid-liquid

Table 3.3: Measured interfacial tensions between the liquid–liquid interfaces at 298 K.

Liquid–liquid interface	Interfacial tension (N m^{-1})
Dichloromethane–water	0.0281
Dichloromethane–2% (w/w) PVA aqueous solution	0.0194
2 g L^{-1} PLA (2kDa) dichloromethane solution–water	0.0269
2 g L^{-1} PLA (2kDa) dichloromethane solution–2% (w/w) PVA aqueous solution	0.0189

interface. Furthermore, the viscosity of polymer solutions generally increases with increasing polymer concentration and polymer molecular weight.[16]

It was confirmed that the viscosity of the PLA dichloromethane solutions increased with increasing PLA concentration and PLA molecular weight by measuring the viscosity of the solutions using a tuning fork vibration viscometer (SV-10, A&D Company, Japan) (Appendix 2). The measured viscosity of dichloromethane was 0.43×10^{-3} Pa s at 298 K. Upon the addition of 2 kDa PLA, the measured viscosities at 298 K were 0.47×10^{-3} and 1.07×10^{-3} Pa·s for concentrations of 2 and 70 g L^{-1}, respectively (see Supporting Information S3).

To explain the bubble release mechanism at the liquid-liquid interface, the following must be proven:

(1) A droplet has sufficient potential energy for continuous bubble release
(2) A force sufficient to break the interfacial tension can be produced at or near the interface

Assuming that a bubble is spherical with a radius of r_0, the energy required for a single bubble to pass through the interface is given by the following equation:

$$E_0 = \pi r_0^2 \gamma , \tag{3.1}$$

where γ is the interfacial tension at the liquid–liquid interface. The potential energy of a droplet of a dichloromethane solution of PLA is equivalent to the energy of the buoyancy of the bubbles when the dissolved air is nucleated. Assuming that the droplet is spherical with a radius of r and bubbles initially nucleate at the center of the droplet and then elevate to the top of the droplet, the potential energy of a single bubble due to buoyancy is given by

$$E_1 = \rho g r \times \frac{4}{3} \pi r_0^3 , \tag{3.2}$$

where ρ is the liquid density and g is gravitational acceleration. Since the volume ratio of dissolved air to dichloromethane is about 0.13,[17] the volume of dissolved air inside the droplet is $0.13 \times 4/3\pi r^3$. If the droplet shrinks by n times, the total volume of the nucleated bubbles is $(1-1/n) \times 0.13 \times 4/3\pi r^3$; thus, the total number of nucleated bubbles is

$$N = \left(1 - \frac{1}{n}\right) \times 0.13 \times \left(\frac{r}{r_0}\right)^3. \tag{3.3}$$

From Equation (2) and (3, the total potential energy of a droplet of dichloromethane solution of PLA is

$$E_N = NE_1 = \left(1 - \frac{1}{n}\right) \times 0.13 \times \frac{4}{3}\pi\rho g r^4. \tag{3.4}$$

Assuming that r_0 is 10^{-6} m, r is 5.0×10^{-4} m, γ is 2.0×10^{-2} N m^{-1}, ρ is 1.33×10^3 kg m^{-3}, and g is 9.8 m^2 s^{-1}, E_0 and E_N are calculated to be 6.28×10^{-14} J and $(1-1/n) \times 4.43 \times 10^{-10}$ J, respectively. Thus, if n = 2, E_N is 3.5×10^3 times larger than E_0. Therefore, the potential energy of a droplet of dichloromethane solution of PLA is large enough for single-bubble release.

The average pressure inside a dichloromethane droplet should equilibrate with the pressure of the surrounding aqueous medium, but, for single-bubble release, the local and instantaneous pressure around a bubble must be larger than the equilibrium pressure. The required pressure difference is given by

$$\Delta p = \frac{2\gamma}{r_0}. \tag{3.5}$$

Assuming that r_0 is 10^{-3} m, Δp was calculated to be 53.8 Pa and 37.8 Pa for γ = 2.69×10^{-2} and 1.89×10^{-2} N m^{-1}, respectively. During the microscopic observations, a circulation flow, which had a maximum velocity in the order of 10^{-4} m s^{-1}, was generated inside the dichloromethane droplets due to the buoyancy of the nucleated bubbles. The Reynolds number for this flow can be estimated to be Re = u (velocity) × r_0 (bubble radius) × η (viscosity) $^{-1}$ × ρ (density) = 10^{-5} m s^{-1} × 10^{-6} m × (10^{-3} Pa s)$^{-1}$ × 10^3 kg m^{-3} = 10^{-5}, which suggests that Stokes flow can be assumed. In fact, when single-bubble

release occurred, no turbulence was observed. Assuming that the dichloromethane droplet is spherical and the dichloromethane flows up along the vertical axis and then down along the circumference from the top to the bottom of the sphere, if the flow in the circumferential direction constantly decelerates, pressure is generated in the radial direction. The pressure in the radial direction can be approximately estimated using the following Stokes equation:

$$\frac{dp_r}{dr} = -\eta \frac{2}{r^2} \frac{du_\theta}{d\theta}, \tag{3.6}$$

where η is the viscosity of the solution, r is the radius of the droplet, θ is the inclination angle, and u_θ is the velocity in the inclination angle direction. It is required to focus on the force balance in a small portion of the outermost spherical shell (i.e., dr, $rd\theta$, $rd\varphi$, where φ is azimuth angle). Assuming that η is 10^{-3} Pa s, r is 10^{-4} m, dr is 10^{-5} m, and $(du_\theta / rd\theta) = -(10^{-5}$ m s^{-1} / 10^{-5} m), dp_r is calculated to be 2×10^{-4} Pa, which is far smaller than the pressure difference required for single-bubble release. Even if the pressure in the radial directions integrated over the surface of the droplet is focused on a single bubble, the pressure affecting a single bubble is calculated to be 8 Pa ($dp_r \times \left(4\pi r^2 / \pi r_0^2\right)$). The radial pressure created by deceleration of circular flow does not reach the required pressure difference. However, in a real system, many bubbles are distributed at the liquid–liquid interface. In such conditions, the bubbles interact with each other and the local and instantaneous pressure affecting each bubble may overcome the pressure required for single-bubble release. The repulsive force between two adjacent bubbles is generally quite large. Furthermore, the deformation of bubbles and the squeezing flow between bubbles may change the direction of a bubble with respect to the aqueous medium.[19] To clarify this release mechanism, it is necessary to make a model of the bubble dynamics at the liquid–liquid interface.

Another possible mechanism for single-bubble release is the imbalance of interfacial tensions around a bubble during the diffusion of dichloromethane into the surrounding aqueous medium. Figure 3.6 shows a schematic of the interfacial tensions at the triple phase interface between an aqueous phase (a), an organic phase (o), and a gas phase (g). The water–air, $\gamma_{w\text{-}air}$, and dichloromethane–air, $\gamma_{d\text{-}air}$, interfacial tensions are 7.18×10^{-2} and 2.72×10^{-2} N m^{-1}, respectively, at 298 K. However, in a real system, water containing PLA, dichloromethane, and PVA is in contact the mixture of air and dichloromethane gas at the interface between the aqueous phase and gas phase. On the other hand, dichloromethane containing PLA and water is in contact with the mixture of air and dichloromethane gas at the interface between the organic phase and gas phase. Therefore, $\gamma_{w\text{-}air} > \gamma_{a\text{-}g}$

> $\gamma_{o\text{-}g}$ > $\gamma_{d\text{-}air}$. When the top part of a bubble is exposed to the aqueous phase (left schematic in Figure 3.6), $\gamma_{a\text{-}o}$ is in the tangential direction of a droplet. Because $\gamma_{a\text{-}g}$ > $\gamma_{o\text{-}g}$, the bubble moves toward the aqueous phase. As this occurs, the direction of $\gamma_{a\text{-}o}$ goes downward (right schematic in Figure 3.6).

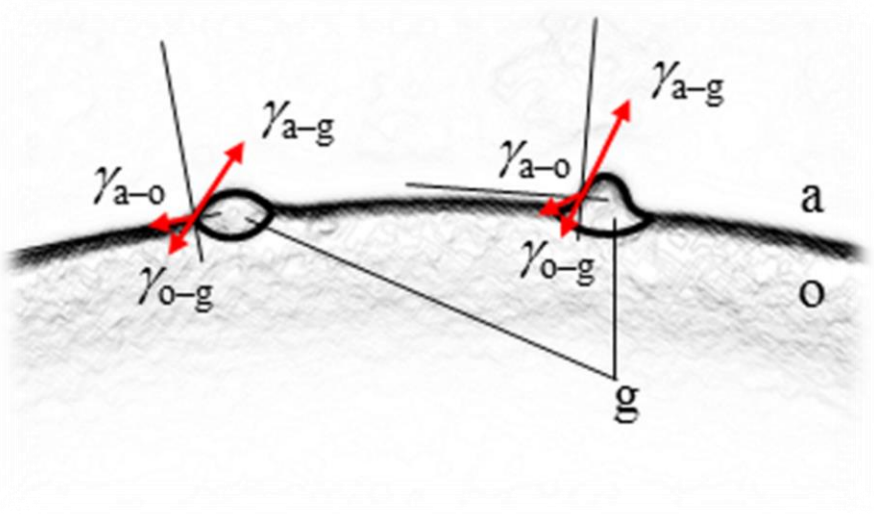

Figure 3.6: Schematics of the interfacial tensions around the bubbles at the triple phase interface between the aqueous phase (a), organic phase (o), and gas phases (g).

However, because the dichloromethane concentration decreases in the aqueous phase, $\gamma_{a\text{-}g}$ increases causing the bubble to still move toward the aqueous phase. To elucidate this release mechanism, it is necessary to predict the interfacial tensions at the triple phase interface by considering the local PLA shell properties.

4.3 Size control using the bubble template method

It is noted that even if the release mechanism is single-bubble release as a result of solvent evaporation (Figure 3.5a), the fabricated hollow PLA microcapsules are smaller than the template microbubbles. Assuming that all of the dichloromethane gas diffuses into the aqueous medium and only air gas remains in the template bubbles, the fabricated hollow PLA microcapsules are still smaller than the template air bubbles. It is possible that the size of the hollow capsules depends on some structural and dynamic properties of the shell materials in addition to the size of template microbubbles. Inside the droplets, the PLA chain configuration is swollen because dichloromethane is a good solvent, while in the surrounding aqueous medium, the PLA chain configuration is globular.[19–21] Therefore, when the microbubbles covered with PLA pass through the interface, the PLA chain configuration changes to form coils. As a result, the possible surface area covered with the PLA coils decreases yielding smaller hollow PLA microcapsules. Furthermore, if PVA is present in the aqueous medium, it hinders the interactions between PLA and water.[16,18-23] In particular, the

hydrophobic segment of PVA adsorbs onto PLA, which reduces the direct interactions between PLA and water and prevents the PLA capsule shell from shrinking.

In the bubble template method of hollow microcapsules, the bubble dynamics and material properties strongly correlate. In general, the size and uniformity of the capsules depend on bubble dynamics, whereas the shell properties depend on material properties. However, these two cannot be completely separated. In this study, the factors that affect the size and uniformity of the fabricated hollow PLA microcapsules and the relationship between the uniformity of the hollow PLA microcapsules and the bubble-release mechanism were clarified. However, further investigations of the bubble dynamics at the liquid–liquid interface and the structural and dynamic properties of PLA and PVA are needed to completely understand how the PLA-covered microbubbles are released from the droplets into the surrounding aqueous medium and, as a consequence, how the solidification of the PLA soft shell proceeds.

5. Conclusion

To precisely control the size of the hollow PLA microcapsules fabricated using the bubble template method, the effect of the initial PLA concentration, the addition of PVA to the aqueous medium, and PLA molecular weight on the capsule radius distribution were investigated. In addition, the relationship between the uniformity of the hollow PLA microcapsules and the bubble release mechanism were clarified. The following conclusions were drawn from this study: (1) The initial PLA concentration should be within 2–3 g L^{-1}, which is much lower than the PLA concentration at which the release of bubbles starts, in order to delay release until the dissolving PLA molecules adsorb on the nucleated bubble surface; (2) PVA should be added to the surrounding aqueous medium as a surfactant; and (3) PLA with a low molecular weight should be used. In view of the above three conclusions, the bubble-release mechanism can be classified as either single-bubble release as a result of solvent evaporation or multiple-bubble release as a result of bubble eruption. The first mechanism is required for the fabrication of uniformly-sized hollow PLA microcapsules. The bubble release mechanism remains to be fully elucidated. Further investigations on the bubble dynamics at the liquid–liquid interface and the structural and dynamic properties of PLA and PVA are needed to completely understand the bubble release mechanism.

6. References

1. Shutt, E.; Klein, D. H.; Mattrey. R.; Riess, J. G., Inyectable Microbubbles as Ultrasound Contrast Agents for Diagnostic Ultrasound Imaging:The Key Role of Perfluorochemicals, *Angewandte Chemie* **2003,** *42,* 3218-3235.
2. Wheatley, M. A.; Schrope, B.; Shen, P., Contrast Agents for Diagnostic Ultrasounds: development and Evaluation of Polymer Coated Microbubbles, *Biomaterials* **1990,** *11,* 713–717.
3. Calliada, F.; Campani, R.; Bottinelli, O.; Bozzini, A.; Sommaruga, M. G., Ulrasound contrast Agents: Basic

Principles, *European Journal of Radiology* **1998,** *27,* S157–S160.

4. Ophir, J.; Parker, K. J. J. Contrast Agents in Diagnostic ultrasound, *Ultrasound Medical Biology* **1989,** *15,* 319-333.
5. Lin, P.; Eckersly, R.; Hall, E., Ultrabubble : A Laminated Ultrasound Contrast Agent with Narrow Size Range, *Advanced Materials* **2009,** *21,* 3949-3952.
6. Lathia, J. D.; Leodore, L.; Wheatley, M. A. Polymeric Contrast Agents with Targeting Potential*, Ultrasonics* **2004,** *42,* 763-768.
7. Wheatley, M. A.; Forsberg, F.; Oum, K.; Ro, r.; El-Sherif, D., Comparison of in vitro and in vivo acoustic response of a novel 50:50 PLGA contrast agent, *Ultrasonics* **2006,** *44,* 360-367.
8. Ferrara, K.; Pollard, R.; Borden, M. Ultrasound Microbubble Contrast Agents: Fundamentals and Application to Gene and Drug Delivery, *Modern Annual Reviews in Biomedical engineering* **2007,** *9,* 415-447.
9. Plesset, M. S.; Sadhal, S. S., On the stability of Gas Bubbles in Liquid Gas Solutions, *Applied Science Research* **1982,** *38,* 133-141.
10. Kabalnov, A.; Bradley, J.; Flaim, S.; Klein, D.; Pelura, T.; peters, B.; Otto, S.; Reynolds, J.; Schutt, E.; Weers, J. Dissolution of multicomponent Microbubbles in the Blood Stream: 2 Experiment, *Ultrasound Medical Biology* **1998,** *2,* 751-760.
11. Leighton, T. G. *The Acoustic Bubble,* 1st ed.; Academic Press: London, 1997.
12. Shchukin, D. G.; Kohler, K.; Mohwald, H.; Sukhorukov, G. B. Gas Filled Polyeelctrolyte Microcapsules, *Agewandte Chemie International Edition* **2005,** *44,* 3310-3314.
13. Lin, P.; Eckersley, R.; Hall, E., Ultrabubble: A Laminated Ultrasound Contrast Agent with Narrow Size Range *Advanced Materials* **2009,** *21,* 3949-3952.
14. Daiguji, H.; Takada, S.; Molino, J. J.; Takemura, F., Fabrication of hollow poly(lactic acid) microcapsules from microbubble templates, *Journal of Physical Chemistry B* **2009,** *2009,* 15002-15009.
15 Molino, J.J; Daiguji, H.; Takemura, F.; Factors affecting the size and uniformity of hollow poly(lactic) acid microcapsules fabricated from microbubble templates, *Journal of Physical Chemistry B* **2011**, *115*, 13828-13828
16. Rubinstein, M.; Colby, R. *Polymer Physics,* 1st ed.; Oxford University Press: Oxford,UK, 2003.
17. Shirono, K.; Morimatsu, T.; Takemura, F., Gas Solubilities (CO2, O2, Ar, N2, H2, and He) in Liquid Chlorinated Methanes, Journal of Chemical engineering Data, **2008**, 53, 1867–1871.
18. Kozlov, M.; Quarmyne, M.; Chen, W.; McCarthy, T. J., Adsorption of Polyvynilc Alcohol onto Hydrophobic Substrates: A general Approach for Hydrophilyzing and Chemically Activating Surfaces, *Macromolecules* **2003,** *36,* 6054-6059.
19. Kozlov, M.; McCarthy, T. J., Adsorption of Poly(Vynil Alcohol) from Water to a Hydrophobic Surface: Effects of Molecular Weight, Degree of Hydrolysis, Salt, and Temperature, *Langmuir* **2004,** *20,* 9170-9176.
20 Sugiyama, K; Takemura, F. J., On the lateral migration of a slightly deformed bubble rising near a vertical plane wall, *Journal of Fluid Mechanics*, **2010**, 662, 209–231
21 Athawale, M. V.; Goel, G.; Ghosh, T.; Truskett, T. M.; Garde, Effects of Lenghtscales and Attractions on the Collpase of Hydrophobic Polymers in Water, Proceedings of the National Academy of Sience U.S.A. **2007**, 104, 733–738
22 Jamadagni, S. N.; Godawat, R.; Dordick, J. S.; Garde, S., How interfaces affect hydrophobically driven polymer folding, J. Phys.Chem. B **2009**, 113, 4093–4101.
23 ten Wolde, P. R.; Chandler, D. Drying Induced Polymer Collapse, *Proceedings of the National Academy of Sience U.S.A.* **2002**,99, 6539–6543.

4

The Effect of PLA on the Microbubble Size

The effect of PLA concentration, c_{PLA}, on the final microbubble size was investigated by measuring the decrease in pressure due the absorption of N_2 into different solutions of PLA in dichloromethane in the temperature range between 15-30 °C. For a given droplet size, the correlation of the Henry's law constant to the average bubble size was experimentally determined and on the basis of the measurements, a final semi empirical correlation for the dependence of the Henry's law constant on c_{PLA} was determined. The experimental results revealed that the solubility of nitrogen in the solutions increases as PLA concentration increases. This result suggests that a high c_{PLA} is a key towards achieving mass production.

1. Introduction

In the previous chapters, the conditions required for spontaneous microcapsule release from the droplet were determined. [1-3] Furthermore, the radius of the microbubble inside the droplet was 1 μm given that the PLA solution is initially diluted (c_{PLA} = 2 g L^{-1}) and made from a low-molecular-weight (2 kDa) PLA and a 2% (w/w) aqueous solution of poly(vinyl alcohol) (PVA). If these capsules were to be fabricated under conditions different than these, the resultant microcapsules were smaller and less uniform. This fabrication technique, although it yielded

highly uniform microcapsules, was not suitable for fabricating large microcapsules. Therefore Sakurai et al[3] introduced a new technique which is disclosed in Appendix 1. This technique required smaller droplets for larger bubbles to appear (i.e. the amount of air content is small). However, eventhough they attained bigger capsules (Gas/O/W method), uniformity was compromised.

In this chapter, special focus was given to the control of the size of the nucleated microbubble. For this purpose the effect of the parameters in the Laplace equation (e.g. the vapor pressure, and the surface tension at the gas liquid interface) on the bubble size were investigated. The measurements indicated that neither the vapor pessure nor the surface tension changed considerably to justify the size increment observed in the microbubbles as the polymer concentration increases. Therefore the theory developed by Ward et al[4]. for the stability of microbubbles (which is discussed extensively in Chapter 2) does not apply to the conditions where high viscosity and a high polymer concentration are present. Furthermore, it was found that the solubility of Nitrogen increases in the solution as the concentration of the polymer is increased. If the solubility of air also increases with the addition of the polymer, then it is possible to make more microbubbles and finally attain mass production.

Eventhough the microbubble radius was increased, the reasons for the dependance of the bubble radius on the concentration of PLA remain to be elucidated. Finally, the measured solubility data was analyzed to determine a semiempirical correlation between the concentration of PLA and the solubility of Nitrogen.

2. Experiment

2.1 Chemicals

The polymeric shell material comprised PLA with molecular weight of 2 kDa (Polysciences, Warrington, PA, USA) and the solvent was CH_2Cl_2 (99.99% purity, Wako Pure Chemical Industries, Ltd., Osaka, Japan)were employed. All the chemicals were of reagent grade.

2.2 Methods

To demonstrate the effect of the initial polymer concentration on the final microbubble size, different solutions of different concentrations of PLA in dichloromethane were prepared. Solutions of 2, 10, 20, and 50 g L^{-1} PLA in dichloromethane were prepared. The interfacial tensions at the liquid-liquid interface were measured by the pendant drop method using the Drop Master Series DM-501 (Kyowa Interface Science, Japan). Likewise, the surface tension at the gas-liquid interface for a bubble nucleated inside different solutions of PLA was also measured to determine the effect of c_{PLA}.

PLA solutions with a c_{PLA} of 0, 2, 10, 20, 30, 40, 50, 60 and 70 gL^{-1} were employed to measure the surface tension at the bubble-solution interface. The interfacial tension values were determined from at least 5 independently formed droplets and bubbles, respectively. The volume of the bubbles and droplets was kept constant and the interfacial tension was monitored for at least 10min. The temperature of the experiments was 298 K.

Furthermore, solutions with 10, 30, 50 and 70g L^{-1} dichloromethane solutions of 2 kDa PLA were prepared. These solutions were placed in a pressure vessel and were degassed to measure the vapor pressure following the same procedure as described by Shirono et al[5]. Afterwards, the solutions were pressurized using nitrogen to determine the solubility of nitrogen into the solutions. A schematic of the setup is shown in Figure 4.1. The total volume of the vessel was $7.892 \times 10^{-5} m^3$ and was calculated from the inner geometry of the vessel. The digital pressure indicator P1 is an AP-53A (Keyence, Japan), which range and resolution are $(0 - 1) \times 10^6$ Pa and 1×10^3 Pa, and the pressure indicator P2 is an AP-V85 (Keyence, Japan) which range and resolution is $(0 - 1) \times 10^5$ and 10Pa respectively. P2 was employed to measure the initial Vapor pressure of the solution after degassing. P2 was employed to measure the total pressure ($P_T = p_1'' + P2$), where p_1'' is the vapor pressure of the solution) in the vessel after applying Nitrogen. After vacuuming, the solutions were mechanically agitated and the pressure sensor was allowed to reach an equilibrium value.

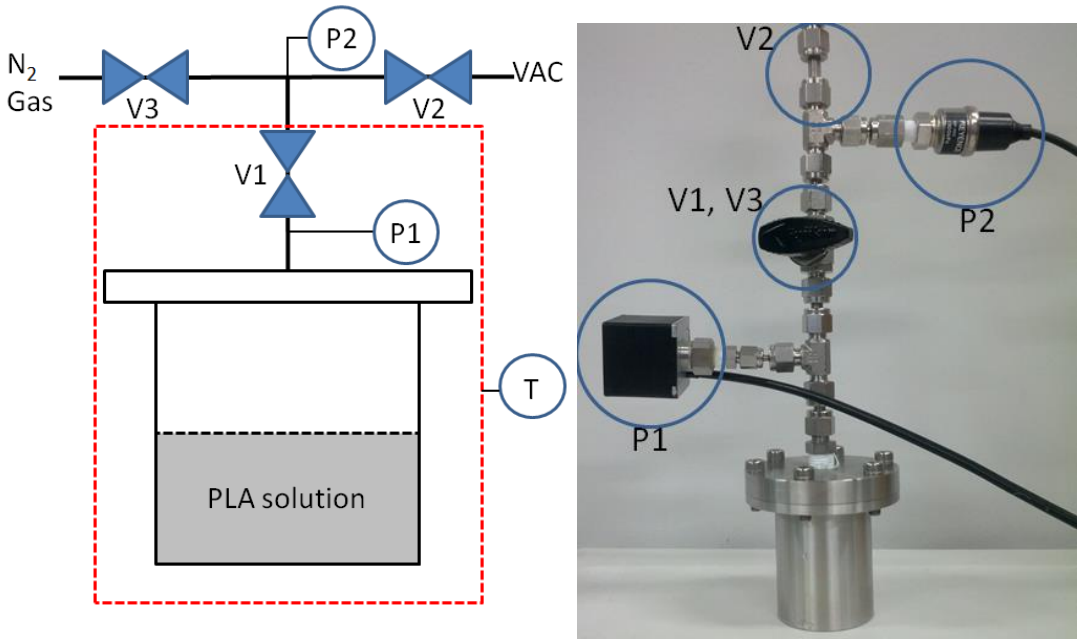

Figure 4.1: Schematic of the experimental setup to measure the vapor pressure and N_2 gas solubilities in different PLA solutions. V1, V2, and V3 are valves. P1 is the total pressure inside the vessel and P2 measures the initial vapor pressure.

The degassed sample was then pressurized with nitrogen and the initial total pressure , P_T was measured from P1. For this purpose valve 3 and 1 were open. After applying pressure valve 3 and 1

were closed. The pressure reading from P1 decreased as Nitrogen dissolved into the PLA solution. The vessel was shaken to enhance the dissolution of air in the vessel. The final pressure reading and the temperature were recorded. The vessel was placed into the thermostat and the pressure was recorded at different temperatures.

The gas solubility of Nitrogen in the PLA solution was calculated by determining the volume of the vapor and liquid phases, $V''$and V' which was measured by calculating the total volume of the pressure vessel, V, the total mole number of the solvent, N_1, at a given temperature, T, by using the following equation (Shirono et al)[5],

$$V = \frac{RT}{p_1''} n_1'' + \frac{M_1}{\rho_1^{sat}} n_1' \quad \text{for } n_1 = n_1' + n_1''$$

Where the universal gas constant, $R = 8.31 J \cdot K^{-1} \cdot mol^{-1}$, $M_1(kg \cdot mol^{-1})$ is the molecular weight of the dichloromethane ($84.93 \times 10^{-3} kg \cdot mol^{-1}$); P_A is the saturation vapor pressure of gas; ρ_1 is the saturated liquid density at the set temperature T; *n* is the mole numbers, subscript 1 and 2 refer to the liquid or gas (nitrogen) and superscript prime and double prime refer to liquid and gas phase respectively. When solutions of PLA are employed, for simplicity, we assume that PLA dissolves completely into the solution and that the volume of the final solution changes (increases) by the addition of PLA. For low concentrations of PLA, the numbers of moles in the solutions is small, which yields to minimal volume changes, however, these changes ought to be consider for high concentrations. The solubility of the gas was determined as follows. The moles of dissolved gas, n_2'were calculated by using the following equation,

$$n_2'' = \frac{P_2 V''^{,i}}{RT^i} - \frac{pV''}{RT}$$

where P_2^i was calculated from the difference between P_T and $p_1^{sat,i}$ and P_2^i is the partial pressure of the gas obtained by substracting the saturated vapor pressure, p_1^{sat} of the solvent from p_T. $V''^{,i}$is the vapor volume of the solution at T^i, and V'' is the vapor volume at T. The superscript i denote the value given at a specific temperature.

The mole fraction of the dissolved gas in the solvent, χ, is defined as

$$\chi = \frac{n_2'}{n_2' + n_1'}$$

And thus the Henry's law constant is given by

$$H = \frac{p''}{\chi}$$

Since it is the same setup, the measurement uncertainties are the same as the ones given by Shirono et al.

2.3 Results

2.3.1 Surface tension, Vapor pressure and Nitrogen solubility

Figure 4.2 shows the dependence of the microbubble size on c_{PLA}. When a higher concentration of PLA was employed, larger microbubbles could be observed. The results are summarized in Table 4.1. It is can be noticed that increasing the polymer concentration reduces the uniformity of the final microcapsule.

Table 4.1: Microbubble radius as a function of the initial PLA concentration.

PLA conc. ($g\ L^{-1}$)	Mean radius (μm)	Standard dev. (μm)	PI (%)
2	1.03	0.14	13.6
10	1.14	0.22	19.3
30	1.31	0.24	18.3
50	1.47	0.35	23.8
60	1.60	0.36	22.5
70	1.72	0.77	44.8
80	2.04	0.92	45.1

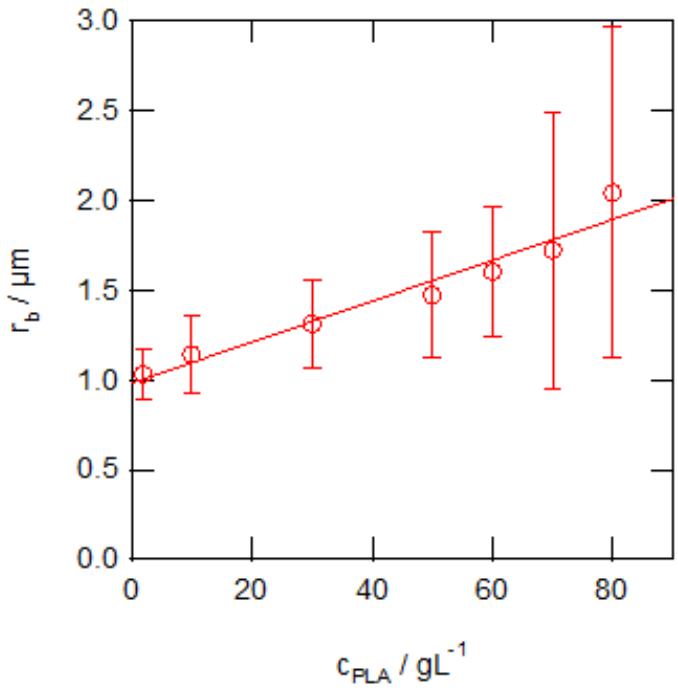

Figure 4.2: The radius of nucleated microbubbles as a function of the initial concentration of PLA, c_{PLA}.

In order to explain the trend shown in Figure 4.2, the Laplace relation was considered. From the Laplace relation it is understood that a decrease in the value of the surface tension at the gas liquid interface or an increase in the vapor pressure, yields to an increase in the microbubble size. However, the results showed that adding PLA reduces the surface tension at most a 12% from its original value. This is, when pure dichloromethane is used, the surface tension is γ=28.3mN m^{-1}, yet when a c_{PLA}= 50g L^{-1} is employed, the surface tension achieves a minimum γ=24.9mN m^{-1}. These results are shown in Figure 4.3. As it can be seen, the only expression left to analyze is the ratio between the actual concentrations of Nitrogen in the solution over the saturation concentration of Nitrogen in the solution (equation 2.38, $\frac{c_2'}{c_{2s}'}$).

The vapor pressure of several solutions of PLA was measured as well. However, it was found that the vapor pressure of the solutions did not change as the polymer concentration or molecular weight was increased. This can be observed from Figure 4.4.

Figure 4.5 shows the Henry's law constant as a function of temperature and Figure 4.6 shows the isotherms for the Henry's law constant as a function of polymer concentration. The solubility of air increases as the concentration of PLA increases, this is, Henry's law constant decreases as c_{PLA} increases. Table 4.2 summarizes these results.

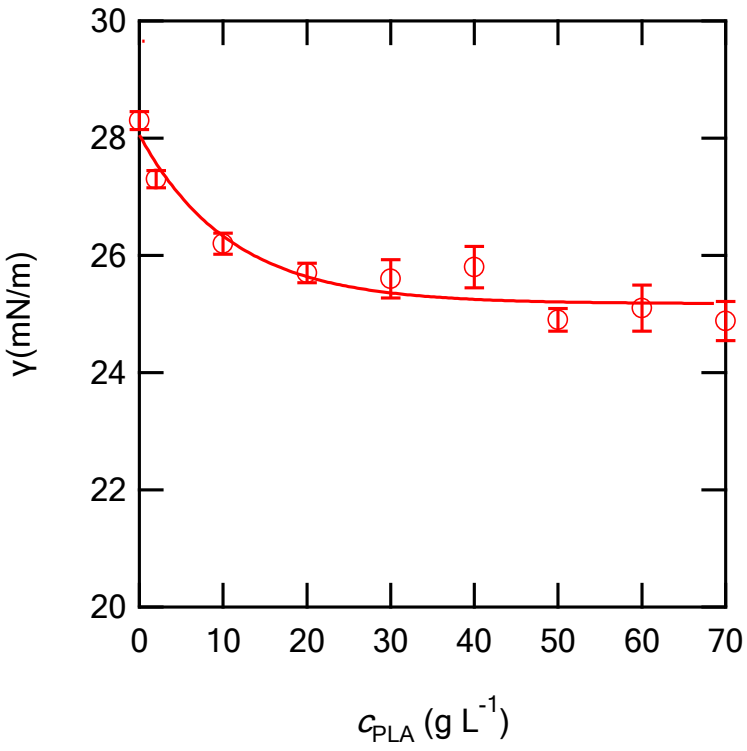

Figure 4.3: Surface tension at the gas liquid interface as a function of c_{PLA}.

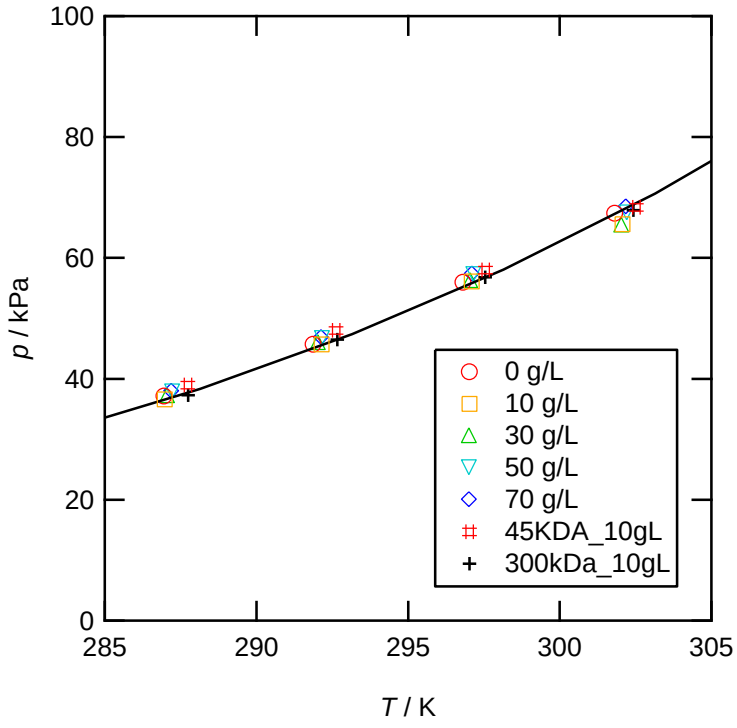

Figure 4.4: Vapor pressure of solutions of PLA with different concentrations of PLA. The solid line is the theoretical prediction.

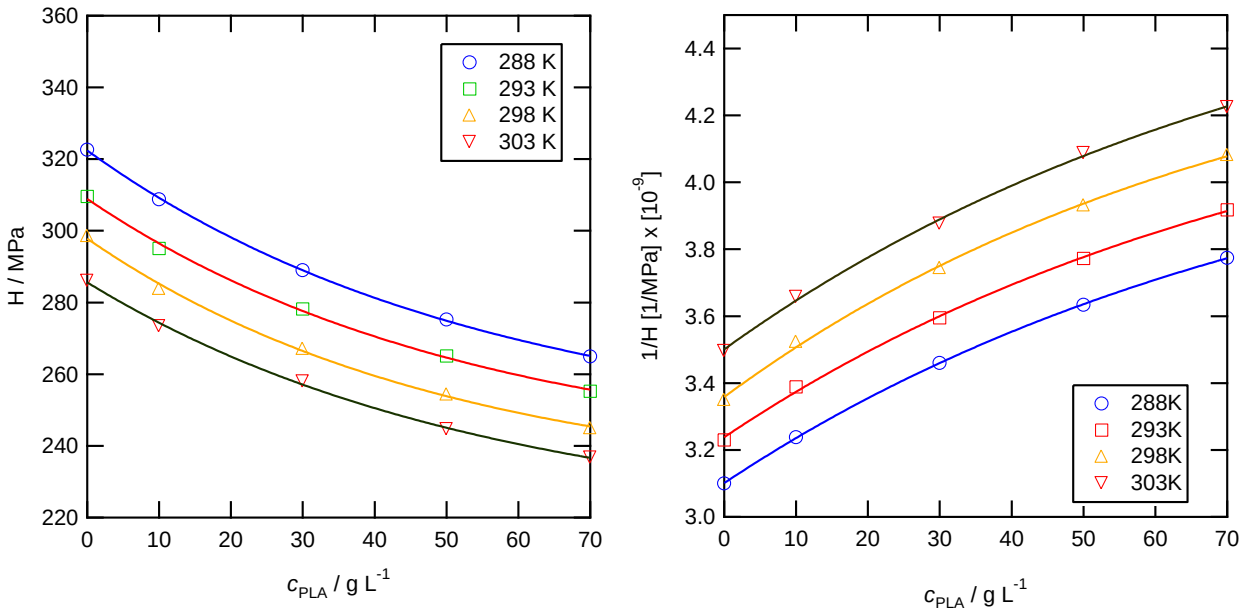

Figure 4.5: Isotherms for the Henry's law constant for N_2 as a function of c_{PLA}. The fit curves are exponential functions.

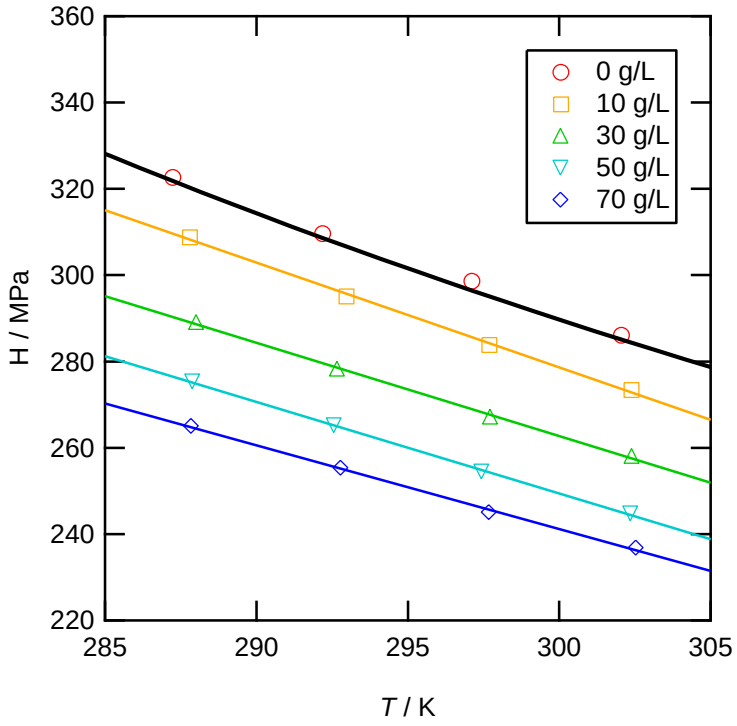

Figure 4.6: Henry's law constant for N_2 as a function of c_{PLA}. The solid black line is the theoretical prediction.

Table 4.2: Henry's law constant for different c_{PLA}

T/K	c_{PLA} [g L^{-1}]	K_H[Mpa]
288	0	322.622
	10	307.164
	30	292.633
	50	284.642
	70	268.085
293	0	309.598
	10	291.759
	30	280.656
	50	272.119
	70	258.472
298	0	298.556
	10	281.381
	30	269.213
	50	262.090
	70	251.339
303	0	286.033
	10	266.840
	30	260.551
	50	255.518
	70	241.559

In the study made by Shirono et. al[5], a semi empirical expression for correlating H and the temperature of the solution, this is, an expression for the solubility of Nitrogen gas in pure dichloromethane, is expressed as,

$$ln\left({}^{H}/_{H_o}\right) = -2.38\left(1 - {}^{T_o}/_{T}\right)$$

Where T_0=298.15K, and H_0=294MPa. By defining a variable χ, which is the difference of the right hand side and the left hand side of the above equation, namely

$$\chi = ln\left({}^{H}/_{H_o}\right) + 2.38\left(1 - {}^{T_o}/_{T}\right)$$

For the measured data, it is found that it's not equal to cero, thus clearly showing the dependence of the Henry law's constant on the polymer concentration. Plotting the quantity χ as a function of the concentration gives us Figure 4.7.

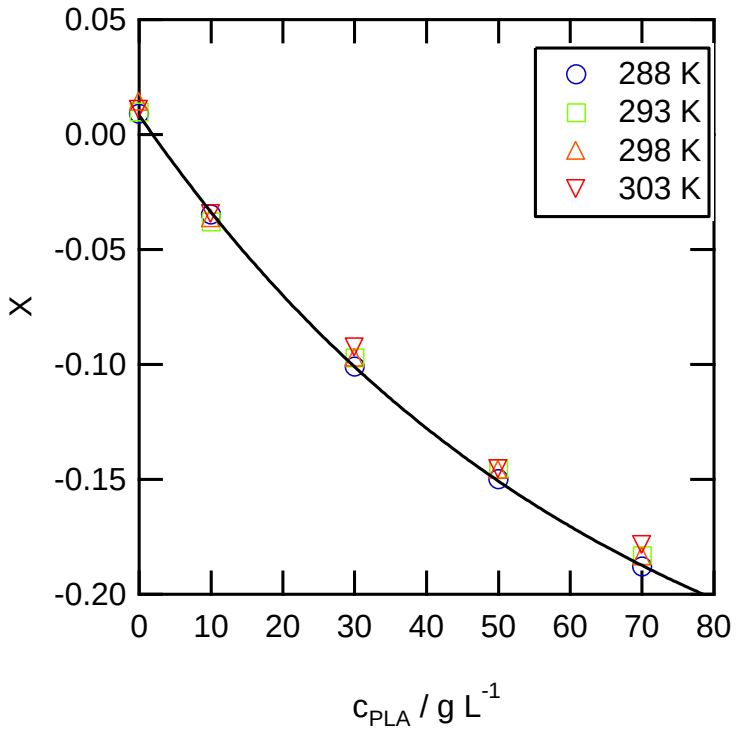

Figure 4.7: χ as a function of c_{PLA}. The solid line is the fitted curve.

From the above results, a semiempirical relationship for the Henry's law constant as a function of temperature and c_{PLA} can be derived. Using a fitting curve it was found that the correlation is,

$$ln\left({}^{H}/_{H_o}\right) = -2.38\left(1 - {}^{T_o}/_{T}\right) + 0.2996e^{-\frac{1}{66}c_{PLA}} - 0.2912$$

It was also found that the solubility of nitrogen increases as the molecular weight of the polymer increases. As the number of molecules increases (i.e. the molecular weight decreases), the Henry's law constant increases, which implies that the saturation concentration increases as the molecular weight increases. This is result is fundamental for manufacturing bigger (yet not so uniform) in the Gas/O/W fabrication (refer to Appendix 1). These results are shown in Figure 4.8. The concentration of the solutions was fixed to c_{PLA}=10gL^{-1}.

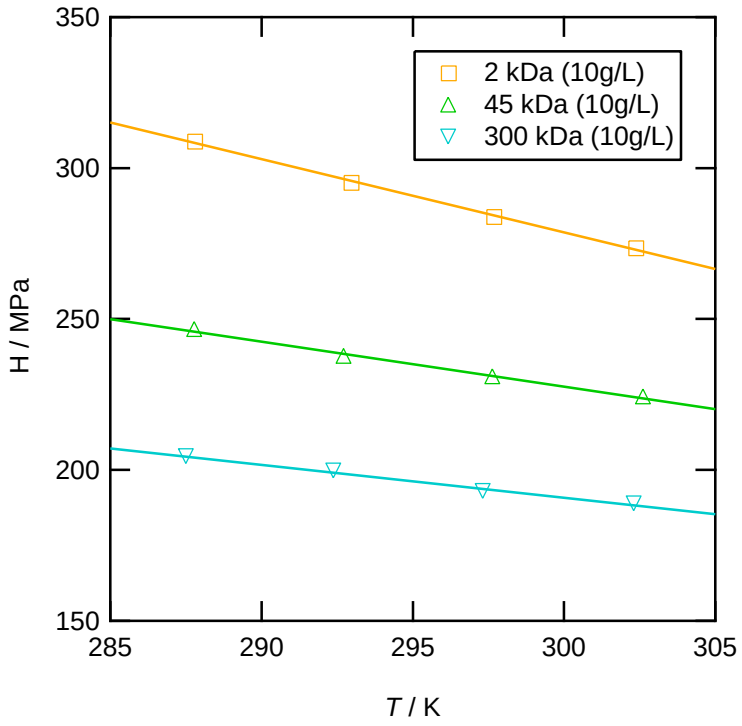

Figure 4.8: Henry's law constant for N_2 as a function of the molecular weight. The solid lines are fitted curve.

2.4 Discussion

2.4.1 Bubble equilibrium size as function of the molar content of Nitrogen in the droplet and microcapsule release

Ward's theory shown previously in chapter 2 (equation 52 and 53)[4] is employed. It was used the derived equation for determining the relation between the total molar amount of nitrogen, N_2, and the equilibrium radius of bubbles, r_b, for different numbers of bubbles, q, at constant p', T, and N_1 is given by the following equation:

$$N_2 = \left[\frac{c'_{2s}}{c'_{01}}\left(N_1 - q\eta\frac{p''_{01}}{RT}\frac{4}{3}\pi r_b^3\right) + q\frac{p'}{RT}\frac{4}{3}\pi r_b^3\right]\left[1 - \eta\frac{p''_{01}}{p'} + \frac{2\gamma}{r_b p'}\right]$$

And the stability condition given by $\frac{dN_2}{dr_b} > 0$. Figure 4.9 show the calculated N_2–r_b curves for a single (q = 1) or multiple ($q \geq 2$) bubbles at p' = 1 atm, T = 298 K, and $N_1 = (4/3)\pi r_d^3/V_{m1}$. Here, r_d is the effective radius of a CH_2Cl_2 droplet and V_{m1} is the molar volume of pure CH_2Cl_2 in the liquid phase. The following parameters are employed: $c'_{01} = V_{m1}^{-1} = 1.56 \times 10^4$ mol m^{-3}, $c'_{2s} = 5.30$ mol m^{-3}, $\gamma = 2.78 \times 10^{-2}$ N m^{-1}, and $p''_{01} = 5.81 \times 10^4$ Pa. For each N_2–r_b curve, if N_2 is lower than a certain minimum, there are no possible equilibrium states for a bubble or bubbles in the system. If N_2 is equal to the minimum, there is only one equilibrium radius, and if N_2 is higher than the minimum, there are two possible equilibrium radii. However, it should be noted that when there are two possible equilibrium radii, the bubble with larger radius is stable while that of smaller radius is unstable.

In Figure 4.9, using equation (13), if the droplet radius in the CH_2Cl_2–nitrogen solution is r_d = 1 mm and the nitrogen concentration of the solution is close to the solubility ($c'_2 \approx c'_{2s}$), the total molar amount of nitrogen inside the droplet is about $N_2 = 2.2 \times 10^{-2}$ μmol. If a droplet of r_d = 1 mm and $N_2 = 2.2 \times 10^{-2}$ μmol is formed gently in an aqueous medium, bubbles with radius of r_b = 0.96 μm will gradually appear [9]. Because the initial nitrogen concentration of the solution is close to the solubility and the solubility of nitrogen in the aqueous medium is much lower than that in the solution, microbubbles are generated due to the dissolution of CH_2Cl_2 into the surrounding aqueous medium and the nitrogen concentration of the solution should remain close to the solubility ($c'_2 \approx c'_{2s}$). This suggests that bubbles with radius of r_b = 0.96 μm will continuously appear. In Figure 4.8, a single bubble (q = 1 and r_d = 1 mm) or multiple bubbles (e.g. $q = 10^4$ and r_d = 1 mm) of r_b = 0.96 μm is unstable because $dN_2/dr_b < 0$. But as time goes on, the number of bubbles, q, increases, while the effective droplet radius, r_d, decreases at constant $N_2 = 2.2 \times 10^{-2}$ μmol. When $q = 2.83 \times 10^7$ and r_d = 0.931 mm, the bubbles of r_b = 0.96 μm become stable because the N_2–r_b curve for $q = 2.83 \times 10^7$ and r_d = 0.931 mm is minimized at r_b = 0.96 μm and the minimum value is $N_2 = 2.2 \times 10^{-2}$ μmol. Subsequently, when the effective droplet radius, r_d, decreases further to 0.8 mm, while $c'_2 \approx c'_{2s}$, the number of bubbles, q, should be in the range from 1.80×10^7 to 7.15×10^7 to keep the system thermodynamically stable. At $q = 1.80 \times 10^7$, the N_2–r_b curve is minimized at r_b = 0.96 μm, whereas, at $q = 7.15 \times 10^7$, the N_2–r_b curve passes through the point (r_b, N_2) = (0.96 μm, 2.2×10^{-2} μmol). According to this analysis, it can be possible that the system keeps stable when q increases while r_b decreases. However, in a real system, if the number density of bubbles is so high, the bubbles cannot stay inside the droplet because of the interactions between bubbles. Since the solubility of nitrogen in the aqueous medium is much smaller than that in CH_2Cl_2, N_2 decreases through the bubble release

from the droplet interior to the surrounding aqueous medium during the process of droplet shrinkage. Inside a droplet of CH_2Cl_2–air solution of PLA, many microbubbles are generated. As CH_2Cl_2 diffuses into the surrounding aqueous solution, microbubbles covered with PLA are released from the droplet interior to the surrounding aqueous medium, and hollow PLA microcapsules whose inner radius is the same as the template bubble radius can be produced. [2]

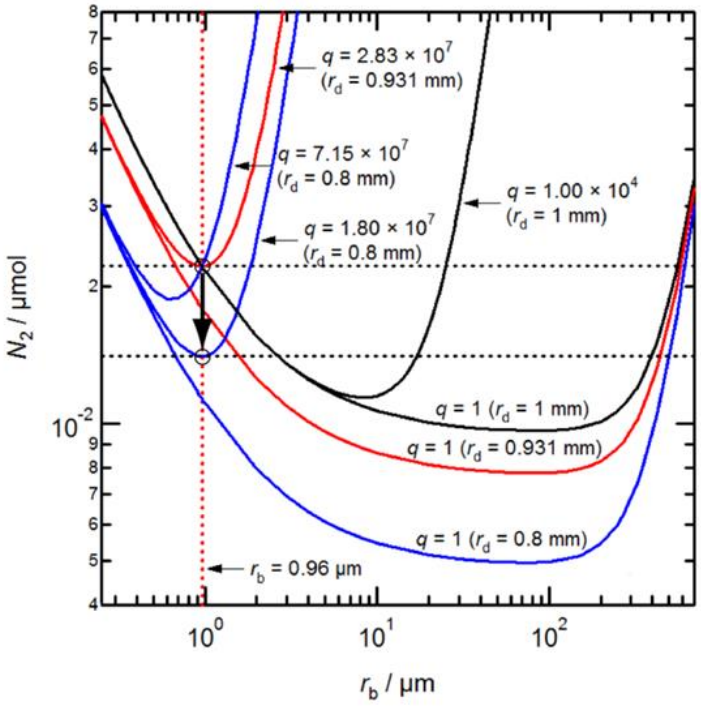

Figure 4.9: Total molar amount of nitrogen in a closed volume of CH_2Cl_2–nitrogen solution including a single (q = 1) or multiple (q > 1) nitrogen bubble vs. bubble radius (N_2–r_b) curves for r_d = 0.8–1 mm. The system is in the equilibrium state at constant pressure, p', temperature, T, and total amount of CH_2Cl_2 in moles, N_1. Here, p' = 1 atm, T = 298 K and $N_1 = (4/3)\pi r_d^3/V_{m1}$, where V_{m1} is the molar volume of pure CH_2Cl_2 in the liquid phase.

In Figure 4.10, if the droplet radius of the CH_2Cl_2-nitrogen solutions is 1mm and assuming that the total bubble count is $q = 10^3$, the equilibrium bubble radius is $r_b \approx 60\mu m$. As the microbubble count increases, the radius of the stable bubble gradually shifts towards lower sizes. When the bubble count is 10^7, the equilibrium size of the bubbles is 10^{-6}μm.

The measured solubility of nitrogen in different solutions of dichloromethane at different temperatures showed that when c_{PLA} is 70gL^{-1} the Henry's law constant at 25C° decreases 16% from its value compared to the case when no PLA is present in the solution. This implies that more air can be dissolved into the solution.

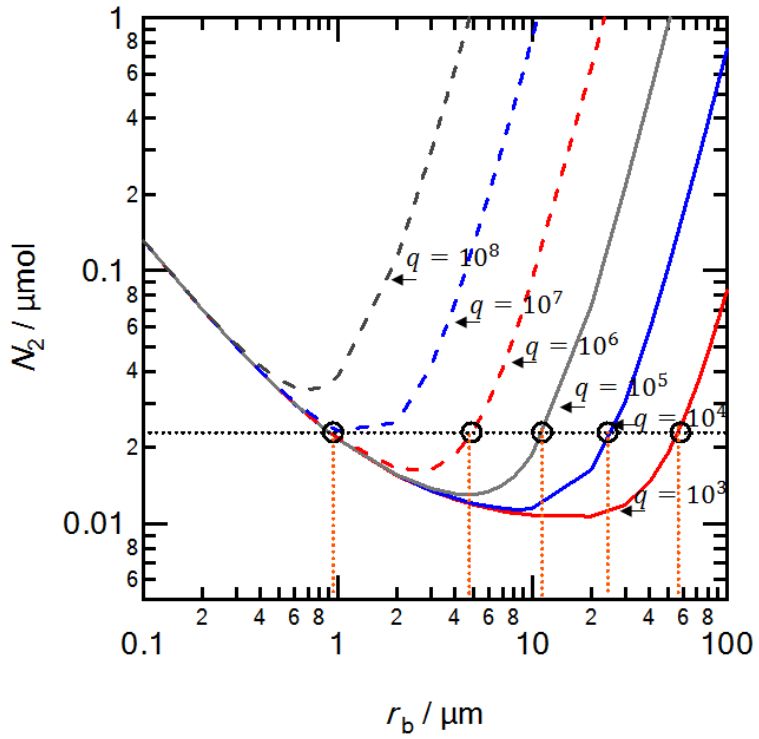

Figure 4.10: **Total molar amount of nitrogen in a closed volume of CH_2Cl_2–nitrogen solution including multiple (q > 1) nitrogen bubble vs. bubble radius (N_2–r_b) curves for r_d = 1 mm.** The system is in the equilibrium state at constant pressure, p', temperature, T, and total amount of CH_2Cl_2 in moles, N_1. Here, p' = 1 atm, T = 298 K.

As the concentration of the polymer increases, the solubility of air increases as well. Since microbubbles are continually nucleating inside the solution the concentration of air in the PLA solution could decrease well below the saturation limit. If so, from theory, the bubble size is expected to increase. However to clarify this scenario a study on the concentration of air at the vicinity of the bubble should be considered.

3. Conclusions

If the concentration of PLA is increased, bigger micro bubbles can be observed. Furthermore, increasing the concentration of PLA also increases the solubility of Nitrogen in the polymer solution. Because there is more dissolved air as the concentration of the polymer increases, it is possible to nucleate more bubbles in the solution and thus attain more microcapsules. Thus increasing the polymer concentration is a key parameter for mass producing the microcapsules.

4. References

1. Daiguji, H.; Takada, S.; Molino, J.J; Takemura, F. Fabrication of hollow poly(lactic acid) microcapsules from microbubble templates. *Journal of Physical Chemistry B* **2009,** *113*, 15002-15009.

2. Molino, J.J.; Daiguji, H.; Takemura, F. Factors affecting the size and uniformity of hollow poly(lactic acid) microcapsules fabricated from microbubble templates. *Journal of Physical Chemistry B* **2011,** *115*, 13828-13834.
3. Sakurai, D.; Molino, J.J.; Daiguji, H.; Takemura, F. Hollow polylactic acid microcapsules fabricated by gas/oil/water and bubble template methods. *Journal of Material Chemistry A* **2013,** *1*, 14562-14568.
4. Ward, C. A.; Tikuisis, P. Bubble stability in closed systems. *Journal of Applied Physics* **1982,** *53*, 6076-6084.
5. Shirono, K.; Morimatsu, T.; Takemura, F. Gas Solubilities (CO2, O2, Ar, N2, H2, and He) in Liquid Chlorinated Methanes. *Journal of Chemical Engineering Data* **2008,** *53*, 1867-1871.

5

Mass Production of Uniform Hollow Poly (Lactic Acid) Microcapsules Fabricated from Microbubble Templates

In the bubble template method it was found that ultrasound enhances bubble nucleation inside the droplets of a dichloromethane solution of poly(lactic acid) (PLA) formed in an aqueous solution of poly(vinyl alcohol), which yields to the mass fabrication of hollow PLA microcapsules without compromising the uniformity of the bubble size. Mass production of hollow PLA microcapsules could be achieved without compromising capsule uniformity when the initial concentration of PLA was 30 g L^{-1}; the final average microcapsule radius was 0.54 μm with a standard deviation of 0.11 μm. From direct observation, it was concluded that the interactions among microbubbles increased locally and instantaneously the pressure inside the droplet, which led to the spontaneous release of PLA coated microbubbles from the droplet interior to the outer aqueous solution.

1. Introduction

In Chapter 3 it was determined that if an initially diluted dichloromethane (CH_2Cl_2) solution of low-molecular-weight (2 kDa) PLA (c_{PLA} = 2 g L^{-1}) and a 2% (w/w) aqueous solution of poly(vinyl alcohol) (PVA) was employed as the dispersed and continuous phases, respectively, uniform microcapsules of about 1 μm radius could be obtained. If capsules were to be fabricated under conditions different than these, the resultant microcapsules were smaller and less uniform.

In this chapter, it is shown the viability of enhancing bubble nucleation by the application of ultrasound. The final produced microcapsule displayed high uniformity. Furthermore, based on the direct observation of microbubble release from the droplet interior when ultrasound was applied or was not applied, it was concluded that the number of released capsules from the droplet interior depends on the number of nucleated bubbles and the bubble size. The effects of the application of ultrasound, and the initial concentration of PLA, c_{PLA}, on the nucleated microbubble and on the final microcapsule size, in addition to the specific conditions at which the highest uniformity could be attained, are disclosed.

2. Experimental

2.1 Chemicals

The following reagents were used: PLA with molecular weights of 2 kDa (Polyscience, U.S.); CH_2Cl_2 (99.99% purity, Wako Pure Chemical Industries, Ltd., Japan) and 2% (w/w) aqueous PVA (Gohsenal T-350, Nippon, Gohsei, Osaka, Japan). All the chemicals used were reagent grade. Water from a Milli-Q Advantage A10 water purification system was used.

2.2 Methods

The following two fabrication processes were employed:

Process A (Chapter 2): The same fabrication process used in chapter 2 was employed to fabricate hollow PLA microcapsules from microbubble templates. During the purification of the microcapsule solution, Millipore water at 313 K was employed to remove PVA which adsorbed onto the capsule shell. The hollow PLA microcapsules were dried in a desiccator at 0.7 kPa for 36 h. Silica gel was used as the desiccant. The final product was a white powder of hollow PLA microcapsules.

Process B: The droplets of a CH_2Cl_2 solution of PLA were formed in a glass dish with 2% (w/w) PVA aqueous solution in the same manner. The glass dish was placed at the water surface in an ultrasonic bath. The output power and frequency of the ultrasonic transducer were 35 W and 38 kHz, respectively. During sonication, the droplets became cloudy, which indicated internal nucleation of microbubbles. Experiments in which each sample was continuously sonicated were performed. The collection, purification, and drying stages were the same as for *process A*.

All the above experiments were performed at room temperature, 298 K. To verify the effect of each parameter on the bubble and capsule size, several bright field images of the microbubbles and capsules were obtained using an inverted microscope (ECLIPSE Ti-E, Nikon, Japan) and the

bubble and capsule size was measured by processing these bright field images. This microscope was also used to observe the release of hollow microcapsules from the interior of the droplets. The size of the nucleated microbubbles inside the droplet was measured at the middle of the droplet, and thus, the measurements did not include coalesced microbubbles that could be mainly found at the top of the droplet due to buoyancy. PLA was stained with Nile Red; when the microscope was used in fluorescent mode, only the capsule shell was observed. This confirmed that the microbubbles served as templates, as they exhibited no fluorescence.

3. Results and Discussion

3.1 Fabrication of hollow PLA microcapsules under sonication

In this study, hollow PLA microcapsules in the bubble template method under sonication (process B) were successfully fabricated. In process A, the total production time was determined solely by the diffusivity of CH_2Cl_2 into the aqueous medium/air (solvent evaporation), this process lasted several hours (>7 hours). Now, the process to fabricate several microcapsules, referred as process B, takes less than an hour. Figure 5.1 shows the pressure waves measured at two different positions in the ultrasonic bath. The positions A and B are near the anti-node and node of the pressure standing wave, respectively. The amplitudes at positions A and B were about 70 and 10 kPa, respectively. At both, position A and B, the bubble nucleation was enhanced but the droplet was stable. In this study, the hollow PLA capsules were synthesized at position A.

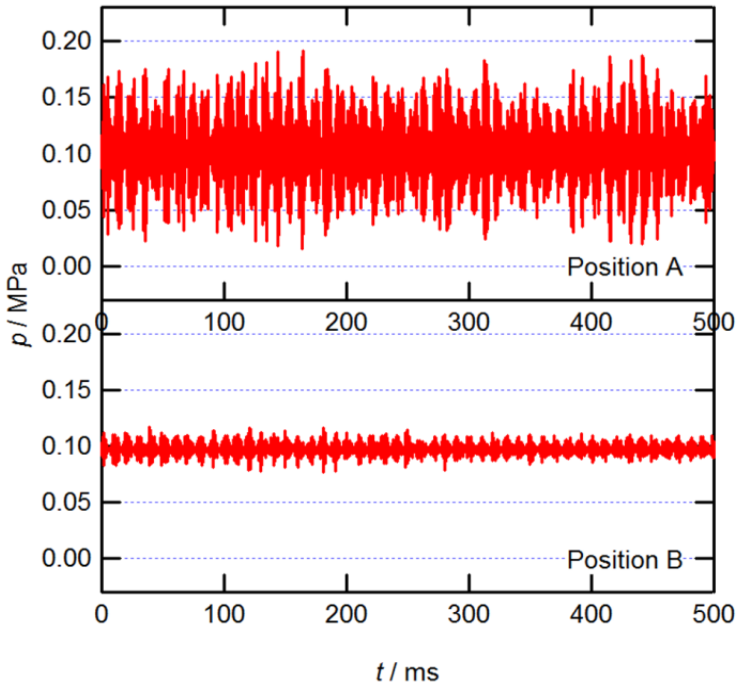

Figure 5.1: Pressure waves measured at two different positions in the ultrasonic bath.

However, when the glass dish was located at some places, the droplet was deformed and PLA particles and films were generated at the droplet surface. Such places were located both near the node and anti-node of the pressure standing wave. In this study, such places were avoided.

The optimum conditions to fabricate hollow PLA microcapsules without compromising uniformity were also clarified. This can be seen from right panels of Figure 5.2. A low or high c_{PLA} considerably deteriorates the final capsule uniformity. A c_{PLA} of 30 g L^{-1} proved to be the optimum condition to fabricate independent hollow and uniform PLA microcapsule. This technique proved to be robust as high uniformity was also attained when a PLA of molecular weight of 100 kDa and a c_{PLA} = 30 g L^{-1} was employed. The mean radius, standard deviation, and PI of these synthesized microcapsules were 0.55 μm, 0.12 μm, and 21.2%, respectively. In spite its robustness, it should be noted that in this technique the mean radius of hollow PLA capsules synthesized with sonication was smaller than that without sonication (ca. 1 μm)

The top panels of Figure 5.2 show a typical bright field image and the radius distribution of microbubbles inside a droplet of a CH_2Cl_2 solution of PLA, respectively, when c_{PLA} = 30 g L^{-1} and ultrasound was employed. During this observation, the ultrasound was not applied to the solution, but the droplets were kept cloudy. The mean values, standard deviations, and polydispersity indices (PI = standard deviation/mean) of microbubble radius were 1.34 μm, 0.23 μm, and 17.4%, respectively.

The bottom panels of Figure 5.2 show bright field & fluorescent images and the outer radius distribution of dry hollow PLA microcapsules, respectively. The mean values, standard deviations, and PI of the outer radius were 0.54 μm, 0.11 μm, and 21.2%, respectively. This result suggests that the hollow PLA microcapsules fabricated under these conditions were smaller than the template microbubbles but highly uniform.

In addition, the size of the bubble was larger than the size of the released wet microcapsule, which was also larger than the final dry microcapsule ($r_b > r_{c,\,wet} > r_c$). This result also agreed with those obtained when capsules were fabricated with process A using EtOH, and can be observed in Figure 2 of Appendix 3.

Using sonication enabled mass production of the capsules in less time and with high uniformity. In process A, the total production time was determined solely by the diffusivity of CH_2Cl_2 into the aqueous medium/air (solvent evaporation); this process lasted several hours (>7 h). Process B now takes less than an hour.

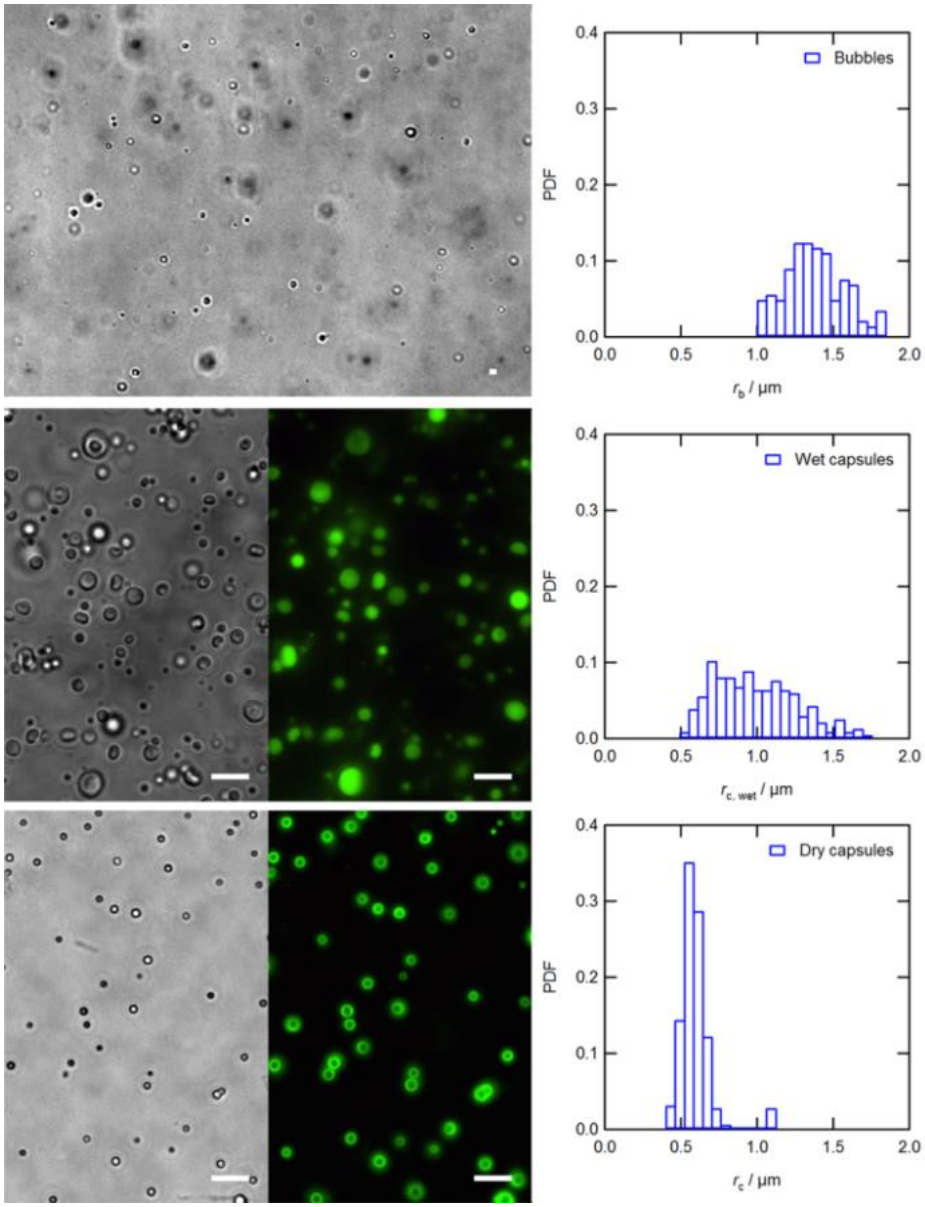

Figure 5.2: Size distribution of Hollow microcapsules fabricated using ultrasound. A bright field image and the radius distribution of microbubbles inside a droplet of a CH_2Cl_2 solution of PLA when ultrasound was employed (top). Bright field and fluorescent images of hollow PLA microcapsules and the radius distribution inside 2% (w/w) PVA aqueous solution (middle) and after drying (bottom). The initial concentration of PLA, c_{PLA}, was 30 g L^{-1}. The scale bars represent 5 μm.

3.2 Effect of ultrasound on the kinetics of bubble release

In process A, it was determined that the minimum required pressure difference Δp for a microbubble to be released from the droplet interior was given by the Laplace equation. In Chapter 3 it was concluded that for a droplet of radius, r_d, of 10^{-3} m, Δp corresponds to 37.8 Pa when 2% (w/w) PVA aqueous solution was employed as the bulk phase.[1] In the present study, to enhance microbubble nucleation, ultrasound was employed. Figure 5.3 shows two representative images of microbubble nucleation and release when ultrasound was not applied (process A), and when

ultrasound was applied (process B), respectively.

The linear resonance frequency of a free bubble is known to be given by the Minnaert formula[2]:

$$f_0 = \frac{1}{2\pi r_b}\left[\frac{3\gamma p'}{\rho'} + \frac{2(3\gamma-1)\sigma}{\rho' r_b}\right]^{1/2} \quad (1)$$

where f_0 is the resonance frequency of a bubble with equilibrium radius r_b; γ is the heat capacity ratio of the gas inside the bubble; p' is the hydrostatic pressure in the surrounding liquid; ρ' is the equilibrium density of the liquid; and σ is the surface tension at the gas-liquid interface. The resonance frequency f_0 was calculated to be 3.4 MHz at r_b = 1 μm. The values of the physical parameters used in the calculations were: p' = 101.3 kPa, ρ' =1330 kg m^{-3}, σ = 0.0278 N m^{-1}, and γ = 1.4. Because the frequency of the acoustic wave employed in this study was 38 kHz, the ultrasonic wave cannot collapse a 1 μm radius bubble and cannot produce shockwaves. The ultrasonic wave just enhances the nucleation of microbubbles and does not produce the large pressure required for bubble release. However, if more bubbles are nucleated an are distributed at the liquid-liquid interface, the frequency of bubble release could increase, because bubbles interact with each other and the local and instantaneous pressure affecting each bubble may overcome the pressure required for bubble release. The repulsive force between two adjacent bubbles is generally quite large, and the deformation of bubbles and the squeezing flow between bubbles may change the direction of a bubble with respect to the external aqueous medium.[3] Several images of microbubble release showed that the number density of nucleated bubbles inside a droplet in process B was about 10 times larger than that in process A, and further, the number density of released bubbles around the droplet in process B was also about 10 times larger than that in process A. Thus, it is reasonable to say that the number of released capsules from the droplet interior depends on the number of nucleated bubbles. The mechanism of bubble release could be the same for processes A and B, but the frequency was different. This is, more capsules were fabricated using Process B.

3.3 Effect of PLA concentration on the bubble and capsule size

When a higher concentration of PLA was employed, larger microbubbles could be observed. This phenomenon was also observed when process A was employed. Figure 5.4 show the dependence of the average bubble radius on c_{PLA} when ultrasound was not applied (process A) or applied (process B). The measured values were summarized in Table 5.1.

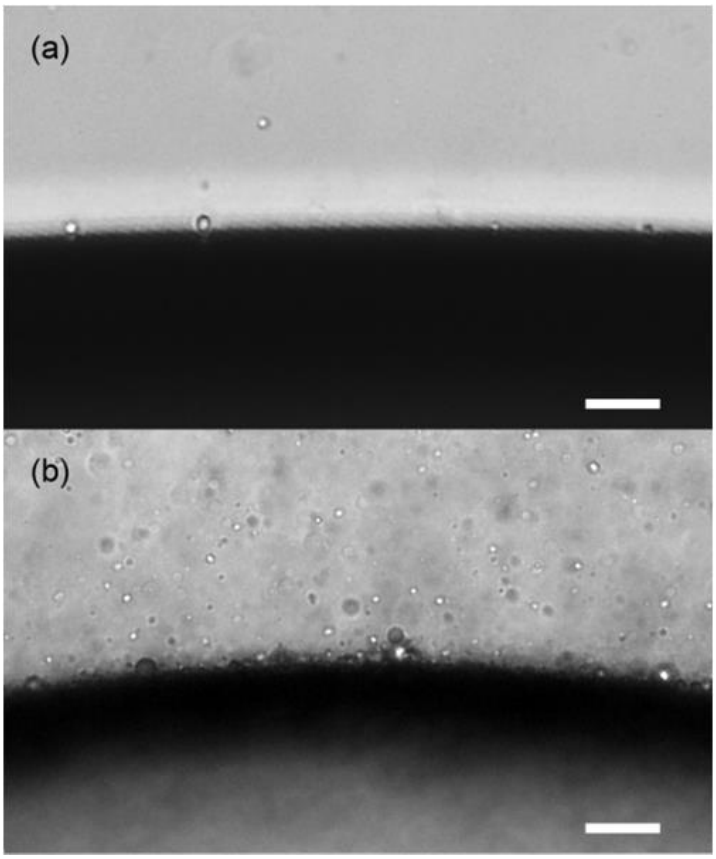

Figure 5.3: Release of hollow PLA microcapsules from the droplets. (a) when ultrasound was not applied and, (b) when ultrasound was applied. The initial PLA concentration, c_{PLA}, was 2kDa g L^{-1}. The scale bars represent 25 μm.

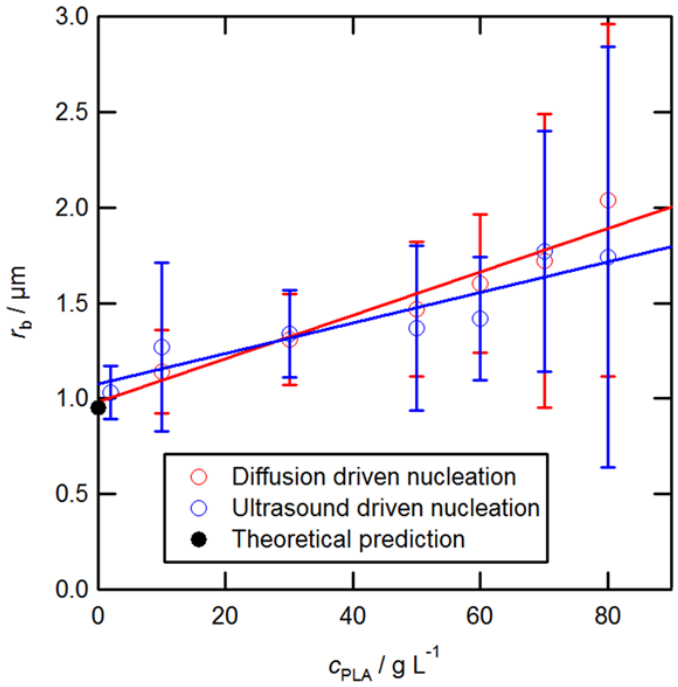

Figure 5.4: The radius of nucleated microbubbles with and without sonication as a function of initial concentration of PLA, c_{PLA}. The black dot is the theoretically predicted equilibrium radius of 0.95 μm for microbubbles nucleated inside a CH_2Cl_2 droplet when p_1'' is assumed to be the saturation vapor pressure of pure CH_2Cl_2.

Table 5.1: Microbubble radius as a function of the initial PLA concentration when ultrasound was not applied (process A) or applied (process B).

	Process A			Process B		
PLA conc. ($g\ L^{-1}$)	Mean radius (μm)	Standard dev. (μm)	PI (%)	Mean radius (μm)	Standard dev. (μm)	PI (%)
2	1.03	0.14	13.6	1.11	0.14	12.9
10	1.14	0.22	19.3	1.27	0.44	34.6
30	1.31	0.24	18.3	1.34	0.23	17.4
50	1.47	0.35	23.8	1.37	0.43	31.4
60	1.60	0.36	22.5	1.42	0.32	23.0
70	1.72	0.77	44.8	1.77	0.63	35.6
80	2.04	0.92	45.1	1.74	1.1	63.2

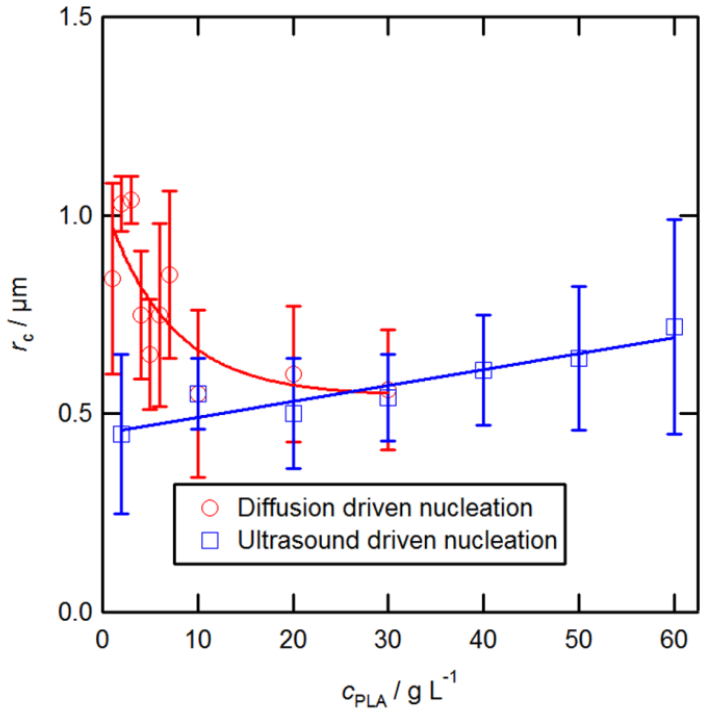

Figure 5.5: Microcapsules fabricated when ultrasound was not applied (process A) or applied (process B) as a function of initial concentration of PLA, c_{PLA}.

Figure 5.5 shows the outer radius of fabricated dry hollow PLA microcapsules as a function of c_{PLA} when ultrasound was not applied (process A) or applied (process B).

The optimum conditions for fabricating hollow PLA microcapsules without compromising uniformity were also clarified. Low or high c_{PLA} values considerably deteriorated the final capsule uniformity, and a c_{PLA} of 30 g L^{-1} proved to be optimal for the fabrication of

independent, hollow, and uniform PLA microcapsules. This technique proved to be robust, as high uniformity was also attained when 100 kDa PLA and c_{PLA} of 30 g L^{-1} were employed. The mean radius, standard deviation, and PI of these synthesized microcapsules were 0.55 μm, 0.12 μm, and 21.2%, respectively. In spite of its robustness, it should be noted that, in this technique, the mean radius of the hollow PLA capsules synthesized with sonication was smaller than that without sonication.

4. Conclusions

It was shown that ultrasound can be effectively employed to mass produce microcapsules within the required range for ultrasound contrast agents and drug delivery applications without compromising uniformity. The optimum conditions at which highly uniform capsules could be obtained when ultrasound was employed were identified: namely, a low intensity ultrasound and a high initial concentration of PLA (c_{PLA} = 30 g L^{-1}). In addition, it was clarified the relationship between the microbubble size and the initial concentration of PLA. Furthermore, the kinetics of the release of the hollow PLA microcapsules created under the bubble template method was clarified. The pressure was increased locally due to the interaction/collision between the microbubbles, which led to spontaneous microbubble release.

5. References

1. Molino, J.J.; Daiguji, H.; Takemura, F. Factors affecting the size and uniformity of hollow poly(lactic acid) microcapsules fabricated from microbubble templates. *Journal of Physical Chemistry B* **2011,** *115*, 13828-13834.
2. Minnaert, M. On Musical Air bubbles and the Sounds of Running Water. *Philosophical Magazine* **1933,** *16,* 235-248.
3. Sugiyama, K.; Takemura, F. On the Lateral Migration of a Slightly Deformed Bubble Rising Near a Vertical Plane Wall. *Journal of Fluid Mechanics* **2010,** *662,* 209-231.

6

Fabrication and Size Control of Hollow PAH/PSS Microcapsules in the Bubble Template Method

In a Na_2CO_3 solution, PAH becomes colloidal particles of carbamate ($R\text{-}NHCOO^-$) and amino $R\text{-}NH3^+$) ions within a certain pH range. When CO_2 bubbles nucleate in this solution, colloidal PAH stabilizes the microbubble via adsorption. In this chapter, the microcapsules radius was successfully controlled by changing the concentration of PAH in the Na_2CO_3 solution. Zeta potential value for these capsules at pH 8.5 is positive, thus allowing PSS adsorption onto the hollow PAH microcapsules and with it, the synthesis of a bilayer PAH/PSS. In addition, the bilayer PAH/PSS capsule solution was titrated until the pH was adjusted to 7.0 and the bilayer microcapsules were stable at this pH. This proved that these bilayer capsules can be potentially employed for medical applications. Nevertheless, the success of the bilayer fabrication strongly depends on the PAH:PSS mass ratios. Increasing this ratio yields to irreversible flocculation. From the analysis of the FTIR-ATR spectra for both PAH and PAH/PSS microcapsules, and analysis from zeta potential measurements, the whole adsorption mechanism of PSS on PAH micrcoapsules was elucidated as well.

1. Introduction

Controlled encapsulation and release has been one of the main focuses over the last decade, especially for hollow polyelectrolyte microcapsules since they have the greatest potential in the pharmaceutical industry due to its low density, optical scattering, [1, 2, 3] large and useful inner

space, and tailorable shell thickness. One common technique for manufacturing polyelectrolyte microcapsules characterized for non covalent interactions in the polymer chains to synthesize nano-thick layers around a liquid or solid core by multiple adsorption of polyanions and polycations groups is the layer-by-layer (LbL) method. [4, 5, 6]

Polyelectrolyte microcapsules also display high biocompatibility and controllable shell properties such as permeability, adhesion, and mechanics. In addition, there is great flexibility for embedding several types of functional groups in the shell. Commercially, two of the most used polymers are poly alyllamine hydrochloride (PAH) and poly styrene sulfonate (PSS). Yet, sequential addition of polyelectrolyte requires exact ratios of polyelectrolyte. Failure to achieve this increases the chances of forming free polyelectrolyte or particle aggregates. [7, 8, 9]

Recent studies [3] proposed the use of microbubbles as templates. In this procedure microbubbles are created via sonication and first stabilized in a tween-span suspension. Then, by sequential adsorption of PAH and PSS, microbubbles are completely covered. Yet, the inclusion of surfactant molecules makes this procedure disadvantageous for medical applications.

In a Na_2CO_3 aqueous solution, CO_2 microbubbles were covered with colloidal PAH particles [10, 11, 12, 13] containing carbamate ions, $R\text{-}NHCOO^-$, and amino ions, $R\text{-}NH_3^+$. These colloidal PAH particles can only be present within a specific pH range $7.5 < pH < 9.0$, and PAH microcapsules can exist in the same pH range. Furthermore, when PSS is added in the diluted solution of PAH it is possible to form bilayer microcapsules that can exist at pH = 7. Furthermore, the mean radius for these human pH resistant microcapsules was measured to be about 2.5 μm.

Daiguji et al made possible the stabilization of a microbubble in an aquous solution and employed these microbubbles as templates by directly absorbing PAH onto their surface [14, 15]. Since the size control of capsules and the condensation of capsule solutions are required for more practical applications, this chapter focuses on (1) the size control of PAH microcapsules, (2) the fabrication of PAH/PSS microcapsules, and (3) the PSS layer formation around PAH microcapsules.

2. Theory

2.1 Fabrication of colloidal PAH:

The theory was developed by Daiguji et. al. They found that in a Na_2CO_3 aqueous solution, if bicarbonate is dissolved in water, a re-equilibration takes place according to the following equations:

$$CO_2(aq) + H_2O \Leftrightarrow HCO_3^- + H^+ \quad (6.1)$$

$$HCO_3^- \Leftrightarrow CO_3^{2-} + H^+ \quad (6.2)$$

PAH reacts with carbonate and bicarbonate as follows:

$$R\text{-}NH_3^+ + HCO_3^- \Leftrightarrow R\text{-}NHCOO^- + H_2O + H^+ \quad (6.3)$$

$$R\text{-}NHCOO^- + H_2O \Leftrightarrow R\text{-}NH_2 + CO_3^{2-} + H^+ \quad (6.4)$$

By adding equation 3 and equation 4 and then subtracting equation 2 from the addition, the following equation can be obtained [16]:

$$R\text{-}NH_3^+ \Leftrightarrow R\text{-}NH_2 + H^+ \quad (6.5)$$

The logarithmic measure of the acid dissociation constants for equation (1), (2) and (5) are pK_{a1}=6.352, pK_{a2}=10.329, and pK_{a5}=8.7, respectively. The pK_a for eqs 3 and 4 are unknown, but the following relationship must be satisfied:

$$pK_{a3} + pK_{a4} = pK_{a2} + pK_{a5} \quad (6.6)$$

Thus, the logarithmic measure of the acid dissociation constants for equations 3 and 4 were to be pK_{a3}=7 and pK_{a4}=12.029, respectively. Furthermore, PAH reacts with CO_2 and this reaction yields to the formation of carbamate ion as follows [17]:

$$R\text{-}NH_2 + CO_2(aq) \Leftrightarrow R\text{-}NHCOO^- + H^+ \quad (6.7)$$

The logarithmic measure of the acid dissociation constant for this reaction, pK_{a7}, is 4.8 [17]. R-NH_2 and R-NH_3^+ are fully dissolved in the solution. However, if R-NH_3^+ and R-$NHCOO^-$ co-exist in the solution, these two different states of PAH can co-aggregate and form neutral colloidal particles due to electrostatic interactions. This is a key aspect event for our technique to work. Figure 6.1 shows the calculated compositions vs. pH curves in two different titration conditions: (a) The overall mass of carbon dioxide, $m\_CO_2^* = m\_CO_3^{2-} + m\_HCO_3^- + m\_CO_2$ (aq) + m_R-$NHCOO^-$, is constant and (b) the mass of carbon dioxide in the aqueous phase, m_CO_2 (aq), is constant.

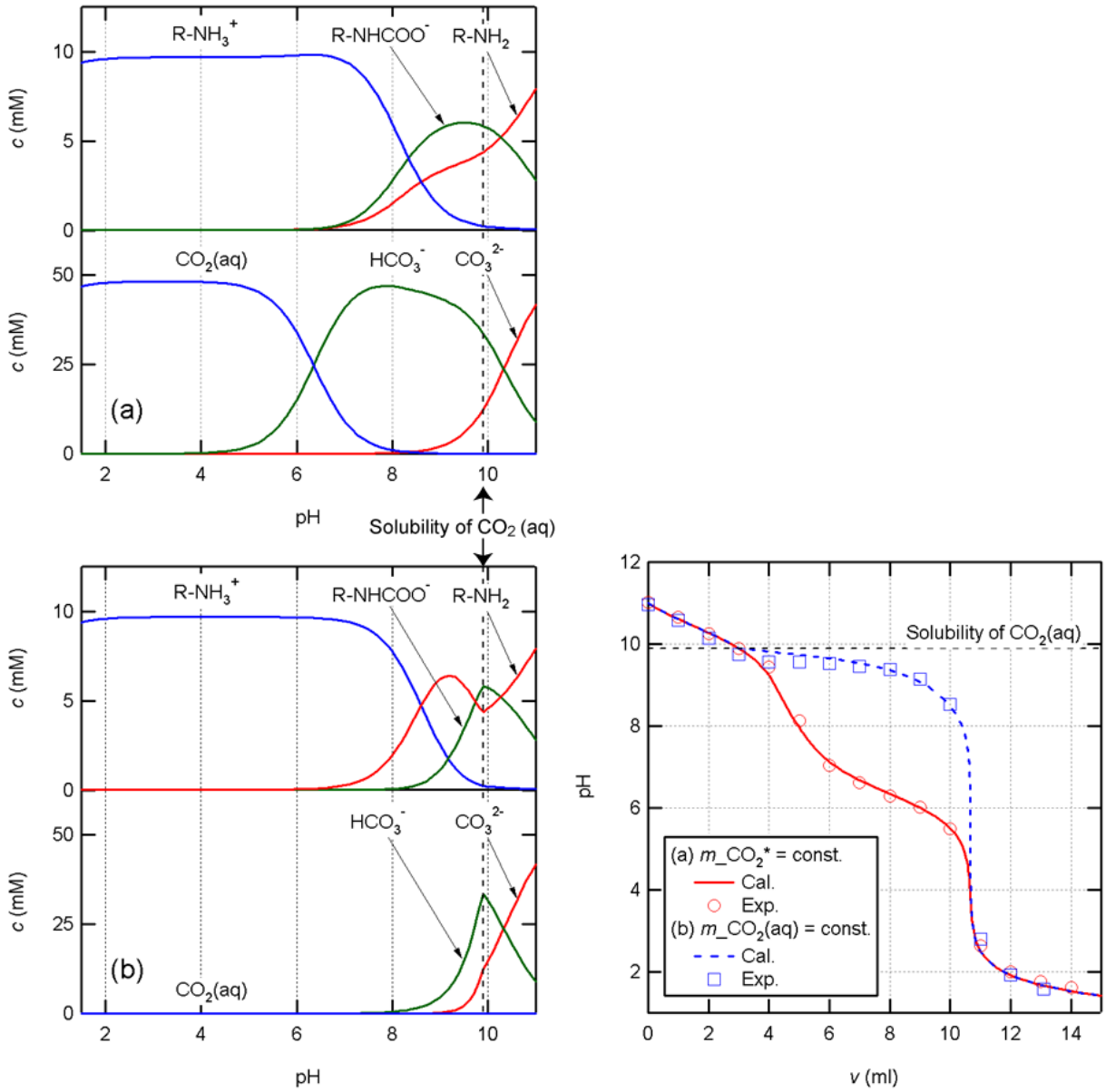

Figure 6.1: Titration curves, and calculated composition vs pH curve. *(left)*: Measured and calculated titration curves of 100 ml of 0.054 M Na_2CO_3 aqueous solution containing PAH titrated with 1 M HCl under two different conditions: (a) The overall CO_2 mass m_CO_2* = m_CO_3^{2-} + m_HCO_3^- + m_CO_2(aq) + m_R–NHCOO$^-$ is constant and (b) the CO_2 mass in the aqueous phase, m_CO_2(aq), is constant. *(right)* Calculated compositions vs. pH curves under two different titration conditions: (a) The overall CO_2 mass m_CO_2* = m_CO_3^{2-} + m_HCO_3^- + m_CO_2(aq) + m_R–NHCOO$^-$ is constant and (b) the CO_2 mass in the aqueous phase, m_CO_2(aq), is constant (Daiguji et al).[14]

The calculation results showed that R-NHCOO$^-$ and R-NH_3^+ coexisted when the solution became cloudy (7.5 < pH <9), suggesting that the colloidal state of PAH was the aggregates of R-NHCOO$^-$ and R-NH_3^+. When the solution was cloudy, in the case of (a), the concentration of CO_2 (aq) was larger than the solubility, thus CO_2 bubbles were generated. Whereas in the case of (b), the concentration of CO_2 (aq) was the same to the solubility, thus CO_2 bubbles were not generated.

If CO_2 is removed from surrounding environment during the synthesis process of hollow PAH microcapsules, the titration curves and compositions vs. pH curves will change as shown in Figure

6.1 (from condition (a) to condition (b)). Not only the concentrations of R–NHCOO$^-$ decreases, but also the equimolar point of R–NHCOO$^-$ and R-NH$_3^+$shifts to higher pH. It will be more difficult to control pH near the equimolar point, that is, it is more difficult to control PSS layer forming process.

If CO_2 is removed from surrounding environment after forming hollow PAH microcapsules but before forming PSS layer, the hollow PAH microcapsules will disappear gradually because the hollow PAH microcapsules are stable for several hours in a closed bottle. If CO_2 is removed from surrounding environment after forming hollow PAH/PSS bilayer microcapsules, the CO_2 leakage rate will increase, but the effect will not be so crucial as the PAH shell contains the gas. Other titration curves for different concentrations of PAH are shown in Appendix 4.

2.2 Size distribution of Colloidal PAH:

Daiguji et al[14] performed Dynamic Light Scattering (DLS) measurements to two different solutions of aqueous PAH with different amounts of CO_2. One solution was prepared by adding NaOH to the PAH aqueous solution until the pH of the solution became 11.0, and then CO_2 gas was dissolved into this solution. CO_2 pressurization lasted few minutes. The other solution was prepared using the aforementioned procedure, however, for this case CO_2 was applied until the solution became cloudy (whitish). Then the pressure was released a little. The colloid mean diameter for the first solution (transparent) was *ca.* 20 nm, whereas that for the cloudy solution was *ca.* 3 μm. The results are displayed in Figure 6.2. These results not only indicated that PAH molecules formed colloidal particles transparent, but the concentration of the particles was so low that the solution

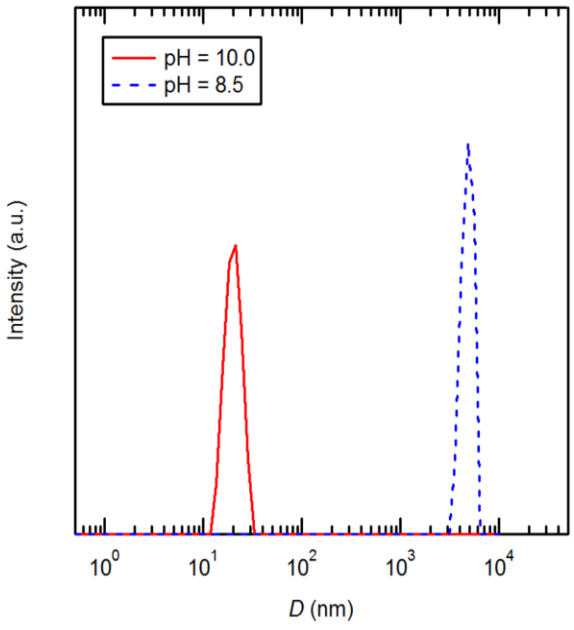

Figure 6.2. Mean diameters of colloids and hollow capsules at two different pH for a 1 g/L PAH. [14]

was transparent, whereas the colloidal particles of PAH encapsulated the CO_2 microbubbles, and the solution became cloudy. The results strongly implied that the mean diameter of the colloidal particles was ca. 20 nm, whereas the mean diameter of the hollow PAH microcapsules was ca. 3 μm. This is, when the CO_2 bubble nucleates, they can be stabilized by adsorbing colloidal PAH to the surface, a layer can form and thus hollow PAH microcapsules can be attained.

3. Experimental

3.1 Materials:

The polyelectrolyte shell materials were PAH (molecular weight: ca. 56 000) (Sigma-Aldrich, US) and PSS (molecular weight ca. 70 000). FITC-PAH (molecular weight: ca. 56 000) (Sigma-Aldrich, US) was used for fluorescence microscopy. The pH adjusted were 1 M NaOH solution (Wako, Japan), 1 M HCl (Wako, Japan), and sodium carbonate (Wako, Japan). All chemicals used in this study were reagent grade. Water with resistivity higher than 18.2 MΩ cm was obtained from a Milli-Q Advantage A10 water purification system.

3.2 Methods:

Hollow PAH microcapsules were fabricated at atmospheric pressure by titration of a Na_2CO_3 aqueous solution including PAH with HCl. Prior to these series of experiments, a 1 M Na_2CO_3 solution was prepared. Size control was attained by changing the concentration of the polyelectrolyte in the solution. While titrating, the solution was gently stirred at 300 rpm at 25 ºC and atmospheric pressure and the final pH for all experiments was adjusted to pH=8.5.

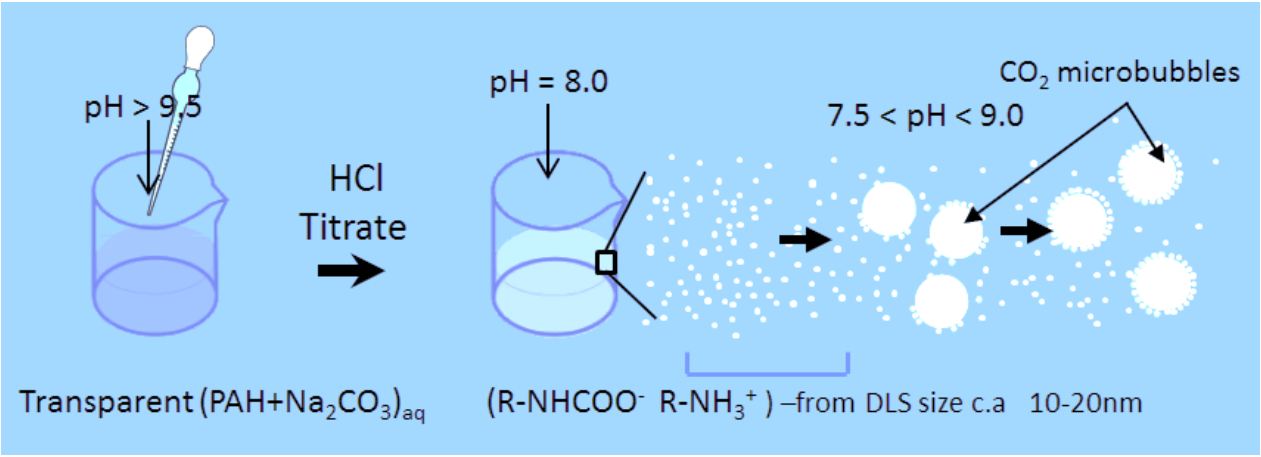

Figure 6.3: Fabrication of PAH microcapsules. When CO_2 microbubbles nucleate in this solution, the colloidal particles of PAH stabilize the micro bubbles via adsorption.

Experimental and theoretical titration curves were in good agreement, which validated the experimental procedures.

Several 1 M solutions of Na_2CO_3 with different concentration of PAH (0.1, 1.0, 2.0, 3.0, 7.0, 15.0, and 20.0 g/L) were prepared to analyze PAH concentration effect on final microcapsules size. Likewise several solutions of Na_2CO_3 (0.5, 1.0, 2.0, and 3.0 M) were prepared to analyze the effect of Na_2CO_3 concentration on final capsule size. A schematic of this process is shown in Figure 6.3.

Bilayer microcapsules were fabricated by adsorbing PSS onto the FITC-PAH stained PAH microcapsule. The concentration of PAH solutions was kept at 0.5 g/L and the concentrations of PSS solution were set to be 0.5, 1.0 and 2.0 g/L, respectively. The pH of PSS solutions and PAH solutions respectively, was adjusted to pH=8.5. Then the PAH microcapsule solution was added slowly to the PSS solution stirring at 300 rpm for more than 5 min to guarantee adsorption of PSS to the PAH microcapsule surface. Then it followed titration of the solution until this solution was stabilized at pH of 7.0.

Size measurements on PAH and PAH/PSS microcapsules were performed 2 hours after microcapsules were synthesized to allow for microcapsules to achieve its equilibrium size. The time evolution of microcapsule size was also measured during standing time. The microcapsule size was obtained by processing several bright field images of microcapsules in several focused planes inside a solution using an inverted microscope system. The electrical properties of PAH and PAH/PSS microcapsules were evaluated by measuring zeta potentials. FTIR-ATR spectra for PAH microcapsules and PAH/PSS bilayer microcapsules in Na_2CO_3 solutions were measured.

Transmission and epifluorescense images were obtained and analyzed using an inverted microscope system (Eclipse Ti-E, Nikon Corporation, Tokyo, Japan). The zeta potential measuremnt was performed using a zeta potential analyser (ZEECOM, Microtec Corporation, Chiba, Japan). The FTIR measurement was performed using an FTIR spectrometer (Nicolet 6700 FTIR, Thermo Scientific, US) with a diamond attenuated total reflectance (ATR) smart accessory.

4. Results and Discussion

4.1 Fabrication of hollow PAH microcapsules:

Figure 6.4 shows the bright field and epifluorescent images of hollow PAH microcapsules. These images clearly show microspheres and the epifluorescent image shows PAH adsorbed on the microspheres. These images confirmed that the generated CO_2 microbubbles were covered with the aggregates of $R\text{-}NHCOO^-$ and $R\text{-}NH_3^+$.

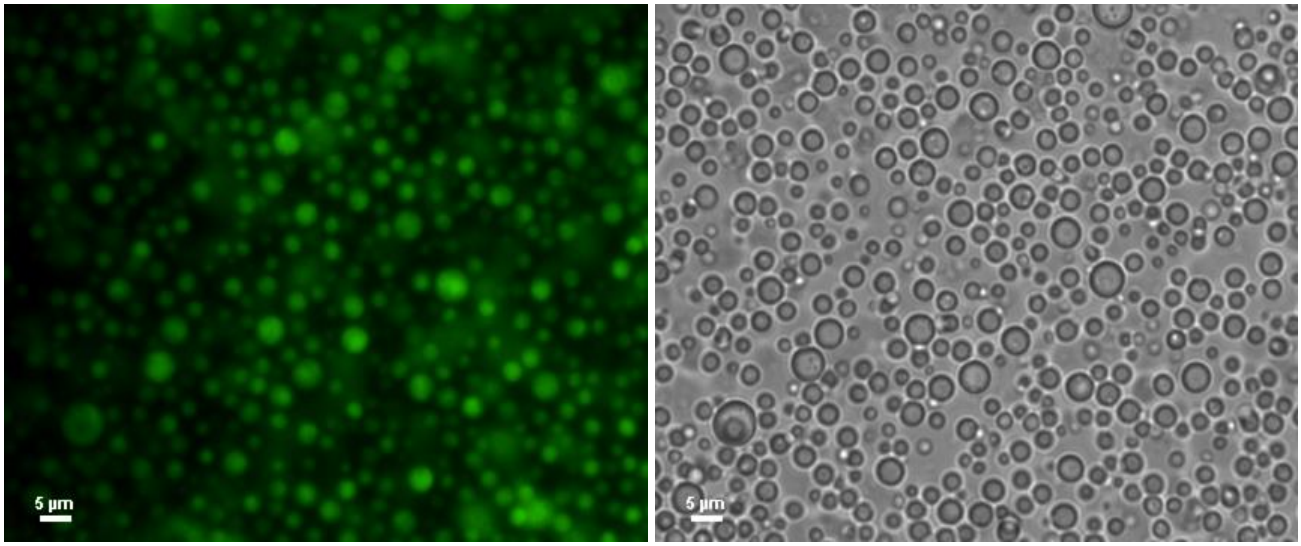

Figure 6.4: Hollow PAH microcapsules. For a concentration of PLA, c_{PLA} = 1g/l in a 0.05 M Na_2CO_3aq solution, it is seen (to the left) a fluorescent image of hollow PAH microcapsules, and (to the right) its corresponding bright field image.

Furthermore, the average diameter of the fabricated microcapsules was about 1 µm. Even more interesting is the fact that before some bubbles coalesced, these were covered with the aggregate. By adjusting the concentration and diffusivity of the aggregates, the diameter could be controlled.

4.2 Size control of hollow PAH microcapsules:

Figure 6.5 shows the effect of standing time on the mean radius of hollow PAH microcapsules for two different PAH concentrations, c_{PAH}=1 and 3 g/L. The time was set as t=0 when the pH of the solutions decreased down to 8.5. Before t=0, because CO_2 gas was generated, the bubbles expanded and the colloidal particles of PAH were accumulated on the surface of the bubbles. Once CO_2 bubbles are nucleated in the solution, CO_2 bubbles should grow due to either the coalescence of bubbles or the heterogeneous nucleation of CO_2 gas at the surface of the bubbles because the solution is oversaturated with CO_2 and bubbles in the bulk solutions are unstable and there is no equilibrium radius. After t=0, because CO_2 gas was no longer generated, the bubbles remained the same or shrunk due to the leakage of CO_2 gas. At t = 0**,** if CO_2 bubbles are covered with the colloidal particles of PAH, the bubbles will survive. However, if not, the bubbles will disappear soon.

Furthermore, it takes about 1 hour before reaching the final radius of bubbles, suggesting that it takes about 1 hour before forming a continuous layer of PAH on the surface of CO_2 bubbles.

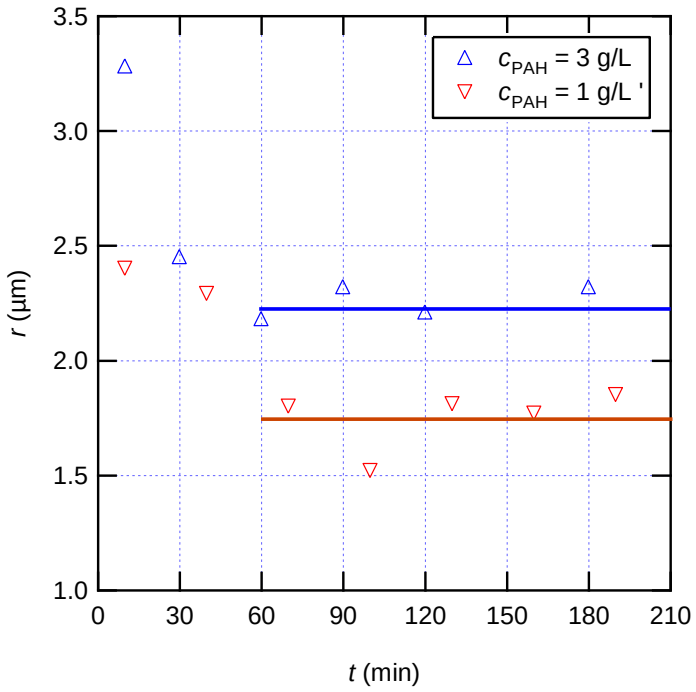

Figure 6.5: Effect of standing time on the mean radius of hollow PAH microcapsules for two different PAH concentrations, c_{PAH}=1 and 3 g/L. The pH of the solutions was 8.5.

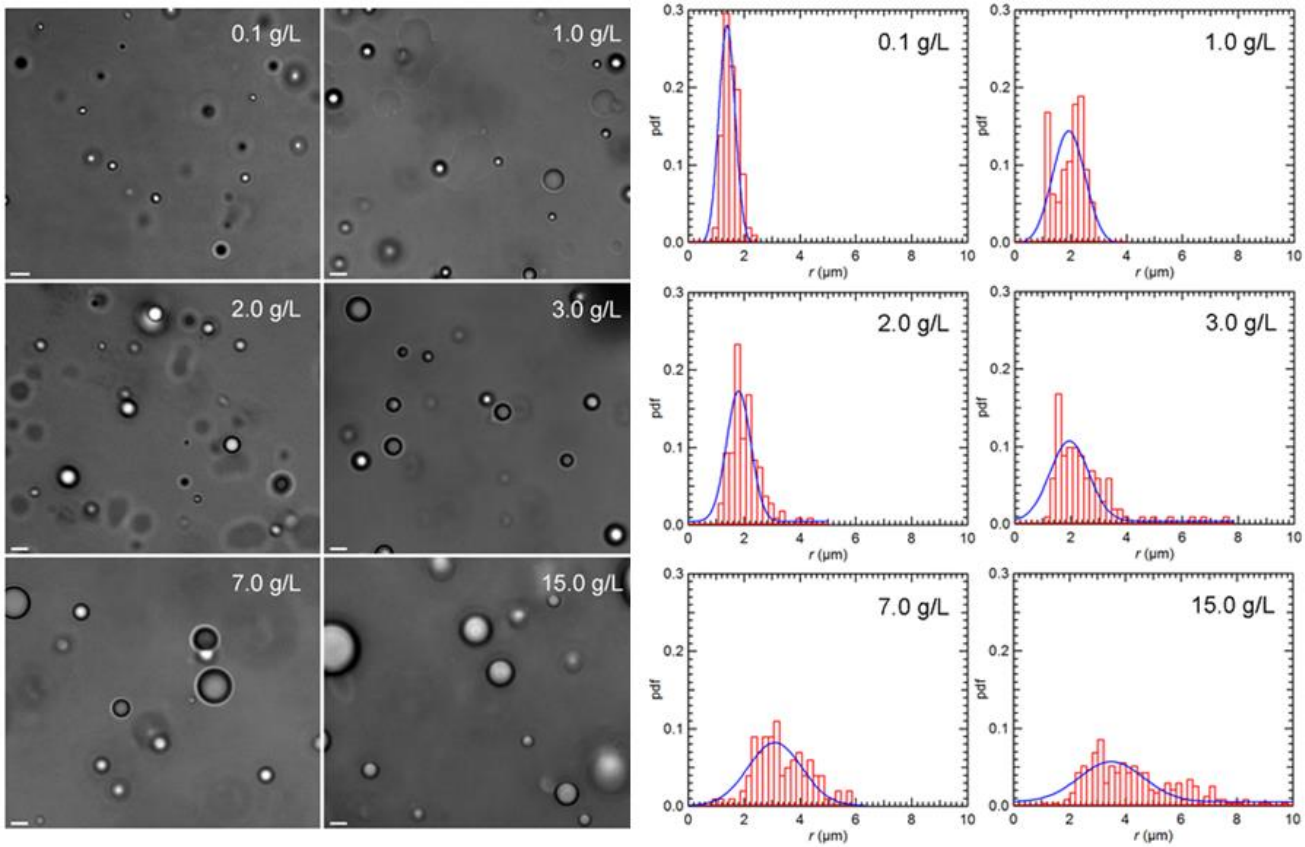

Figure 6.6: Radius distribution (PDF) of the hollow PAH microcapsule radius at pH=8.5 (right) and the corresponding bright field images of hollow PAH microcapsules (left). The scale bar is 5 µm. The PAH concentration of the solutions were 0.1, 1.0, 2.0, 3.0, 7.0, and 15.0 g/L, respectively.

Figure 6.5 also shows that the final mean radius increases with increasing PAH concentration and the time required for reaching the final mean radius is independent of PAH concentration.

Figure 6.6 shows the frequency histogram of microcapsule radius and the representative bright field images of microcapsules floating in the solution as a function of PAH concentration. The radius of microcapsules in this solution was measured from several bright field images. The curves in the graphs show the fitted Gaussian curves.

Table 6.1 summarizes the effect of PAH concentration on final capsule size. The mean radius of microcapsules and their standard deviation increase with increasing polymer concentration.

Figure 6.7 shows the mean radius of microcapsules vs. PAH concentration curves. The curve fit on the graph corresponds to a power function of exponent 1/2, making evident the proportionality between the mean surface area of microcapsules and PAH concentration. To interpret this result, here, the following two assumptions were employed:

(1) PAH colloidal particles are uniform in size, and the number is proportional to PAH concentration.
(2) Total number of nucleated bubbles is the same and independent of PAH concentration, and all microbubbles have mean radius.

If all PAH colloidal particles are adsorbed on microbubbles and the number density on the microbubble surface is constant, the mean surface area of microcapsules should be proportional to PAH concentration. Furthermore, when PAH concentration is 20 g/L, PAH were sedimented from the solution. PAH could no longer be dispersed in the solution as a colloidal form, therefore, no capsules were observed.

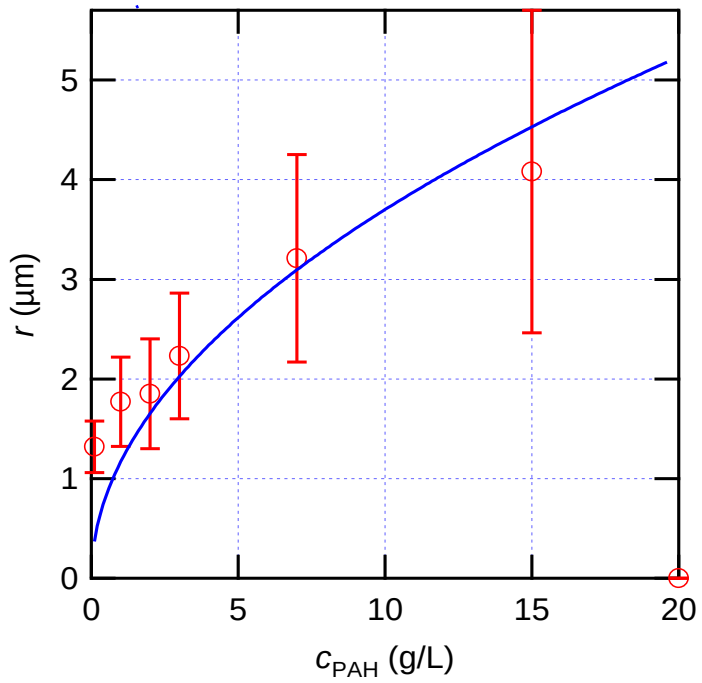

Figure 6.7: The mean radius of hollow PAH microcapsules as a function of PAH concentrations. The pH of the solutions was 8.5.

Table 6.1: Measured capsule radius at pH = 8.5 as a function of PAH concentration, c_{PAH}.

PAH conc. (g/L)	Mean radius (μm)	Standard dev. (μm)	PI (%)
0.1	1.32	0.26	20.41
1.0	1.77	0.45	25.30
2.0	1.84	0.55	30.11
3.0	2.23	0.63	28.40
7.0	3.21	1.04	32.46
15.0	4.08	1.62	39.85

To interpret the deviations of capsule size (see Table 6.1), the time course of number density of PAH colloidal particles dispersed in the solution should be considered. The number density of dispersed PAH colloidal particles decreases as time goes on due to the adsorption on the microbubble surface. The change in number density of dispersed PAH colloidal particles increases with increasing PAH concentration. Therefore, both of the mean radius and standard deviation of PAH microcapsules increase with increasing PAH concentration.

Figure 6.8 shows the mean radius of hollow PAH microcapsules as a function of Na_2CO_3 concentrations. PAH concentration was kept at 1.0 g/L. The mean radius was independent of Na_2CO_3 concentration, suggesting that the amount of nucleated CO_2 bubbles does not affect the capsule size.

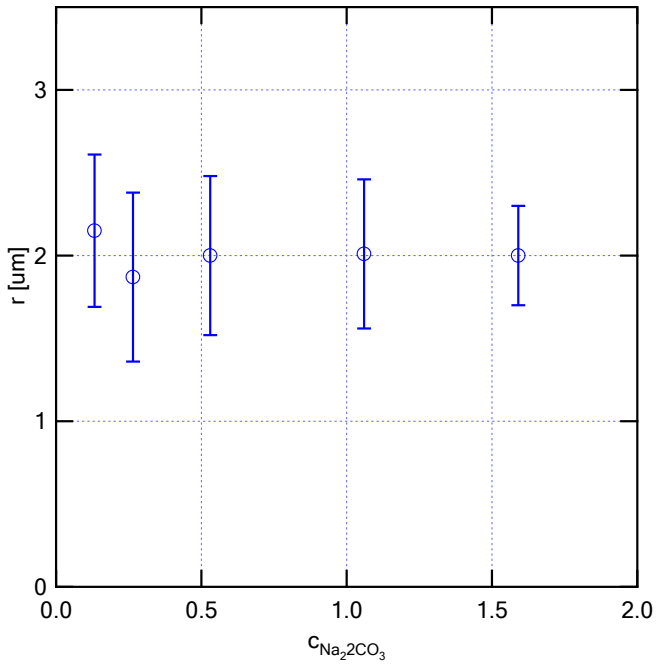

Figure 6.8. The mean radius of hollow PAH microcapsules as a function of Na_2CO_3 concentrations. PAH concentration was 1.0 g/L.

Table 6.2: Measured zeta potentials of PAH microcapsules at pH = 9.0, 8.5, and 7.5.

Type of microcapsules	pH	Zeta potential (mV)
PAH	9.0	-64.8
PAH	8.5	21.2
PAH	7.5	63.9

4.3 PSS layer formation around hollow PAH microcapsules:

Once hollow PAH microcapsules are synthesized, if the pH was decreased, colloids disappeared from the solution since the concentration of R-NHCOO$^-$ decreases and that of R-NH_3^+ increases, resulting in nonequimolar particles. Since the pH of 7.0 is required for medical applications, it is vital that hollow capsules can be stable at this pH. First, to confirm the electrical properties of PAH microcapsules, zeta potential was measured at two different pHs of the solution. Table 6.2 summarizes the result. The measured velocity profiles of the particles are shown in Appendix 4.

The measured zeta potential of PAH microcapsules at pH=8.5 was positive and the value increased with decreasing pH. This result suggests that the concentration of R-NHCOO$^-$ decreases and that of R-NH3$^+$ increases with a decrease in the pH.[12] In the aqueous solution with CO_2, amino group of PAH reacts with CO_2 and becomes carbamate ion R-NHCOO$^-$. As shown in the above graph, the concentration of R-NH_3^+ is larger than that of R-NHCOO$^-$ at pH < 8.5,

while the concentration of R-NHCOO$^-$ is larger than that of R-NH_3^+ at pH > 8.5.Therefore, a low pH is preferable for the sequential adsorption of PSS. However, the solution at pH = 7.5 was more transparent than that at pH = 8.5, suggesting that parts of the PAH colloidal particles could be decomposed and dissolved in the solution and that parts of the PAH microcapsules could disappear. Therefore, if it is desired to adsorb a counter ion to the PAH shell at this pH to form a bilayer, it can be done.

PSS aqueous solutions with concentration of 0.5, 1.0 and 2.0 g/L were also adjusted to pH=8.5. Then, the PAH microcapsule solution was uniformly mixed with each of the PSS solutions and thus enabling bilayer formation around the CO_2 cores. Bilayer microcapsules were synthesized in a solution of which mass ratios of PAH and PSS were m_{PAH}:m_{PSS}=1:1, 1:2, and 1:4, respectively. The volume ratio was kept constant at 1:1 throughout the experiments. After hollow PAH/PSS bilayer microcapsules were synthesized at pH=8.0, the pH of the solution was carefully decreased down to pH=7.0 by titrating with HCl.

Figure 6.9 shows the bright field and epifluorescent images of hollow PAH/PSS bilayer microcapsules at pH=7.0. The mass ratio of PAH and PSS were m_{PAH}:m_{PSS}=1:1, 1:2, and 1:4, respectively. In the solution of m_{PAH}:m_{PSS}=1:4, each capsule was independent.

However, after decreasing the mass ratio of PAH and PSS, hollow PAH/PSS bilayer microcapsules tended to form the aggregates. This result suggests that when the mass ratio of PAH and PSS is large, hollow PAH microcapsules are completely covered with PSS and independent hollow PAH/PSS bilayer microcapsules can be formed, whereas, if it is small, PSS plays a role as a binder to connect several hollow PAH microcapsules and aggregates can be formed. To verify the electrical properties of hollow PAH/PSS bilayer microcapsules, the zeta potentials were measured for m_{PAH}:m_{PSS}=1:2 at pH=8.5 and 7.0.

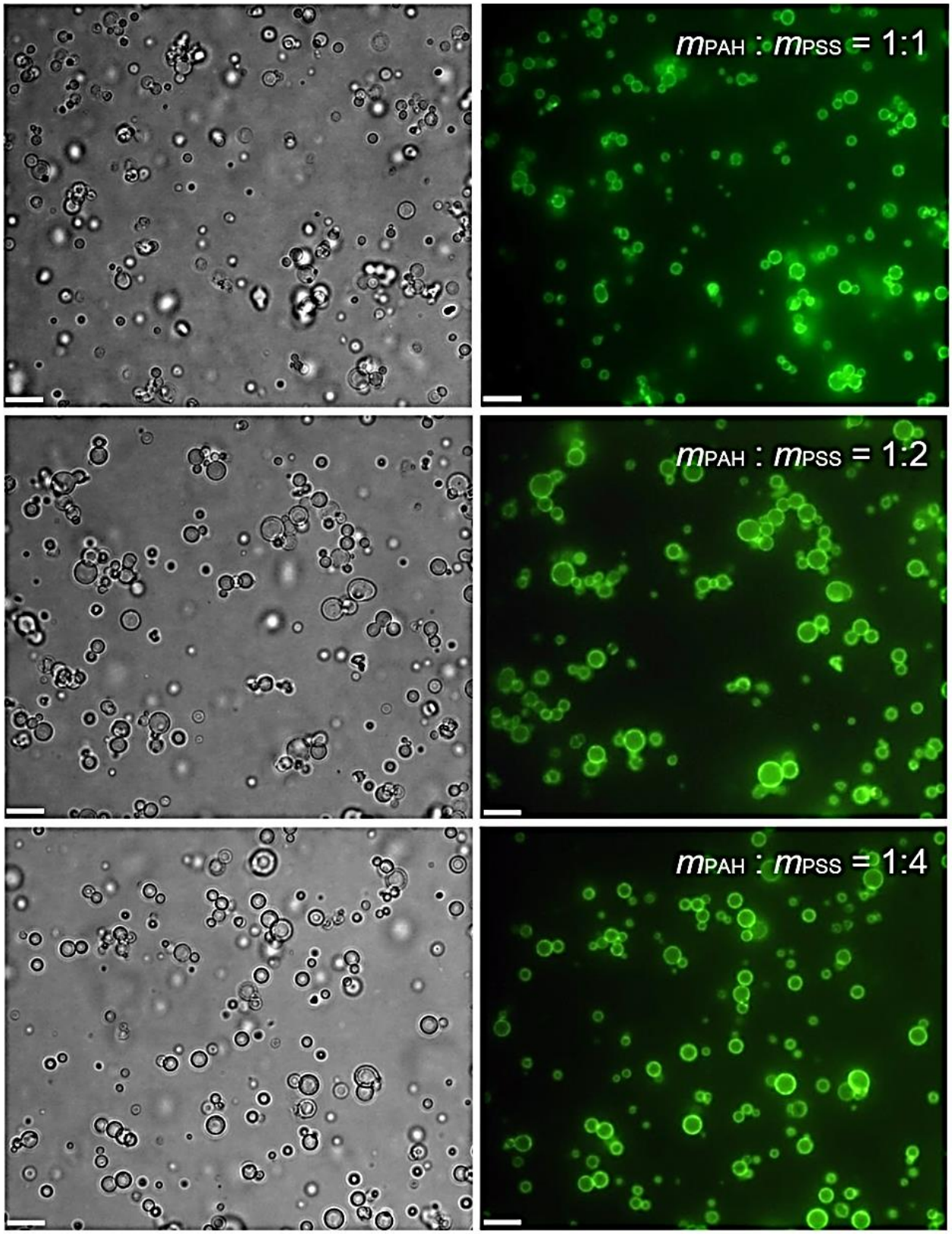

Figure 6.9: Bright field (left) and epifluorescent (right) images of hollow PAH/PSS bilayer microcapsules. The scale bar is 5µm. The mass ratios of PAH and PSS were m_{PAH}:m_{PSS}= 1 : 1 (top), 1 : 2 (middle), and : 4(bottom). The pH of the solution was 7.0.

Table 6.3 summarizes the result. The zeta potential of hollow capsules was changed from positive to negative by adding a hollow PAH microcapsule solution into PSS aqueous solution at pH=8.5, suggesting that PSS adsorbed on hollow PAH microcapsules. Sequentially, when the pH of the solution was decreased to 7.0 by titrating with HCl, the magnitude of zeta potential slightly decreased but the value was still negative.

Table 6.3: Measured zeta potentials of PAH/PSS microcapsules at pH = 8.5.

Type of microcapsules	pH	Zeta potential (mV)
PAH/PSS	8.5	-92.9
PAH/PSS	7.0	-83.3

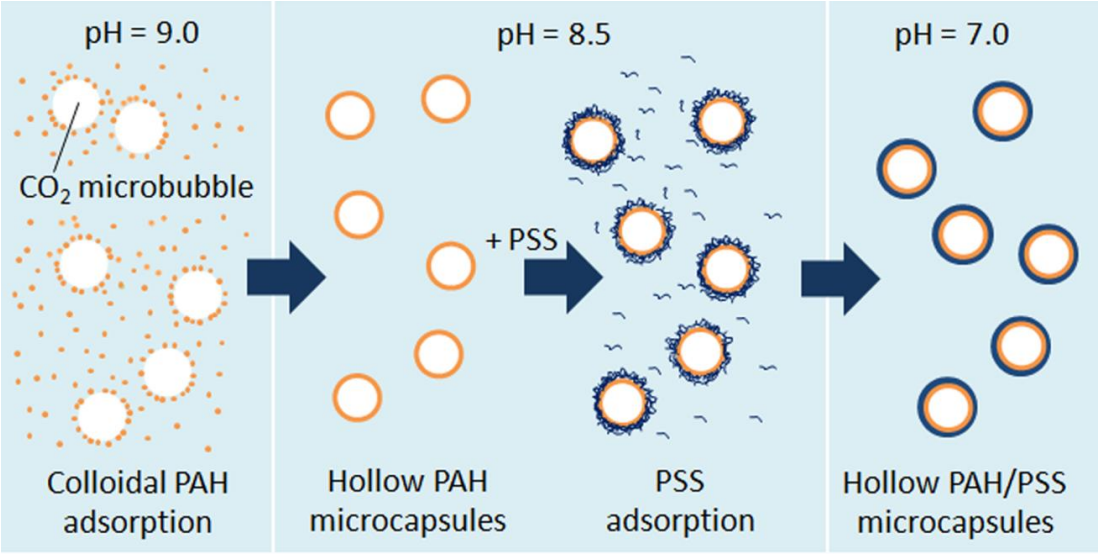

Figure 6.10: Bilayer Fabrication procedure. *(pH = 9)* CO_2 Microbubbles nucleate in a Na2CO3aq solution and will keep growing due to microbubble coalescence or microbubble nucleation at the CO_2 microbubble interface; simultaneously, the colloidal PAH starts to stabilize the microbubbles. *(pH = 8.5)* At this pH the concentration of amino group and carbamate group is equimolar and a PAH shell is completely formed around the microbubbles. At this pH ζ potential is positive and PSS can be adsorbed to the surface. *(pH = 7.0)* The bilayer shell is formed and the microcapsules can withstand this pH.

Figure 6.10 shows a complete schematic of the bilayer formation kinetics process. CO_2 microbubbles nucleate and because the solution is oversaturated with CO_2, the system is unstable, therefore CO_2 microbubbles will keep growing until they are completely stabilized by PAH colloidal particle. After some time these particles form a PAH shell that entirely wraps the bubble preventing its diffusion. A solution of PSS stabilized at pH = 8.5 was made using the procedure shown in *Section 3* of this chapter. Both solutions are mixed and PSS adsorbs to the

PAH capsule surface. Finally a PSS layer forms and the pH of the solution is reduced to pH = 7.0.

Concerning the stability of PAH/PSS microcapsules, it was found that these could last for several weeks. Figure 6.11 shows the FTIR-ATR spectra of 0.05-M aqueous Na_2CO_3 solutions with PAH and with PAH + PSS titrated with 1-M HCl. 128 scans were collected for each measurement over the spectral range of 800–1800 cm^{-1} with a resolution of 2 cm^{-1}. *Daiguji et al* [14] performed the FTIR measurements for the PAH microcapsules solution using a FTIR spectrometer with a diamond attenuated total reflectance (ATR) smart accessory.

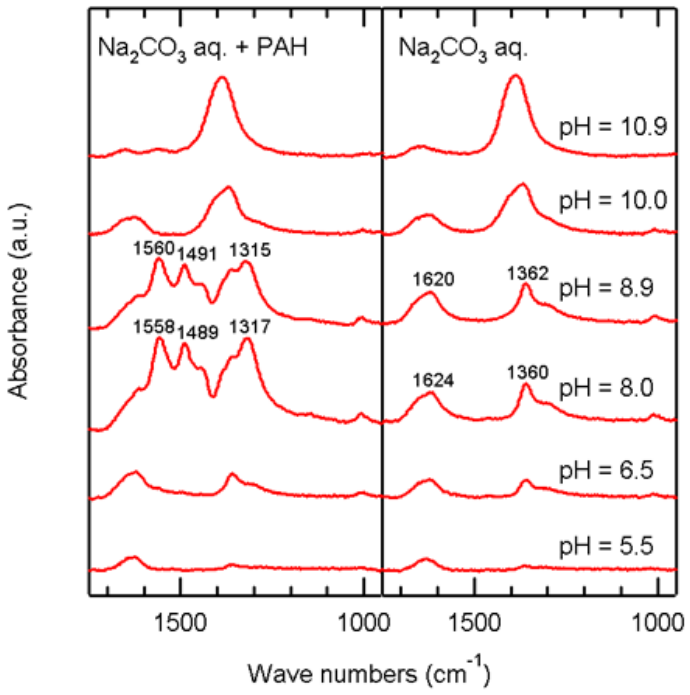

Figure 6.11: FTIR-ATR spectra of 0.054 M Na_2CO_3 aqueous solutions with (left) and without PAH (right) titrated with 1 M HCl. The initial concentration of PAH was set to be 1.0 g /l. [14]

In this work they identified the corresponding band for the amide II and amide III. Since this band only appeared at pH 8.9 and 8.0 , it can be derived from the carbamate group. The FTIR-ATR spectra of the solution without PAH at pH = 8.9 and 8.0 show bicarbonate bands due to stretching vibrations of the carbonate groups at 1362 and 1620 cm^{-1}. The FTIR-ATR spectra of the solutions at pH . 10.9 and 10.0 do not show the bands observed at pH . 8.9 and 8.0. Further, the spectra of the solutions with PAH at pH . 8.9 and 8.0 show bands typical for carbamates within the range of 1200–1600 cm^{-1}.These results confirmed the reaction shown in *section 2* of this chapter.

However Figure 6.12 shows a comparison FTIR-ATR spectra of a solution of pure PAH and

that including PSS. The solutions containing PAH at pH = 7.0 and 6.5 were transparent, but those solutions that had PSS microcapsules were cloudy at the same pH. The FTIR-ATR spectra, Figure 6.14, of the solutions with PAH at 7.0 < pH < 9.0 shows, again, the bands typical for carbamates within the range of 1200–1600 cm^{-1}.

The band around 1500–1600 cm^{-1} is the amide II and is attributed mainly to the distortion oscillations of N–H and the stretching oscillations of C–N in the carbamate.[18] Further, the band around 1300 cm^{-1} is the amide III. The band at 1320 cm^{-1} can also be attributed to the carbamate. The FTIR-ATR spectra of the solution with PAH at pH = 6.5 shows the bicarbonate bands due to the stretching vibrations of the carbonate groups at 1360 and 1622 cm^{-1}.[19-21]

The FTIR-ATR spectra of the solutions with PAH + PSS show that the bands typical for carbamates disappeared.

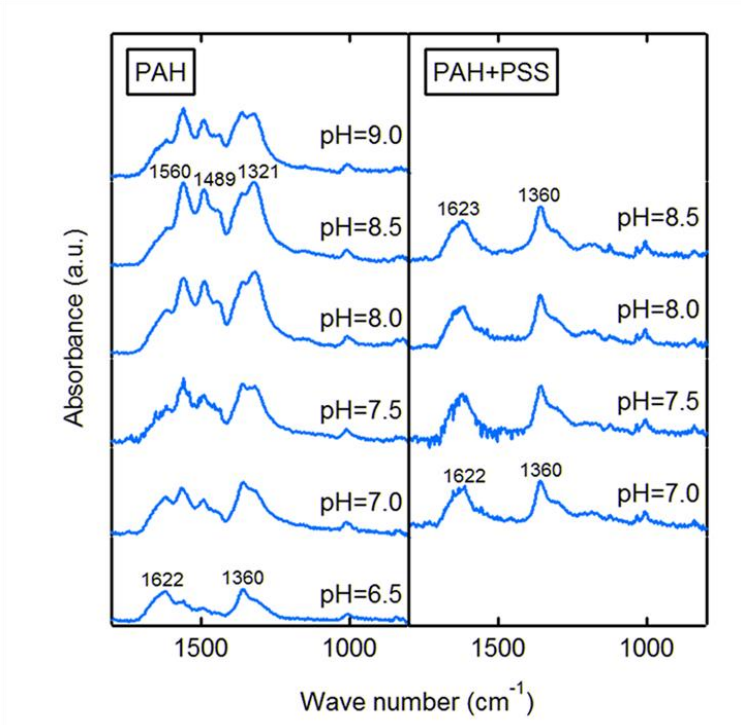

Figure 6.12: FTIR-ATR spectra of bilayer capsules. FTIR-ATR spectra of 0.05-M aqueous Na_2CO_3 solutions with PAH (left) and with PAH + PSS (right) titrated with 1-M HCl. The initial concentrations of PAH and PSS were set to be 0.5 and 1.0 g/L, respectively.

This result suggests that R-$NHCOO^-$ changes to R-NH_3^+ in aqueous PSS solutions and the negative PSS firmly adsorbs on the positive PAH capsule shell. The hollow PAH microcapsules were stable in the solution for several hours in a closed bottle, while, the hollow PAH/PSS bilayer microcapsules were stable more than a week in the same condition. Because the hollow PAH/PSS microcapsules are stable and have a negative charge, the sequential layer formation

can be performed in the same way as that in the normal LbL method.

5. Conclusions

The radius of the hollow PAH microcapsules was successfully controlled by changing the PAH concentration in an aqueous Na_2CO_3 solution in the bubble template method. The radius was independent of the Na_2CO_3 concentration. The zeta potential of the hollow PAH microcapsules was negative at pH = 9.0 and this value changed to positive above pH = 8.5, and then increased with a decrease in the pH. A low pH value was preferable for the sequential adsorption of PSS, but if the pH was very low, the hollow PAH microcapsules disappeared since the PAH colloidal particles could be decomposed and dissolved in the solution.

Hollow bilayer PAH/PSS microcapsules were successfully fabricated by adding a hollow PAH microcapsule solution to an aqueous PSS solution at pH = 8.5. Nevertheless, the success of bilayer fabrication strongly depended on the mass ratio of PAH and PSS. Decreasing the mass ratio of PSS yielded irreversible flocculation. The zeta potential of the hollow PAH/PSS microcapsules was negative because of the adsorbed PSS. The FTIR-ATR spectra revealed that the $R\text{-}NHCOO^-$ band peak disappeared when PSS adsorbed to the PAH shell, suggesting that PSS firmly adsorbed on the hollow PAH microcapsule because of the transformation of $R\text{-}NHCOO^-$ to $R\text{-}NH_3^+$.

6. References

1. Narayan, P.; Wheatly, M. Preparation and Characterization of Hollow Microcapsules for use as Ultrasound Contrast Agents. *Polymer Engineering and Science* **1999,** *39,* 2242-2255.
2. Lin, P.-L.; Eckersley, R. J.; Hall, E. A. H. Ultrabubble: A Laminated Ultrasound Contrast Agent with Narrow Size Range. *Advanced Materials* **2009,** *21,* 3949-3952.
3. Shchukin, D. G.; Kohler, K.; Mohwald, H.; Sukhorukov, G. B. Gas-Fillerd Polyelectrolyte Capsules. *Angewandte Chemie International Edition* **2005,** *44,* 3310-3314.
4. Straub, J. A.; Chickering, D. E.; Church, C. C.; Shah, B. Porous PLGA Microparticles: AI-700, an Intravenously Administered Ultrasound Contrast Agent for Use in Echocardiography. *Journal of Controlled Release 108* **2005,** 21-32.
5. Zhao, Q.; Han, B.; Wang, Z.; Gao, C.; Peng, C.; Shen., J. Hollow Chitosan-Alginate Multilayer Microcapsules as Drug Delivery Vehicle Doxorubicin Loading and in Vitro and in Vivo Studies. *Nanomedicine: Nanotechnology, Biology, and Medicine* **2007,** *3,* 63-74.
6. Decher, G. *in Comprehensive Supramolecular Chemistry,* 1st ed.; J.P. Sauvage, Pergamon Press, 1996; Vol. 9.
7. Peyratout, C.; Dahne, L. Tailor-Made Polyelectrolyte Microcapsules From Multilayers to Smart Containers. *Angewandte Chemie* **2004,** *43,* 3762-3783.
8. Park, J.; Choi, Y.-W.; Kim, K.; Chung, H.; Sohn, D. Aggregation Processes of a Weak Polyelectrolyte, Poly(allylamine) Hydrochloride. *Bulletin of the kKorean Chemical Society* **2008,** *29,* 104-110.
9. Calliada, F.; Campani, R.; Bozzini, A.; Sommaruga, M. Ultrasound contrast agents: basic principles. *European Journal of Radiology* **1998,** *27,* 157-160.
10. Stuart, M. A. C.; Hoogendam, C. W.; Keizer, A. d. Kinectics of polyelectrolyte adsorption. *Journal of Physics: Condensed Matter* **1997,** *9,* 7767-7783.
11. Adamczyk, Z.; Siwek, B.; Musiał, E. Kinetics of Colloid Particle Adsorption at Heterogeneous Surfaces. *Langmuir* **2001,** *17,* 4529-4533.

12. Dobrynina, A. V.; Rubinstein, M. Theory of Polyelectrolytes in solutions and surfaces. *Progress in Polymer Sience* **2005,** *30,* 1049-1118.
13. Hershkovits, E.; Tannenbaum, A.; Tannenbaum, R. Polymer Adsorption on Curved Surfaces: A Geometric Approach. *Journal of Physical Chemistry B* **2007,** *111,* 12369-12375.
14. Daiguji, H.; Matsuoka, E.; Muto, S. Fabrication of hollow poly-allylamine hydrochloride/poly-sodium styrene sulfonate microcapsules from microbubble templates. *Soft Matter* **2010,** *6,* 1892-1897.
15. Molino.J.J.; Matsuoka, E.; Daiguji, H. Size control of hollow poly-allylamine hydrochloride/poly-sodium styrene sulfonate microcapsules using the bubble template method. *Soft Matter* **2011,** *7,* 1897-1902.
16. Petrov, A. I.; Antipov, A. A.; Sukhorukov, G. B. Base-Acid Equilibria in Polyelectrolyte Systems: From Weak Polyelectrolytes to Interpolyelectrolyte Complexes and Multilayered Polyelectrolyte Shells. *Macromolecules* **2003,** *36,* 10079-10086.
17. McCann, N.; Phan, D.; Wang, X.; Conway, W.; Burns, R.; Attalla, M.; Puxty, G.; Maeder, M. Kinetics and Mechanism of Carbamate Formation from CO2(aq), Carbonate Species, and Monoethanolamine in Aqueous Solution. *Journal of Physical Chemistry A* **2009,** *113,* 5022-5029.
18. Krol, P.; Wietrazynska-LalakL, Z. Study on Sturucture and Properties of Carbamates as Model Compounds for Urethane Polymers. *European Polymer Journal* **1995,** *31,* 689-699.
19. Naik, V. M. Vibrational Spectroscopty Studies of L,D-alternating Valine Peptides. *Vibrational Spectroscopy* **1992,** *3,* 105-113.
20. Nickolov, Z. S.; Ozcan, O.; Miller, J. D. FTIR analysis of water structure and its significance in the flotation of sodium carbonate and sodium bicarbonate salts. *Colloids and Surfaces A: Physicochem. Eng. Aspects* **2003,** *224,* 231-239.
21. Karmali, K.; Karmali, A.; Teixeira, A.; Curtob, M. J. M. The use of Fourier transform infrared spectroscopy to assay for urease from Pseudomonas aeruginosa and Canavalia ensiformis. *Analytical Biochemistry* **2004,** *331,* 115-121.

7

Conclusions

In order to functionalize micro bubbles with a shell in the micrometer size range, a simple technique was developed in which hollow biodegradable microcapsules have been fabricated by using micro bubbles as a template. This method was called The Bubble Template Method. In this method, hollow microcapsules of poly(lactic acid) (PLA) were fabricated using bubbles. The process consist on the nucleation of bubbles inside droplets of a dichloromethane solution of PLA prepared in a continuum medium of an aqueous solution of either poly(vinyl alcohol) (PVA) or water. Furthermore two other variants of this method were developed to manufacture bigger PLA microcapsules and bilayer polyelectrolyte microcapsules that can withstand human pH. This is, three types of hollow biodegradable microcapsules made from microbubble templates were successfully manufactured in a facile way.

Regarding hollow PLA microcapsules, the experimental conditions required for the stability of the uniformly sized microbubbles inside a droplet of a dichloromethane solution of PLA were identified, for which it was theoretically and experimentally found that the equilibrium radius is given by Laplace equation. Furthermore, the conditions required for the release of hollow PLA microcapsules from the droplet were also elucidated. There exist a required minimum amount of microbubbles in order to attain a stable radius. Moreover, size control of the fabricated capsules was attained, and it was concluded that in order to attain high uniformity, a low initial concentration of PLA, the addition of PVA, and a low molecular weight of PLA is required. At this condition, the energy barrier at the liquid-liquid interface is reduced. On the other hand, in order to mass produce them, a higher concentration of polymer is required. A higher concentration increases the solubility

of air in the system and by enhancing the nucleation process using ultrasound, much more microcapsules of uniform size were fabricated.

As for PAH/PSS (poly-allylamine hydrochloride/ poly-sodium styrene sulfonate) bilayer capsules, the success of fabricating a bilayer strongly depends on the mass ratio of PAH and PSS. If this ratio is below one, irreversible flocculation is produced. On the basis of the analysis of the zeta potentials and Fourier transform infrared-attenuated total reflection (FTIR-ATR) spectra for hollow microcapsules of both PAH and PAH/PSS it was understood that it was the transformation of the carbamate ion (anion) into the amino ion (cation) in the PSS solutions which allowed the negative PSS to firmly adsorbs on the positive PAH capsule shell.

Future Research

1. **PLA microcapsules fabricated using the Bubble template method:**

(1) Better understanding of bubble nucleation and growth in polymer solutions is required. It is understood that adding PLA into dichloromethane increases the solubility of Nitrogen in the solution, yet we cannot explain the mechanism of bubble growth in the ternary system. Furthermore, the in vitro analysis of the acoustic properties of the microcapsules, the degradation kinetics and the mechanical characterization (e.g. nano identation) of the capsules must be performed in detail. **(2)** Because of the standing free geometry of hollow capsules, the clarification of their stress-strain curves is desirable from the scientific and engineering point of view. Furthermore, current theoretical models cannot properly describe the whole stress-strain curves because these are based on the important assumption that deformation is completely reversible (which is not). It is important to determine these curves, and develop better models. **(3)** In addition, a new research direction can be considered as the appropriate modeling of the dynamics of ultrasound contrast agents is based on a modified Rayleigh Plesset equation in which the main assumption is that ultrasound contrast agents are surrounded by an infinite fluid and remain spherical until collapse. This view is not accurate because it is a poor description of the system considering the space in small blood vessels. **(4)** Future studies should also analyze mass transport through the polymer shell in several flow conditions that characterize blood flow in human bodies (vessels, capillaries, blood clots, etc). It is possible to load the capsules with hydrophobic drugs, however, the fabrication methods displayed in this thesis can be adjusted to load hydrophilic drugs. **(5)** Furthermore, the shown process can be potentially employed for manufacturing inorganic capsules that can serve as acoustic or heat insulator systems.

2. **The Gas/O/W method:**

(1) Capsules manufactured using the Gas/O/W method must be tested as well to assess the

mechanical properties of the capsules as they are intended to be employed as shock absorbers. Because of their size and its potential size tailorability over a wider range of sizes, these capsules have the great potential to host phase change materials, be employed as bioreactors or as scaffolds for cell cultivation. Because of their size, they can also be employed in the food industry and cosmetics.

Appendix 1

1. Bigger bubbles bigger capsules: The Gas/O/W method

In the work of Sakurai et al (Sakurai, D.; Molino, J. J.; Daiguji, H.; Takemura, F. *Journal of Material Chemistry A* **2013,** *1*, 14562-14568) based on the theoretical analysis in Chapter 2, if the droplet radius in the CH_2Cl_2–nitrogen solution is r_d = 10 μm and the nitrogen concentration of the solution is close to the solubility ($c'_2 \approx c'_{2s}$), the total nitrogen molar amount inside the droplet is about $N_2 = 2.2 \times 10^{-8}$ μmol. If a single bubble appears inside the droplet of r_d = 10 μm and $N_2 = 2.2 \times 10^{-8}$ μmol, the equilibrium radius is 4.8 μm. The smaller radius of 0.96 μm is unstable. Now, lets imagine that such a droplet of CH_2Cl_2–nitrogen solution is located in an aqueous medium. If the solution includes bubble nuclei, microbubbles will appear from the nuclei. Initially, bubbles with radius of $r_b \approx 2\gamma/p''_1 \approx 2\gamma/p''_{01}$ (= 0.96 μm) may appear because $c'_2 \approx c'_{2s}$. However, a single bubble (q = 1) or multiple bubbles (e.g. q = 5) of r_b = 0.96 μm is unstable because $dN_2/dr_b < 0$. In addition, the N_2–r_b curve for r_d = 10 μm and q = 15 does not cross $N_2 = 2.2 \times 10^{-8}$ μmol, suggesting that there is a limitation on the number of bubbles in a droplet. Thus, bubbles grow and/or coalesce, and ultimately become a single bubble of r_b = 4.8 μm, while the nitrogen concentration of the solution decreases below the solubility ($c'_2 < c'_{2s}$). According to this analysis, it can be possible that a single bubble is formed in a droplet by keeping the CH_2Cl_2–nitrogen solution in a closed volume. In a real system, dissolution of CH_2Cl_2 into the surrounding aqueous medium should be slow enough to form a single bubble without appreciable change in size of the droplet. Subsequently, even if the dissolution of CH_2Cl_2 is extremely slow, CH_2Cl_2 dissolves into the aqueous medium as time goes on, while most of the nitrogen stays inside the droplet because CH_2Cl_2 is miscible with the aqueous medium but the solubility of nitrogen in the aqueous medium is much lower than that in CH_2Cl_2. Furthermore,

the dissolution rate of CH_2Cl_2 is much lower than the relaxation rate needed to achieve bubble–liquid equilibrium inside the droplet. Thus, it could be considered that a droplet of CH_2Cl_2–nitrogen solution is in a closed system at each time step. Under such conditions, if N_1 decreases (i.e., r_d decreases) and N_2 stays constant, the final bubble radius, r_b, can be estimated by substituting $q = 1$ and $N_1 = (\eta p''_{01}/RT)(4/3)\pi {r_b}^3 = (p''_1/RT)(4/3)\pi {r_b}^3$ into equation 9 Specifically,

$$N_2 = \frac{p'}{RT}\frac{4}{3}\pi r_b^3\left(1-\eta\frac{p''_{01}}{p'}+\frac{2\gamma}{r_b p'}\right) = \frac{p''_2}{RT}\frac{4}{3}\pi r_b^3 \qquad (10)$$

The relation of N_2 and r_b given by equation 10 is also shown in Figure 1. When $N_2 = 2.2 \times 10^{-8}$ μmol, the final bubble radius r_b = 6.3 μm. It should be noted that a single bubble in the droplet is thermodynamically stable during the entire process of droplet shrinkage, which is shown by an arrow in Figure 1. This suggests that a single bubble inside the droplet stays stable during the following fabrication procedure.

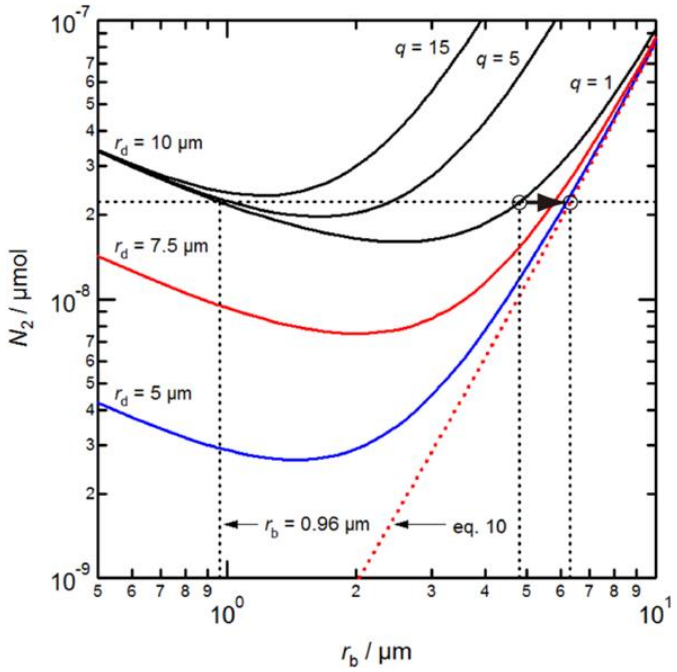

Figure 1: Total molar amount of nitrogen in a closed volume of CH_2Cl_2–nitrogen solution including a single (q = 1) or multiple (q > 1) nitrogen bubble vs. bubble radius (N_2–r_b) curves for an effective droplet radius r_d = 5–10 μm.[1]

Figure 2 shows a schematic diagram of the proposed fabrication method of hollow PLA microcapsules (gas/O/W method). Here, a CH_2Cl_2 solution of PLA is used instead of pure CH_2Cl_2. Droplets of CH_2Cl_2 solution of a PLA–air solution are distributed in a continuous aqueous solution. With time, CH_2Cl_2 diffuses into the surrounding aqueous solution and a single air bubble is covered with PLA. If uniformly sized droplets of CH_2Cl_2 solution of PLA containing the same amount of air (more than the minimum amount of air is required for bubble stability) were distributed in the aqueous medium, uniformly sized hollow PLA microcapsules can be produced.

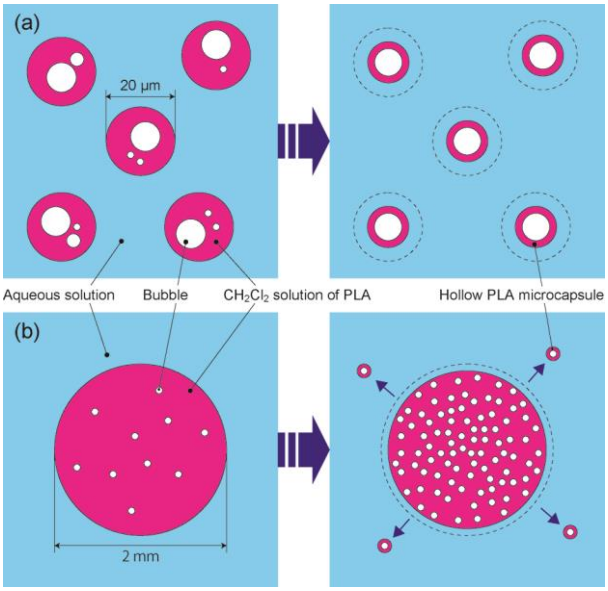

Figure 2: Schematic diagrams of two different fabrication methods of hollow PLA microcapsules: (a) gas/O/W method and (b) bubble template method.[1]

Figures 3a and 3b show the procedures for two different fabrication methods of hollow PLA microcapsules: (a) the gas/O/W method and (b) the bubble template method, respectively. In the gas/O/W method, a droplet of CH_2Cl_2 solution of PLA (300 kDa) was formed in an aqueous solution of CH_2Cl_2 [Figure 3a (left)]. The initial concentration of PLA was 10 g L^{-1} and the initial concentration of air in the solution was close to the solubility at atmospheric pressure ($c'_2 \approx c'_{2s}$).

In order to visualize the fabricated hollow PLA microcapsules by fluorescence imaging, Nile Red was also dissolved in the CH_2Cl_2 solution of PLA; the color of the droplets was pink. The solution was sonicated for 10 s using an ultrasound bath. Microbubbles were generated in a droplet of CH_2Cl_2 solution of PLA, and the droplet changed from transparent to cloudy [Figure3a (center)].

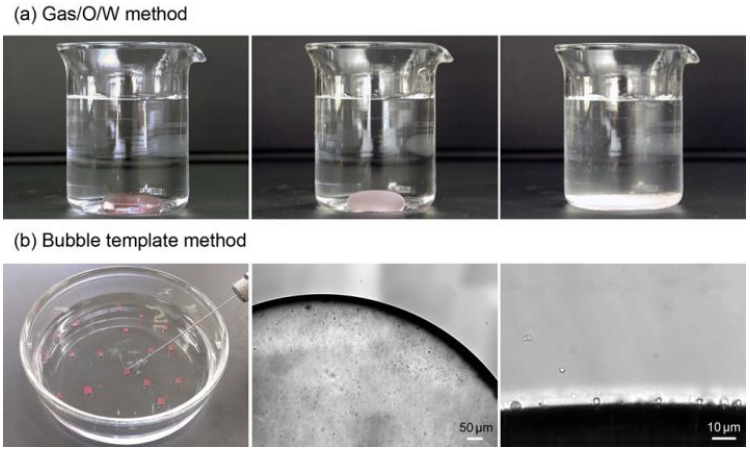

Figure 3: Procedures of two different fabrication methods of hollow PLA microcapsules: (a) gas/O/W method and (b) bubble template method.[1]

The average radius of the microbubble was about 5 μm. Since the droplet size was much larger than the bubble size, the system, i.e., the droplet of CH_2Cl_2–air solution in an aqueous medium, could be regarded as an open system and there should be no equilibrium bubble radius. However, the bubble radius was quite uniform. Then the droplet and the surrounding aqueous solution were mixed using a homogenizer at 3500 rpm for 10 s. A droplet of CH_2Cl_2 solution of PLA containing microbubbles was broken down into micro scale droplets containing a single microbubble or multiple microbubble, and they were dispersed in aqueous solution. If the droplet and the surrounding aqueous solution were mixed using a homogenizer without sonication, many microscale droplets that did not contain any bubbles were produced.

Figures 4a and 4b show the bright-field and fluorescent images of hollow PLA microcapsules fabricated by the gas/O/W method and bubble template method, respectively. Both images have the same magnifications. These images clearly show that the size of hollow PLA microcapsules fabricated by the gas/O/W method is about one order larger than that of the microcapsules produced by the bubble template method. In Figure 4a, most of the microspheres are hollow microcapsules with a single internal void, but microspheres containing multiple voids or no void could also be observed.

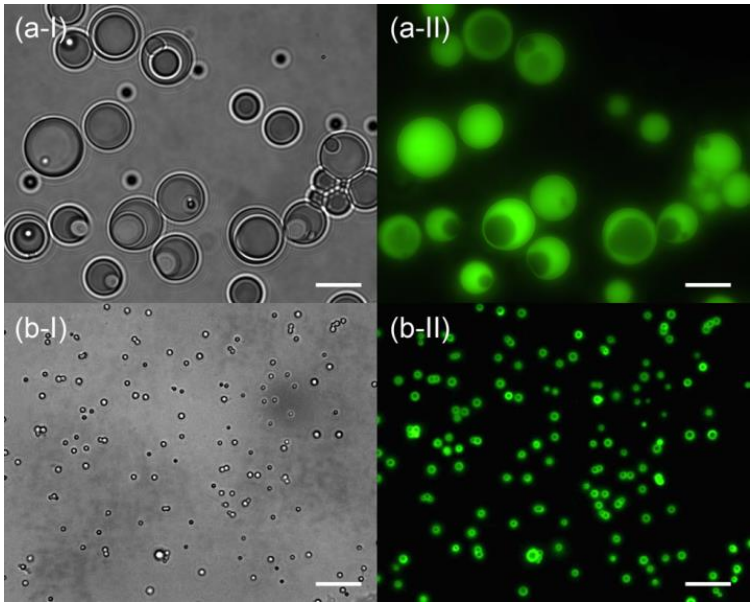

Figure 4: **(I) Bright-field and (II) fluorescence microscopy images of hollow PLA microcapsules fabricated by (a) gas/O/W method and (b) bubble template method.** The scale bar is 10 μm.[1]

Figures 5a and 5b show the radius distributions of hollow PLA microcapsules fabricated by the gas/O/W method and bubble template methods, respectively. For the microcapsules fabricated by the gas/O/W method, the mean values (m), standard deviations (σ), and polydispersity indices (PI = standard deviation/mean) of the outer and inner radii are (m = 5.49 μm, σ = 2.14 μm, and PI = 39.0%) and (m = 2.35 μm, σ = 0.93 μm, and PI = 39.6%), respectively. For the microcapsules

fabricated by the bubble template method, these values are (m = 0.78 μm, σ = 0.060 μm, and PI = 7.69%) and (m = 0.42 μm, σ = 0.058 μm, and PI = 13.6%), respectively. The PI of hollow PLA microcapsules fabricated by the gas/O/W method was larger than that of those produced by the bubble template method, indicating lower uniformity of the hollow PLA microcapsules fabricated by the gas/O/W method.

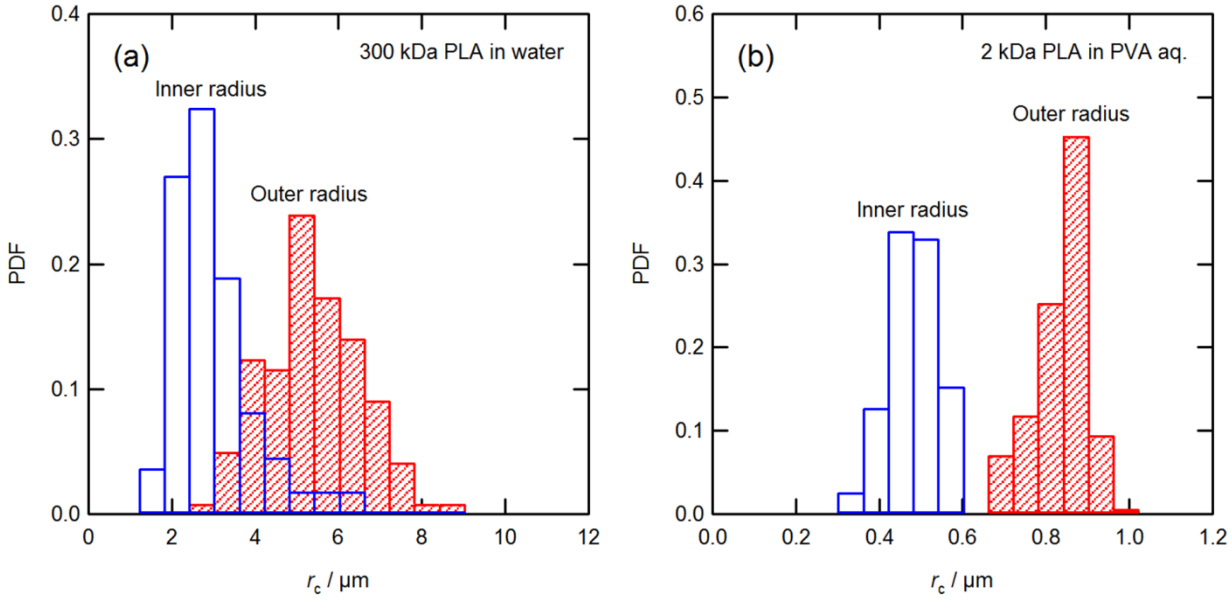

Figure 5. Radius distribution of hollow PLA microcapsules fabricated in (a) gas/O/W method and (b) bubble template method.

2. Radius distributions of microbubbles in a droplet of CH_2Cl_2 solution of PLA in the Gas/O/W method

Figure 6 shows a bright-field image of microbubbles inside a droplet of CH_2Cl_2 solution of PLA (300 kDa) when the initial concentration of PLA in CH_2Cl_2 was 10 g L^{-1}. The central part of a droplet was observed just after sonication as shown in Figure 3a (center). The bubble size was quite uniform and did not change considerably during the observation.

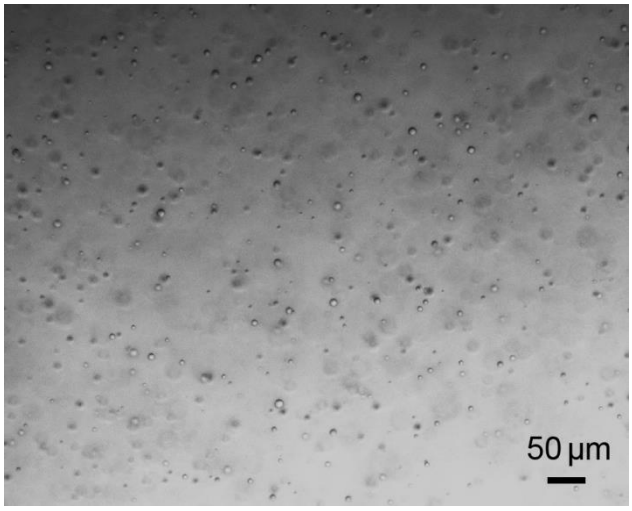

Figure 6: Bright-field image of microbubbles inside a droplet of CH_2Cl_2 solution of PLA (300 kDa). The initial concentration of PLA in CH_2Cl_2 was 10 g L^{-1}. [1]

Figure 7 shows the radius distributions of microbubbles in a droplet of CH_2Cl_2 solution of PLA (300 kDa). The initial concentrations of PLA in CH_2Cl_2 were 5, 10, and 20 g L^{-1}. The mean values (m), standard deviations (σ), and polydispersity indices (PI = standard deviation/mean) of the bubble radius for the initial concentrations of 5, 10, and 20 g L^{-1} were (m = 3.78 µm, σ = 1.23 µm, and PI = 32.5%), (m = 4.23 µm, σ = 1.26 µm, and PI = 29.8%), and (m = 6.34 µm, σ = 2.63 µm, PI = 41.5%), respectively. As the initial concentration of PLA increased, the size increased and the uniformity deteriorated.

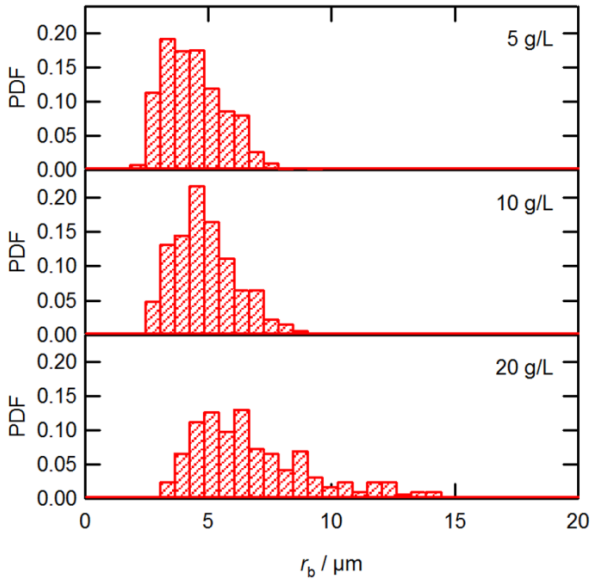

Figure 7: Radius distributions of microbubbles in a droplet of CH_2Cl_2 solution of PLA (300 kDa). The initial concentrations of PLA in CH_2Cl_2 were 5, 10, and 20 g L^{-1}.[1]

3. The condition for constant dr_d/dt

If the dissolution of the PVA aqueous solution into methylene chloride is negligible, the dissolution rate of the a spherical methylene chloride droplet into the surrounding PVA aqueous solution, $\dot{m}_1$, can be expressed as follows:

$$\dot{m}_1 = c_1 S_\mathrm{d} \frac{dr_\mathrm{d}}{dt}, \tag{1}$$

where c_1 is the concentration of methylene chloride inside the droplet, and r_d is the radius of the droplet. By using the mass flux of methylene chloride from the surface of a spherical droplet into the surrounding PVA aqueous solution, J_1, $\dot{m}_1$ can also be expressed as follows:

$$\dot{m}_1 = S_\mathrm{d} J_1, \tag{2}$$

where S_d is the surface area of a methylene chloride droplet. From eqs. a17 and a18, dr_d/dt can be expressed as follow:

$$\frac{dr_\mathrm{d}}{dt} = \frac{J_1}{c_1}, \tag{3}$$

If J_1 is constant, that is, the dissolution rate of methylene chloride is restricted by the surface area of a droplet and is not restricted by the diffusion in the PVA aqueous solution, dr_d/dt remains constant.[2]

4. Measurements of the external and internal radii

A 60x water immersion lens that has a depth of field of 0.4 μm was employed. The focusing plane is the plane at which the measurements were made. This plane was intended to be at the middle of the microcapsules. This plane is located at a height z = 0 μm. Thus, planes located between -0.2 μm $\leq z \leq$ 0.2 μm, are in focus.

Several planes above and below the focusing plane for a single microcapsule were analyzed. Figure 8 shows the sequential micrographs of the same microcapsule taken at different planes. Notice that the micrographs that lie within -0.2 μm $\leq z \leq$ 0.2 μm are exactly the same image. As we deviate from this range, error in the measured data increases as well.

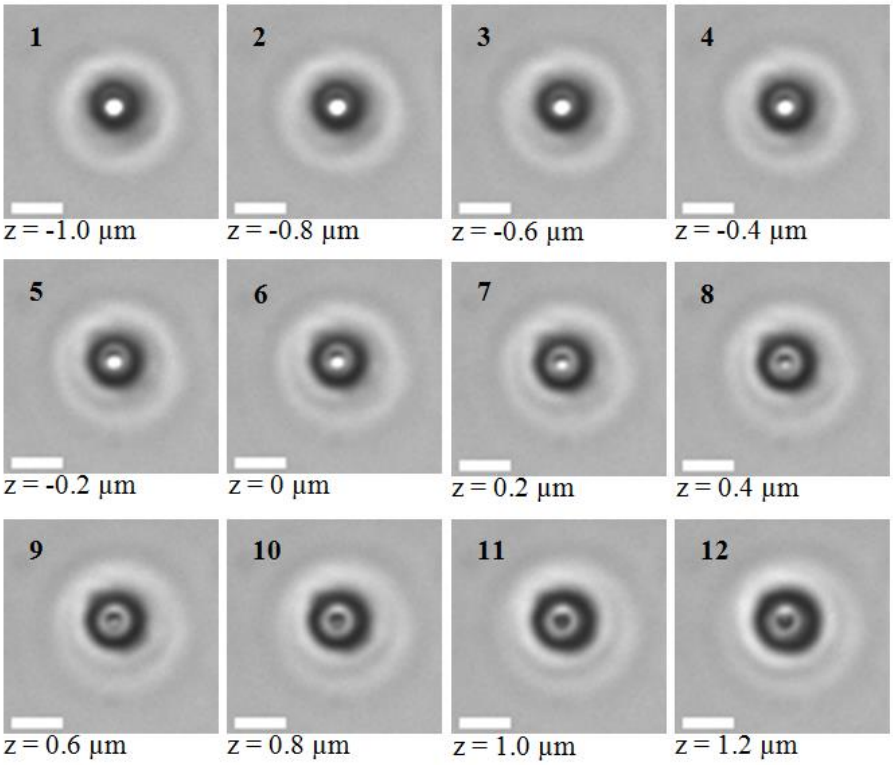

Figure 8: Sequential micrographs of a hollow microcapsule taken at different planes. Micrograph #6 is the plane of focus. The scale bar is 2 µm long.

In the images and distributions shown, small number of microcapsules is located outside of the depth of field. Even if the center of capsules was located below or above the focusing plane, the error was about 0.1 µm. However, the number of capsules outside the depth of field was negligible compared to the population located within the depth of field. Thus the measured average radius was unaffected by the errors in measurements made on those capsules that were out of focus.

5. References

1. Sakurai, D, Molino, J.J., Daiguji, H., Takemura, F., Hollow polylactic acid microcapsules fabricated by gas/oil/water and bubble template methods," *Jourtnal of Materia. Chemistry A* **2013**, *1,* 14562-14568
2. Daiguji, H.; Takada, S.; Molino, J. J.; Takemura, F., Fabrication of hollow poly(lactic acid) microcapsules from microbubble templates, *Journal of Physical Chemistry B* **2009,** *24,* 15002-15009.

Appendix 2

1. Measurement of interfacial tensions

Interfacial tension measurements were performed via the pendant drop method using the Drop Master Series DM-501 (Kyowa Interface Science, Japan). Dichloromethane drops with or without 2 g/L PLA were formed in either pure water or a 2% (w/w) PVA aqueous solution. The interfacial tension values were determined from at least 5 independently formed drops. The volume of the drops was constant and the interfacial tension was monitored for at least 12 min. The temperature of the experiments was 298 K. As shown in Figure A1, the sizes of the droplets were kept at 17, 16, 10, and 8 μL for the dichloromethane–water (CH_2Cl_2–H_2O), 2 g L^{-1} PLA (2kDa) dichloromethane solution–water (CH_2Cl_2+PLA–H_2O), dichloromethane–2% (w/w) PVA aqueous solution (CH_2Cl_2–PVA aq.), and 2 g L^{-1} PLA (2kDa) dichloromethane solution–2% (w/w) PVA aqueous solution (CH_2Cl_2+PLA–PVA aq.), respectively. The measured initial interfacial tensions were 2.81×10^{-2}, 2.64×10^{-2}, 1.94×10^{-2}, and 1.89×10^{-2} N m^{-1} and the standard deviations were estimated to be 2×10^{-4}, 2×10^{-4}, 4×10^{-4}, and 7×10^{-4} N m^{-1}, respectively. The measured interfacial tension decreased as time continued. In the cases of CH_2Cl_2–H_2O and CH_2Cl_2+PLA–H_2O, the value decreased almost linearly because dichloromethane diffused into the surrounding aqueous medium. In contrast, in the cases of CH_2Cl_2–PVA aq. and CH_2Cl_2+PLA– PVA aq., the value exponentially decayed in the early stages because PVA in the aqueous medium adsorbed onto the droplet surface. These results indicated that the addition of PVA reduced the interfacial tension by about 30%, but the effect of PLA on the interfacial tension was much smaller than that of PVA.

During the measurements of interfacial tension, the size of the droplet was kept constant by forcing either dichloromethane or a PLA dichloromethane solution from a microsyringe to compensate for the diffusion of these liquids into the surrounding aqueous medium. Without the addition of liquid,

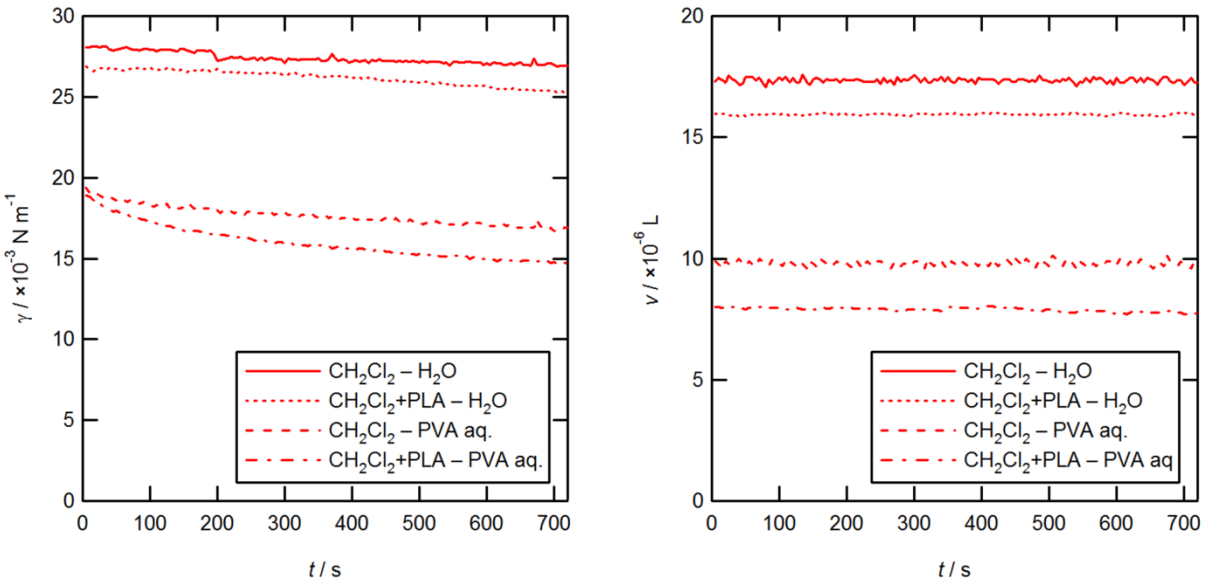

Figure 1: Time courses of interfacial tension, γ (left) and droplet volume of either dichloromethane or 2 g L^{-1} PLA (2 kDa) dichloromethane solution, *v* (right). The surrounding aqueous medium is either water or 2% (w/w) PVA aqueous solution.

the size of the droplet decreased as time went on due to diffusion.

Figure 2 shows the time course of the droplet volume; the volume of the droplet decreased almost linearly. The measured volume reduction rates of the droplet were 5.12×10^{-2}, 3.31×10^{-2}, 5.51×10^{-3}, and 2.40×10^{-3} μL s^{-1} for CH_2Cl_2–H_2O, CH_2Cl_2+PLA–H_2O, CH_2Cl_2–PVA aq., and CH_2Cl_2+PLA–PVA aq., respectively. This result indicates that the volume reduction rate decreased by 35.4% in water and 56.4% in the PVA aqueous solution due to the addition of PLA.

1. Measurement of viscosity

Viscosity measurements were performed using a tuning fork vibration viscometer SV-10 (A&D Company, Japan). The viscometer was calibrated using pure water. The measured viscosity of dichloromethane was 0.43×10^{-3} Pa s at 298 K. Figure 3 shows the specific viscosity of PLA dicholoromethane solutions as a function of PLA concentration for three different PLA molecular weights, 2, 45, and 100 kDa, at 298 K. The specific viscosity is defined as $\eta_{sp} = (\eta - \eta_0)/\eta_0$, where η_0 and η were the measured viscosities of dichloromethane and the PLA dichloromethane solution, respectively. The curve fit on the graph corresponded to power functions of $\eta_{sp} = 0.0123 \times c_{PLA}^{1.14}$, $\eta_{sp} = 0.0300 \times c_{PLA}^{1.52}$, and $\eta_{sp} = 0.0709 \times c_{PLA}^{1.62}$ for PLA molecular weights of 2, 45, and 100 kDa, respectively. The viscosity of the solution increases with increasing PLA concentration and molecular weight.

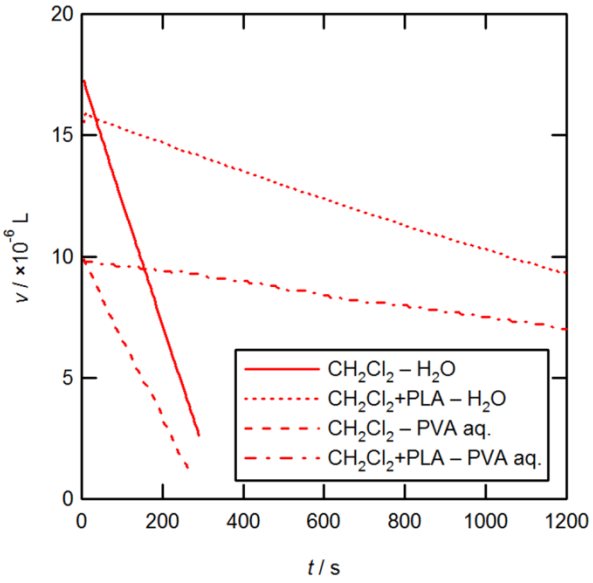

Figure 2: Time courses of the droplet volume of either dichloromethane or a 2 g L^{-1} PLA (2 kDa) dichloromethane solution, *v*, without the addition of liquid. The surrounding aqueous medium is either water or a 2% (w/w) PVA aqueous solution.

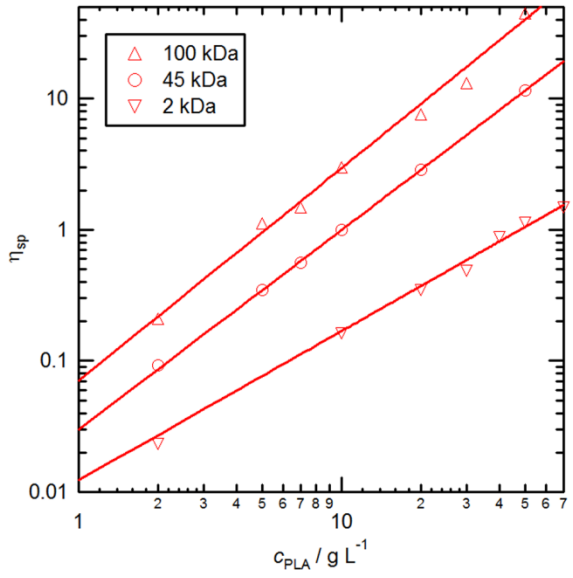

Figure 3: Specific viscosity of the PLA dicholoromethane solutions, η_{sp}, as a function of the PLA concentration, c_{PLA}.

Appendix 3

1. The Effect of EtOH on the bubble and capsule size

The inclusion of EtOH in the PLA polymer solution enhanced bubble nucleation. As the concentration of EtOH increased, the average microbubble size increased but its uniformity decreased. The presence of a higher volatile component yielded to the continuous nucleation and growth of microbubbles.[1,2] This can be observed from left panels of Figure 1. This suggests that the theoretical model of bubble stability and equilibrium bubble radius cannot be used when EtOH is added because the system no longer can be regarded in the equilibrium state and the nucleation of EtOH have to be considered explicitly. Hollow PLA microcapsules created using EtOH have low uniformity. In addition, as the concentration of EtOH increases (i.e. 20% EtOH) size distribution deteriorates. This is shown in right panels of Figure 1. The largest hollow PLA microcapsules are attained when the concentration of EtOH is 5%. This fabrication condition is similar to the fabrication conditions reported in our previous studies (Daiguji, H.; Takada, S.; Molino, J.J.; Takemura, F.; *Journal of Physical Chemistry B*, 2009, **113**, 15002-15008). Thus, increasing the content of volatile solute, which in turn increases the number of nucleated microbubbles inside the droplet, does not yield to larger capsules; but rather it yields to smaller capsules with deteriorated uniformity.The addition of EtOH to the CH_2Cl_2 solution of PLA reduces the quality of the solvent. Indeed, when EtOH was added to the CH_2Cl_2 solution of PLA slowly, a part of dissolved PLA polymer precipitated. Subsequently, when the solution was agitated, the polymer dissolved again. This simple experiment also suggests that the addition of EtOH reduces the quality of the solvent. When adding EtOH, the size of the bubble is larger than the size of the wet microcapsule, which is also larger than the final dry microcapsule ($r_b > r_{c,\,wet} > r_c$) as reported in the previous section.

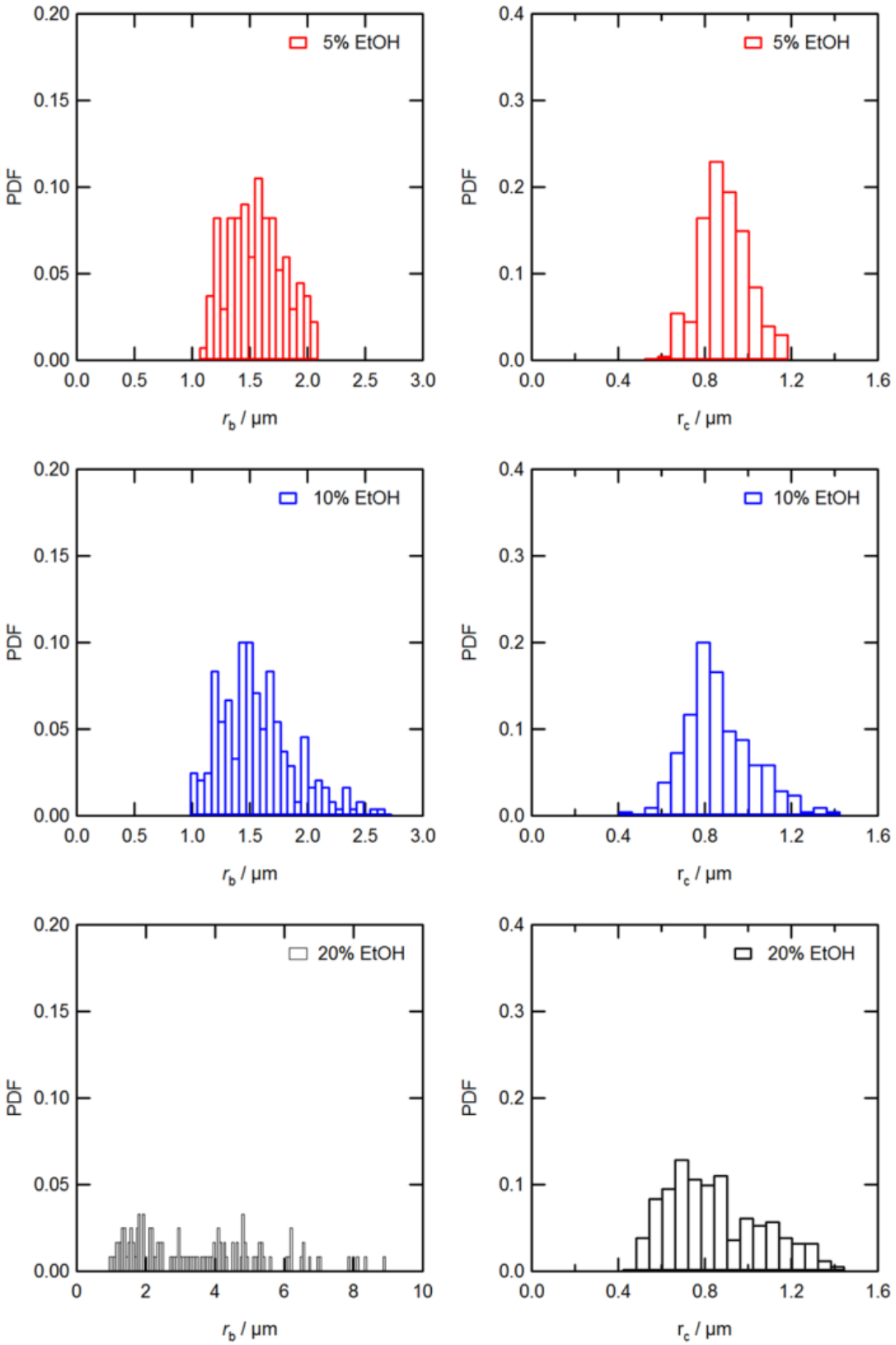

Figure 1: Radius distributions of nucleated microbubbles (left) and hollow PLA microcapsules (right). The concentrations of 5, 10 and 20% volume of EtOH in CH_2Cl_2 were employed using a PLA of molecular weight of 2 kDa and an initial c_{PLA} of 2 g L^{-1}.

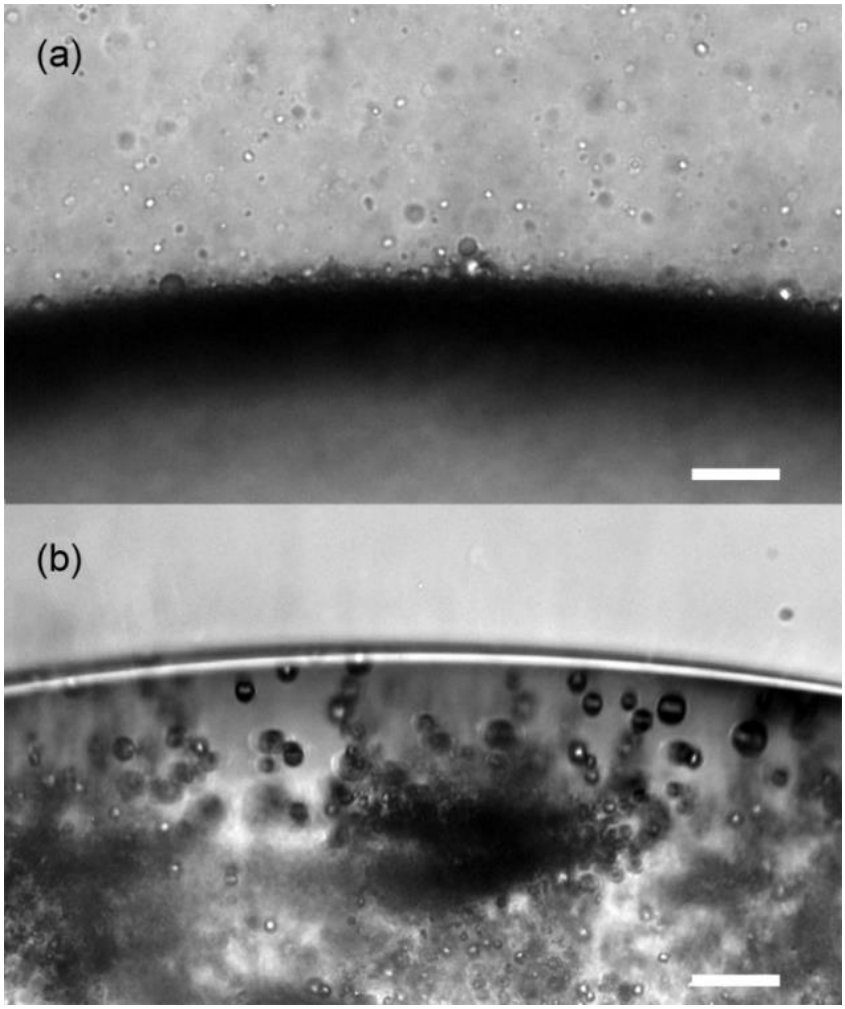

Figure 2: Release of hollow PLA microcapsules from the droplets (a) when ultrasound was applied and (b) when 20% volume of EtOH was employed. The PLA molecular weight was 2 kDa and the surrounding aqueous medium was 2% (w/w) PVA aqueous solution in both cases. The scale bar is 50 μm long.

2. Shrunken and Bridged microcapsules

The analysis of the experimental results suggested that shrinkage was a two-stage process. The first stage happened as the bubble crossed the liquid-liquid interface (top and middle of Figure 5.2 in Chapter 5), and the second stage happened when the microcapsules were dried (middle and bottom, Figure 5.2 in chapter 5). Inside the organic solvent in the first stage, the hydrophobic portions of PLA prefer the swollen state to a compact, collapsed state. When the polymeric shell of PLA contacts the aqueous phase, the hydrophobic areas of the polymers reduce their size to minimize surface exposure and to avoid any inclusion of water. Furthermore, because the encapsulated gas is a mixture of air and CH_2Cl_2 (the volume ratio of air to CH_2Cl_2 is about 0.13[3]), more CH_2Cl_2 gas diffuses into the surrounding aqueous medium. The capsule shrinkage is attributed not only to the shell shrinkage but also to the dissolution of the CH_2Cl_2

gas into the bulk aqueous medium. Especially when ultrasound was employed, bubble nucleation was enhanced, and thus the amount of PLA per bubble could also affect the capsule size. If this value was not large enough, the bubble could not be covered with PLA completely, and thus gas leakage could take place in the aqueous phase. As for the second stage, it is important to understand that the capsule shell is not completely solid. In fact, it is more accurately described as a gel state because CH_2Cl_2 has not been removed completely. Only a very dry/low pressure environment or heating will completely remove CH_2Cl_2 from the shell structure. In the end, the fabricated hollow PLA capsules become smaller than the template bubbles, and the dried capsules are even smaller than the wet ones. Figure 3a shows the FE-SEM images of dried hollow PLA microcapsules.

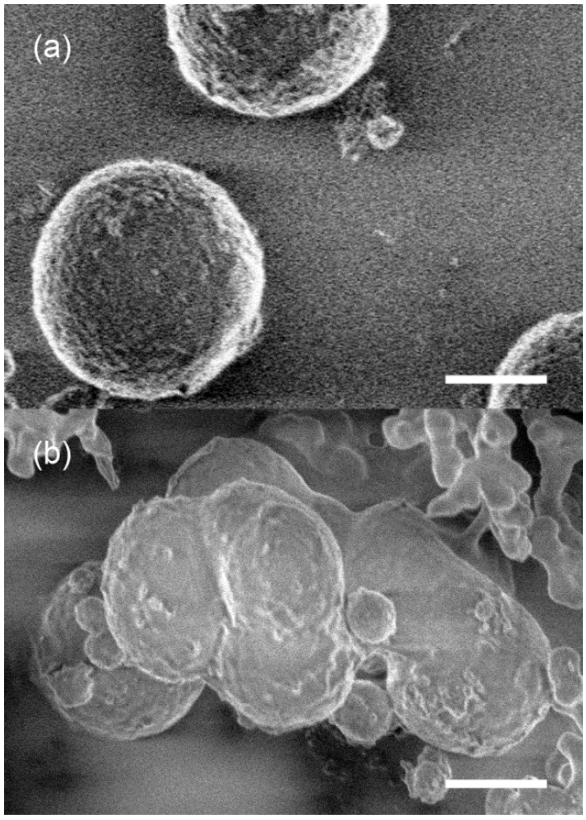

Figure 3: FE-SEM images of hollow PLA microcapsules fabricated using process A from 2 kDa PLA solutions with different initial PLA concentrations. (a) c_{PLA} = 2 g L^{-1} and (b) c_{PLA} = 30 g L^{-1}. The scale bars represent 1 μm.

Regarding microcapsule bridging, the probability of fabricating bridged capsules increased as c_{PLA} increased in process A (diffusion only driven pocess). This can be explained from the fact that, in a higher viscosity solution, the energy transferred is greatly damped by the viscous medium. Therefore, PLA-coated microbubbles have the opportunity to agglomerate at the interface. Furthermore, as solvent diffusion took place, a highly viscous layer of PLA solution was formed close to the liquid-liquid interface. This layer has completely different rheological

properties compared to the bulk solution.[4–6] De Gennes[7] provided a theoretical discussion of this layer, which was considered an elastic layer in the sol-gel transition. Therefore, the outermost part of this layer can solidify into a solid skin at the liquid-liquid interface. The initial c_{PLA} is an important parameter, as it determines the time required to achieve such a solid skin, which also increases the opportunity to form agglomerated capsules at the interface. When a sufficiently strong energy can be transferred to the agglomerated capsules, they are released and become bridged capsules, as confirmed in Figure 3.b.

Another scenario for the formation of bridged capsules is that the PLA polymer solidifies around the bubble and the PLA-covered bubbles agglomerate inside a CH_2Cl_2 droplet. This happens frequently, when the PLA concentration is high and EtOH is added. The addition of EtOH to the CH_2Cl_2 solution of PLA reduced the quality of the solvent. Indeed, when EtOH was added to the CH_2Cl_2 solution of PLA slowly, part of the dissolved PLA polymer precipitated. Subsequently, when the solution was agitated, the polymer dissolved. This simple experiment also suggests that the addition of EtOH reduced the quality of the solvent. The addition of EtOH could segregate PLA to the bubble surface. Figure 4 shows bridged microcapsules inside a CH_2Cl_2 droplet. Microcapsules of non-spherical shape retained those shapes inside the polymer solution during the entire period of experimental observation. This phenomenon occurred not only when EtOH was employed but also in processes A and B.

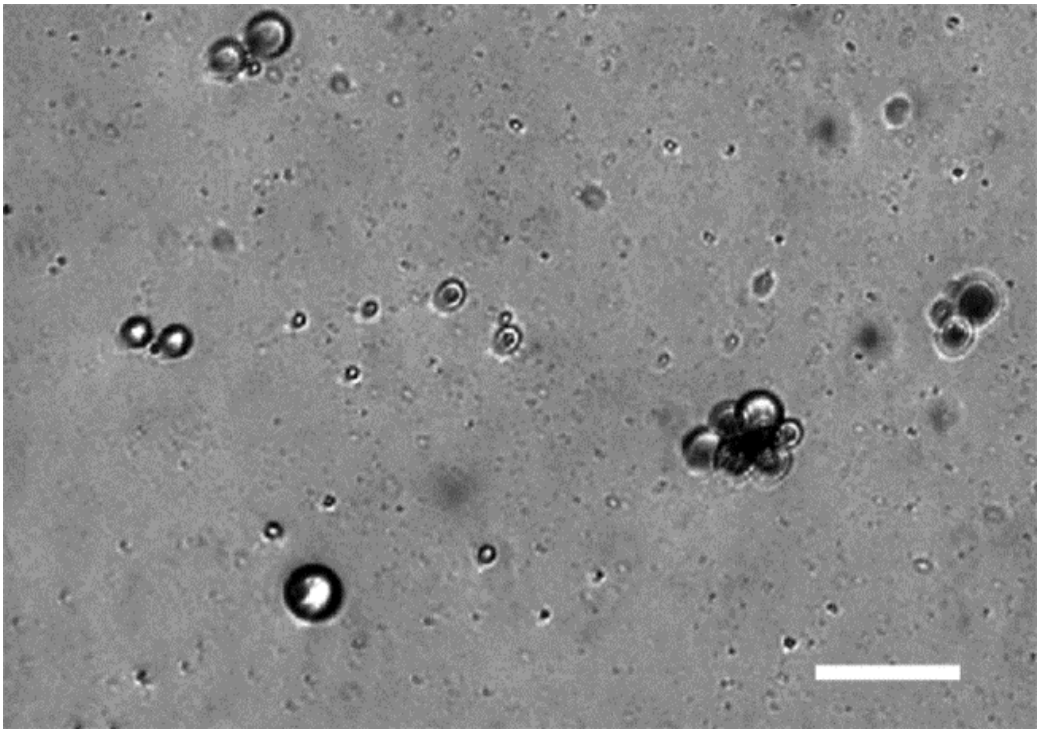

Figure 4: Bridged microcapsules inside a CH_2Cl_2 droplet. The capsules kept their shapes (deformed and bridged) throughout the entire observation time (20 min). The PLA molecular weight was 2 kDa, the surrounding aqueous medium was 2% (w/w) PVA aqueous solution, c_{PLA} = 30 g L^{-1}, and 5% (v/v) EtOH. The scale bar represents 25 µm.

3. References

1. C. A. Ward, P. Tikuisis and R. D. Venter, *J. Appl. Phys.*, 1982, **53**, 6076.
2. S. Goldman, *J. Phys. Chem. B*, 2008, **112**, 16701.
3. K. Shirono, T. Morimatsu and F. Takemura, *J. Chem. Eng. Data*, 2008, **53**, 1867.
4. B. Ewen, D. Richter, T. Shiga, H. H. Winter and M. Mours, *Neutron Spin Echo Spectroscopy-Viscoelasticity-Rheology*, Advances in Polymer Science, **134**, Springer-Verlag, Berlin Heidelberg, 1997.
5. M. Rubinstein and R. Colby, *Polymer Physics*, Oxford University Press, Oxford, 1st ed., 2003.
6. I. Teraoka, *Polymer Solutions: An Introduction to Physical Properties*, Wiley InterScience, New York, 1st ed., 2002.
7. P. G. de Gennes, *Eur. Phys. J.*, 2002, **7**, 31.

Appendix 4

1. Titration Curves and Velocity Profiles at different pH

Several 0.05-M solutions of Na_2CO_3 with different concentrations of PAH (0.1, 1.0, 2.0, 3.0, 7.0, 15.0, and 20.0 g/L) were prepared to analyze the effect of the PAH concentration on the final microcapsule size. Some titration curves for the different concentration of PAH are shown in Figure 4.8. As it is seen experimental results agreed with the theoretical titration curves. Likewise, several solutions of Na_2CO_3 (0.0125, 0.025, 0.05, 0.10, and 0.15 M) were prepared to analyze the effect of the Na_2CO_3 concentration on the final capsule size.

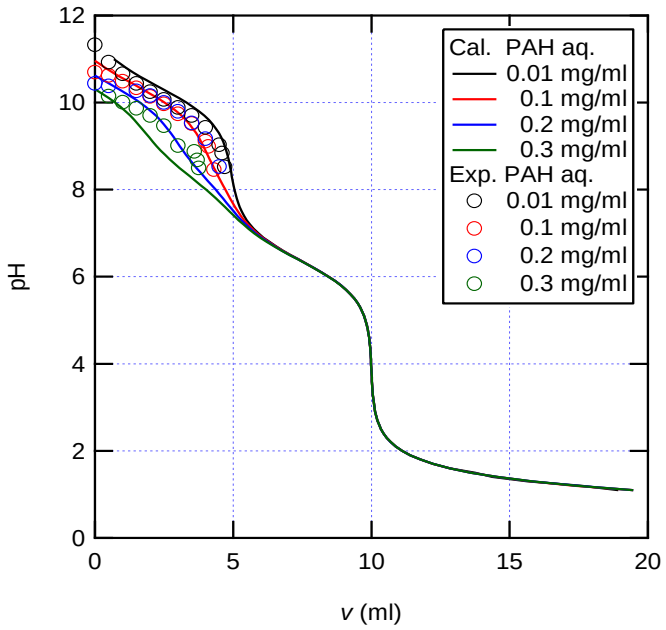

Figure 1: Titration curves. Measured and calculated titration curves of 100 ml of 0.054 M Na_2CO_3 aqueous solution with a concentration of PAH, cPAH = 0.1, 1.0, 2.0, and 3.0.

Figure A10 shows the velocity profile of the microcapsules inside the electrophoretic cell at different pH. The measured zeta potential of the PAH microcapsules at pH = 9.0 was negative, and this value changed to positive, and then increased with a decrease in the pH. This result suggests that the concentration of R-NHCOO^{-} decreases and that of R-NH3^{+} increases with a decrease in the pH.

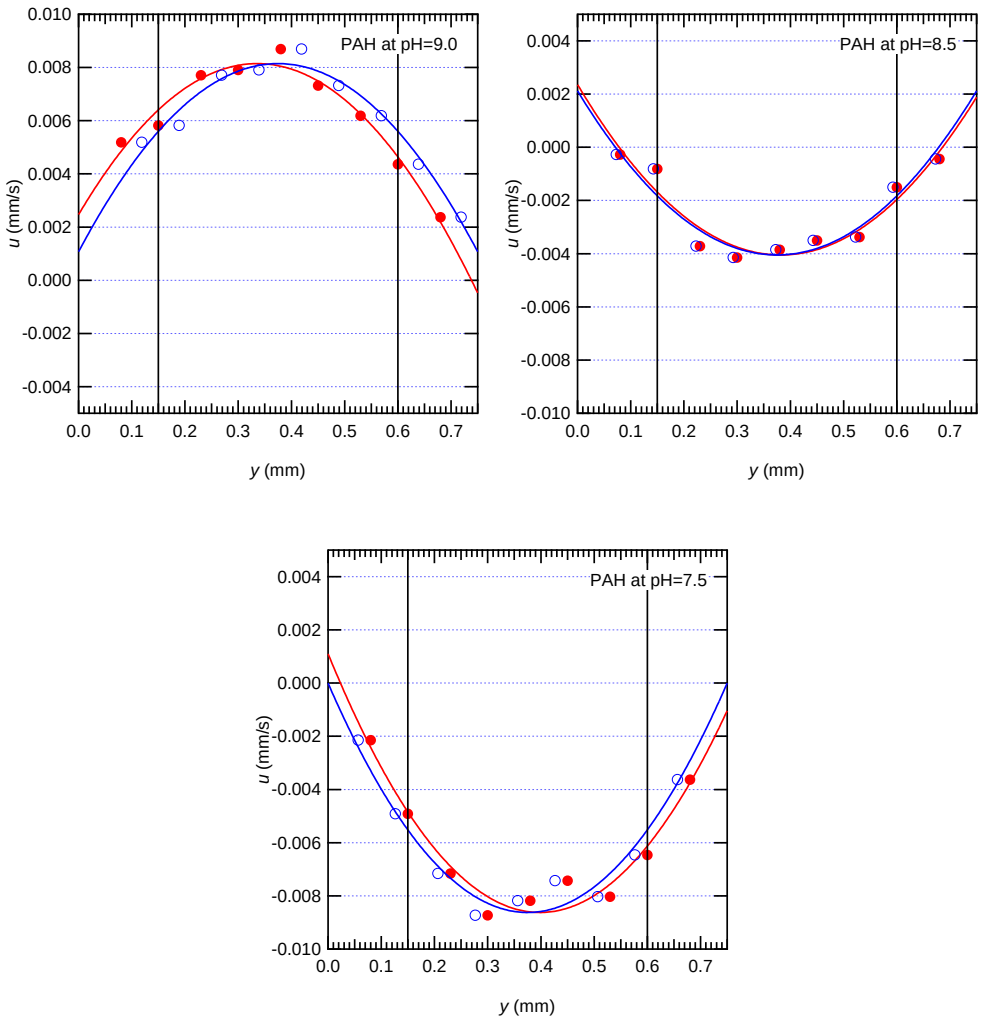

Figure 2: PAH microcapsules velocity profile at different pH At low pH zeta potential is positive, whereas at high pH it is negative.

Nomenclature

In order of appearance here it is the list of nomenclatures employed through this thesis:

1. Φ scattering section, azimuth angle
2. R radius of the scatterer
3. λ wavelength
4. k $2\pi/\lambda$ is the wave number
5. k_s compressibility of the scatterer
6. K compressibility of the continuous phase
7. ρ_s density of the scatterer
8. ρ density of the continuous phase
9. ΔP pressure difference
10. P_b blood pressure
11. P_d drop pressure
12. γ,σ surface tension
13. L Ostwald coefficient
14. D_w diffusivity of the gas in water
15. f ratio of gas concentration in the bulk to saturation
16. R_{shell} Resistance of the shell to the encapsulated gas permeation
17. PI, CV polydispersivity index, coefficient of variation.
18. G Gibbs energy
19. T Temperature
20. p pressure
21. N_k moles of the k^{th} component
22. F Helmholtz free energy
23. ν_0 specific volume of the pure liquid
24. $0, 1,2,3$ subscript for the initial value, the liq., the gas and the polymer substance respectively
25. $',''$ prime and double prime for the liquid and gas phase respectively.
26. c_{2s} saturation concentration of the gas
27. μ_2'' chemical potential of the pure gas in the gas phase
28. μ_2' chemical potential of the gas in the liquid phase
29. μ_1'' chemical potential of the pure liquif in the gas phase
30. μ_1' chemical potential of the liquid in the liquid phase
31. p_{10}'' saturation vapor pressure of the pure liquid
32. K_H, H Henry constant
33. R Universal gas constant
34. c concentration

35. V volume
36. q amount of nucleated bubbles
37. r_b radius of the bubble
38. N_2 total amount of moles of Nitrogen
39. $\Gamma_{bc}^{eq}(c_3)$ the equilibrium area density of PLA on the surface of the bubbles
40. ΣS_{bc} total surface area of bubbles and microcapsules
41. ΣV_{bc} total volume of bubbles and capsules
42. $\bar{\Gamma}_{bc}$ average area density of PLA at the surface of the bubbles
43. c_{PLA} initial concentration of PLA
44. E_0 the energy required by a single bubble to pass through the interface
45. N total number of nucleated bubbles
46. η kinematic viscosity
47. θ inclination angle
48. χ mole fraction of the dissolved gas in the liquid

Dedication

Above all, to the maximum glory of God.
To Jay (Papá), Mayra (Mamá), Alejandro(Hermano),
and Marina(abuela) for helping and letting me
chase comets for so long...so far away…
&
To my beloved wife Laura,
for being my conscience,
my inspiration, my heart, my will…
together always in all ways for Him.
For she gave me new dreams
and a life to pursue.

ad Romanos 8: 37-39

Publications

Journal papers

1. Hirofumi Daiguji, Shingo Takada, Jay Jesus Molino, and Fumio Takemura
   "Fabrication of hollow polylactic acid microcapsules from microbubbles templates"
   Journal of Physical Chemistry B **113**, 15002-15009, 2009.
2. Jay Jesus Molino, Eitaro Matsuoka and Hirofumi Daiguji
   "Size control of hollow poly-allylamine hydrochloride/poly-sodium styrene sulfonate microcapsules in bubble template method"
   Soft Matter **7**, 1897-1902, 2011.
3. Jay J. Molino Cornejo, Hirofumi Daiguji and Fumio Takemura
   "Factors affecting the size and uniformity of hollow poly(lactic acid) microcapsules fabricated by bubble template method"
   Journal of Physical Chemistry B **115**, 13828–13834, 2011.
4. Daichi Sakurai, Jay J. Molino Cornejo, Hirofumi Daiguji and Fumio Takemura
   "Hollow poly(lactic acid) microcapsules fabricated in gas/oil/water method and bubble template method"
   Journal of Materials Chemistry A, **doi: 10.1039/c3ta12587d**, 2013.

International conferences

1. Jay Jesus Molino, Shingo Takada, Hirofumi Daiguji, and Fumio Takemura
   "Fabrication of hollow polylactic acid microcapsules from microbubbles templates"
   2nd ASME Micro/Nanoscale Heat & Mass transfer International Conference (MNHMT2009)
   Shanghai (China) (2009.12)
   ISBN: 978-0-7918-4390-1, **ASME** (2009) 205−209, **doi: 10.1115/MNHMT2009-18416**
2. Jay Jesus Molino, Fumio Takemura and Hirofumi Daiguji
   "Size control of hollow polylactic acid microcapsules and hollow polyelectrolyte microcapsules in bubble template method"
   8th ASME-JSME Thermal Engineering Joint Conference (AJTEC2011)
   Honolulu, Hawaii (USA) (2011. 3)
   ISBN: 978-0-7918-3892-1, ASME (2011) T30097-T30097-6, **doi: 10.1115/AJTEC2011-44556**
3. Jay Jesus Molino, Hirofumi Daiguji, and Fumio Takemura
   "Factors affecting the size and uniformity of hollow poly(lactic acid) microcapsules fabricated from microbubble templates"
   7th US-Japan Joint Seminar on Nanoscale Transport Phenomena
   Shima (Japan) (2011.12)
   Poster Presentation

4. Jay Jesus Molino, Fumio Takemura and Hirofumi Daiguji
   "On the kinetics of formation of hollow poly(lactic acid) microcapsules fabricated from microbubble templates"
   10th ASME International Conference on Nanochannels, Microchannels, and Minichannels (ICNMM2012)
   Puerto Rico (USA) (2012. 7)
   ISBN: 978-0-7918-4479-3, ASME (2012) 295−302, **doi: 10.1115/ICNMM2012-73257**

Other conferences

1. Jay Jesus Molino, Hirofumi Daiguji, and Fumio Takemura
   "Fabrication of hollow polylactic acid microcapsules from microbubble templates: The effect of surfactant and polymer concentration on capsule size"
   第47回日本伝熱シンポジウム講演論文集, 札幌 (2010.5)
2. Jay Jesus Molino, Hirofumi Daiguji, and Fumio Takemura
   "Size control of hollow polylactic acid microcapsules made from microbubble templates
   第48回日本伝熱シンポジウム講演論文集, 岡山 (2011.6)
3. Jay Jesus Molino, Hirofumi Daiguji, and Fumio Takemura
   "Mechanics of formation and release of hollow polylactic acid (PLA) microcapsules made from microbubble templates"
   第49回日本伝熱シンポジウム講演論文集, 富山 (2012.5)
4. Jay Jesus Molino, Daiichi Sakurai, Hirofumi Daiguji, and Fumio Takemura
   "Mass production of hollow polylactic acid microcapsules using the bubble template method"
   第50回日本伝熱シンポジウム講演論文集, 仙台 (2013.5)
5. Daiichi Sakurai, Jay Jesus Molino, Hirofumi Daiguji, and Fumio Takemura
   "マイクロバブルを用いた中空マイクロカプセルの製造"
   第50回日本伝熱シンポジウム講演論文集, 仙台 (2013.5)

Curriculum

Jay Jesus Molino Cornejo was born on March 7th of 1985 in Panama city, Panama, the bridging exuberant isthmus of America. In 2007 he graduated as a Mechanical Engineer from John Brown University sponsored by the Walton Scholarship Program. In 2008 he entered the University of Tokyo as a research student sponsored by the Ministry of Culture and Education. In April 2009 he started his master degree and completed it in February 2011 under the supervision of prof. Hirofumi Daiguji at Hihara-Daiguji Lab. He graduated in Summa degree and was granted the Head of the Department Award. After his master, he pursued doctoral studies under prof. Daiguji guidance. Both worked on several projects including the fabrication of polyelectrolyte microcapsules using microbubble as templates and mass production of hollow capsules. During this time, he worked on and improved facile procedures to fabricate hollow capsules using microbubble templates, worked on the elucidation of the kinetics of formation of such capsules and achieved size control. From these studies 3 different kind of capsules were synthesized for pharmaceutical and engineering applications.

All his contributions are published in scientific international journals, presented in several local and international conferences and disclosed in this defense.